MONTHLY NOTICES

OF THE

ROYAL ASTRONOMICAL SOCIETY

Volume 117 No. 4 1957

Published and Sold by the

ROYAL ASTRONOMICAL SOCIETY
BURLINGTON HOUSE
LONDON, W.1

Price £1 0s. 0d.; in U.S.A. $3.20

(Annual Subscription for volume of six numbers: £5 5s. 0d.; in U.S.A. $16)

ROYAL ASTRONOMICAL SOCIETY

Founded 1820

ANNOUNCEMENT OF NEW PUBLICATION

First number to appear in 1958 March

The Geophysical Journal

Price (post free) : £3 ($9 in U.S.A.) for a volume of at least four parts.

This is a new journal of the Society for the publication of research in geophysics and related subjects. It is being started because the rapid development in geophysics calls for a journal that will appear at short intervals and contain papers covering the wide range of subjects involved. The increase of geophysical activity now makes it essential that authors should be assured of speedy publication and that their work should become known through a large and world-wide circulation.

The *Geophysical Journal* will contain original papers, short notes and letters, and articles on the progress of geophysics, together with book reviews and reports of geophysical discussions.

The *Geophysical Supplement* to the *Monthly Notices* of the Society will be incorporated in the new *Journal*. The last number of the *Geophysical Supplement* will appear towards the end of 1957.

The *Geophysical Journal* invites papers of high standard on the topics previously covered by the *Geophysical Supplement* and also on related subjects such as, for instance, some aspects of work on the upper atmosphere. To ensure the minimum of delay between acceptance of a paper and its publication, the *Geophysical Journal* will be issued quarterly. It is hoped that these features, together with the wide circulation enjoyed by the Society's publications, will encourage authors (who need not be Fellows of the Society) to contribute to it.

Papers for publication should be sent to the Assistant Secretary of the Royal Astronomical Society, Burlington House, London, W.1, England.

The *Geophysical Journal* will be edited by A. H. Cook, M.A., Ph.D., F.R.A.S., F.G.S. and T. F. Gaskell, M.A., Ph.D., F.R.A.S. in collaboration with the Geophysical Secretary of the Society, R. A. Lyttleton, M.A., Ph.D., F.R.S.

MONTHLY NOTICES

OF THE

ROYAL ASTRONOMICAL SOCIETY

Vol. 117 No. 4

MEETING OF 1957 MARCH 8

Dr W. H. Steavenson, President, in the Chair

The President announced the death of Henry Norris Russell, an Associate of the Society, and paid a tribute to his memory, the Fellows standing.

The election by the Council of the following Fellows was duly confirmed :—

George Anderson, 54 Winton Road, Ashburton, Victoria, Australia (proposed by W. H. Vale) ;

William Bowen Bonnor, 8 Aigburth Drive, Liverpool 17 (proposed by J. Kershaw);

Michael Harvey Briggs, 9 Meadway, Chadderton, Lancs. (proposed by F. W. Land);

Peter John Grant, Uplands, Burley, Ringwood, Hants. (proposed by R. W. Cartmel);

*Michael Guest, 122 Perrywood Road, Great Barr, Birmingham (proposed by P. Moore);

Kenneth William Harrison, 61 Worthing Avenue, Gosport, Hants. (proposed by W. H. Day);

Michael James Hendrie, 25 The Crossways, Westcliff-on-Sea, Essex (proposed by R. L. Waterfield);

James Lawrence, Stonyhurst College Observatory, Lancs. (proposed by P. J. Treanor);

John Vetterlein, 91 Ingrave Road, Brentwood, Essex (proposed by W. H. Julian);

*Roderick Vernon Willstrop, The Observatories, Cambridge (proposed by R. O. Redman); and

Raymond William Henry Wright, University College, Ibadan, Nigeria (proposed by M. W. Ovenden).

The election by the Council of the following Junior Members was duly confirmed :—

Muriel Hodgkinson, 78 Hardy Lane, Chorlton-c-Hardy, Manchester 21 (proposed by Z. Kopal); and

Richard Anthony James, Downing College, Cambridge (proposed by A. W. Vince).

* Transferred from Junior Membership.

One hundred and twelve presents were announced as having been received since the last meeting, including :—

A. G. Meissner, *Astronomischer Hand-Atlas zu Rüdiger's Kenntniss des Himmels* (presented by Flt Lt F. Whalley);

Melbourne Astrographic Catalogue, Vol. V (presented by Sydney Observatory and the International Astronomical Union);

Harold Jeffreys, *Scientific Inference*, 2nd edition (presented by the author);

F. Link, *Die Mondfinsternisse* (presented by Messrs Geest and Portig);

J. Dufay, *Galactic nebulae and interstellar matter* (presented by Messrs Hutchinson & Co.); and

G. C. McVittie, *Distance and Time in Cosmology : the Observational Data* (presented by the author).

MEETING OF 1957 APRIL 12

Dr W. H. Steavenson, President, in the Chair

The President announced that the Council had elected the following Associates of the Society :—

Guillermo Haro, Director of the National Astrophysical Observatory, Tonanzintla, Mexico;

Milton La Salle Humason, Mount Wilson Observatory, California, U.S.A.; and

Miss Inge Lehmann, Chief Seismologist, Copenhagen (retired).

The election by the Council of the following Fellows was duly confirmed :—

John Brian Alexander, 106 Pevensey Road, Eastbourne, Sussex (proposed by R. v. d. R. Woolley);

Winter Horace Barnett, 6 The Bungalows, Pottery Lane, Whittington Moor, Chesterfield, Derbyshire (proposed by R. R. S. Cox);

Thomas James Edgar Palmer, 12A Kenyon Mansions, Queen's Club Gardens, London, W.14 (proposed by F. M. Holborn);

Michael Douglas Scott-Scott, Ferres, Swanage, Dorset (proposed by H. Bondi);

William Smith, 60 Hillcrest Road, Southlands, Weymouth, Dorset (proposed by A. F. Alexander);

George Eric Burdett Stephenson, 124 Duchy Road, Harrogate, Yorkshire (proposed by G. Fielder); and

Harry Wilde, 363 London Road, Ewell, Surrey (proposed by J. Jackson).

The election by the Council of the following Junior Members was duly confirmed :—

Vinod Kumar Gaur, Geophysics Department, Imperial College, London, S.W.7 (proposed by J. M. Bruckshaw); and

Brian Richard May, 3 St George's Mews, Regent's Park Road, London, N.W.1. (proposed by C. W. Allen).

THE VARIATION OF IONIZATION ALONG A METEOR TRAIL

J. S. Greenhow and E. L. Neufeld

(Communicated by A. C. B. Lovell)

(Received 1957 March 29)

Summary

The ionized trails of faint meteors have been investigated by observation of radio echoes at two spaced receiving stations. The mean ionization curve is much shorter than predicted by present theory, and in particular the rise to maximum electron line density is more rapid than expected. Occasional meteors appear almost instantaneously with maximum electron density, and in many cases irregularities in the ionization considerably distort the diffraction effects during trail formation. Evidence for the fragmentation of meteors is also presented. These effects are considered in relation to Jacchia's photographic observations of the light curves of faint visual meteors.

1. *Introduction.*—A meteor in its passage through the upper atmosphere is subject to impacts with air molecules, and the heat liberated is sufficient to vaporize completely the meteoric material. Light and ionization are produced by collisions between air molecules and evaporated meteor atoms, which are moving with relative velocities of 10–70 km sec^{-1} (Sparrow, 1926; Öpik, 1933; Hoppe, 1937). The variation of light and ionization along a meteor trail has been discussed by Whipple (1943) and Herlofson (1948), and the light curves have been investigated photographically by Jacchia (1949). Results for bright meteors of 0 to −7 magnitude are in general agreement with theory, and by analogy it has been assumed that the ionization curves are also of the same form. The ionization curves are of considerable interest in studies of radio echoes from meteor trails, particularly in atmospheric density and temperature measurements, and in the determination of meteor mass distributions (Kaiser, 1954; Evans, 1954).

Recently the photographic observations have been extended to faint visual meteors of approximately +3 mag, and serious anomalies in the light curves have been discovered (Jacchia, 1955). As the majority of radio echoes are obtained from meteors even fainter than this, it is important to determine to what extent the ionization curves agree with those derived theoretically. This paper describes experiments in which the variation of electron line density along a meteor trail has been investigated by observation of the radio echoes at two widely-spaced stations.

2. *Technique*

(*a*) *Measurement of electron line density.*—The linear electron density α in the section of a meteor trail from which the radio echo is obtained may be determined from the echo characteristics, together with a knowledge of the equipment parameters. Thus for $\alpha \lesssim 10^{12}$ electrons cm^{-1} the initial echo amplitude $A_0 \propto \alpha G_T^{1/2} G_R^{1/2} / R^{3/2}$ (Lovell and Clegg, 1948). The amplitude decays exponentially and the decay time to $1/e$ of the initial amplitude is $\lambda^2/16\pi^2 D$ (Herlofson, 1948). G_T and G_R are the gains of the transmitting and receiving aerials, and R

the range of the echo. λ is the radio wave-length and D the diffusion coefficient. When $\alpha \gtrsim 10^{12}$ cm^{-1}, $A_0 \propto \alpha^{1/4} G_T^{1/2} G_R^{1/2} / R^{3/2}$. In this case echo amplitude varies only as the fourth root of α, and is a rather inaccurate measure of the electron density. On the other hand, echo duration T increases with α, where $T = \frac{\alpha \lambda^2}{4\pi^2 D} \left(\frac{e^2}{mc^2} \right)$ (Greenhow, 1952). e, m are the electronic charge and mass, c the velocity of light. Thus if D is known, T gives a measure of the linear electron density.

(*b*) *Transmitter and receiver.*—In order to investigate the shape of the ionization curve it is necessary to obtain radio reflections simultaneously from two or more points along a given meteor trail. In the present experiments a single transmitter generating 300 pulses/sec with a peak power of 50 kw was used. The pulse length was 30 μs and wave-length 8·27 m. The sensitivity of the equipment was such that most of the echoes used in the analysis were from meteors of +6 to +8 visual magnitude. Two receiving stations were set up, one on the same site as the transmitter at Jodrell Bank (O_1, Fig. 1), and the other 20 km to the east.

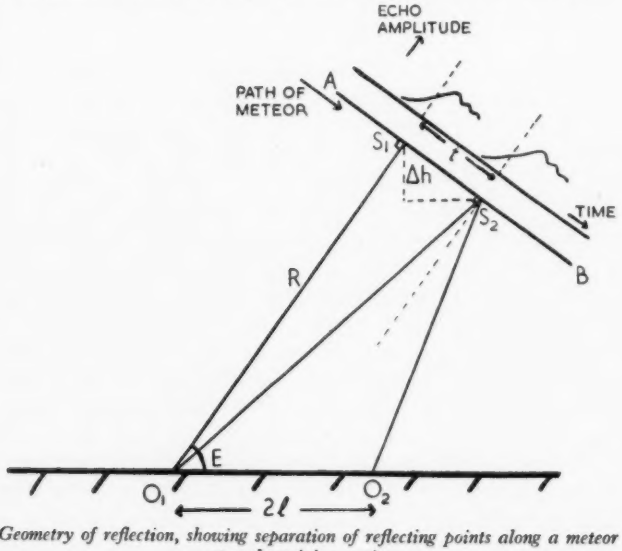

FIG. 1.—*Geometry of reflection, showing separation of reflecting points along a meteor trail with spaced receiving stations.*

Because of the specular reflecting properties of a meteor trail, echoes are received at O_1 and O_2 from points S_1 and S_2. If V is the meteor velocity and t the time taken for the meteor to travel from S_1 to S_2, then $S_1S_2 = Vt$. If observations are restricted to meteors occurring at approximately 90° azimuths, then for a trail AB at any inclination to the plane of the paper the difference in height between S_1 and S_2 is given by $\Delta h \sim (Vt)^2 \cot E / l$. The largest permissible value of Δh is 5 km, and all values less than this are possible for meteor trails suitably orientated. The meteor velocity is estimated approximately from the rate of increase in echo amplitude as the meteor passes through the first Fresnel zone, or, in the case of very slow meteors, from the diffraction fluctuations (Davies and Ellyett, 1949). t is given by the time delay in appearance of the echoes at O_1 and O_2, and E from the height and range of the meteor echo.

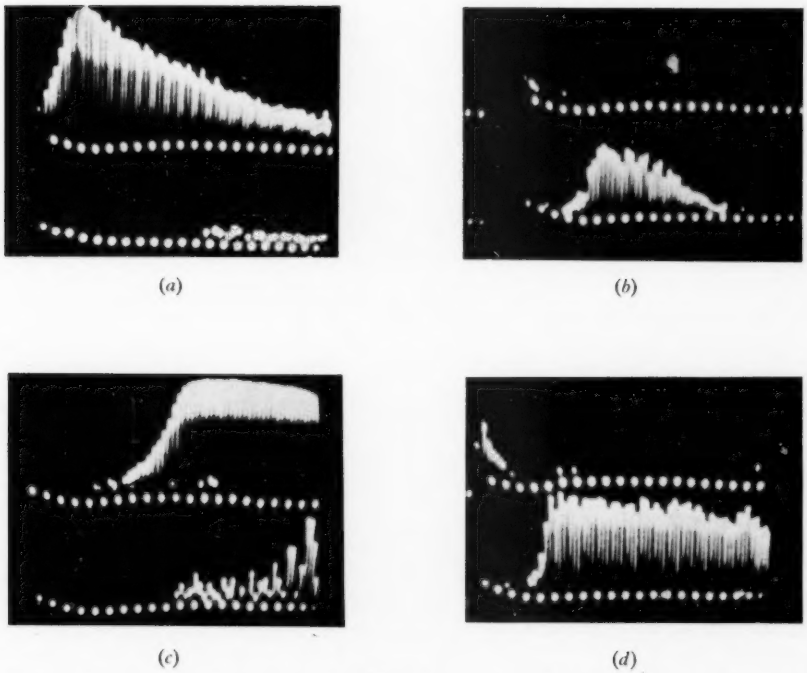

(*a*) (*b*)

(*c*) (*d*)

FIG. 2.—*Film records. Upper trace, echo at* O_1. *Lower trace, echo at* O_2. *150 pulses/sec 50 c/s calibration pulses.*

(*a*) *Echo at* $O_1 \gg$ *echo at* O_2. *Echoes are from near end of trail and no diffraction fluctuations are observed at* S_1.

(*b*) *Echo at* $O_2 \gg$ *echo at* O_1. *Echoes are from near beginning of trail and well marked diffraction effects are visible at* O_2.

(*c*) *Example of irregular ionization between* S_1 *and* S_2, *producing diffraction fluctuations before the lower specular reflecting point.*

(*d*) *Example of "decay" echo with* $\alpha \lesssim 10^{12}\ cm^{-1}$ *at* S_1, *giving place to a "long duration" echo with* $\alpha > 10^{13}\ cm^{-1}$ *at* S_2 ($\Delta h \sim 2{\cdot}5\ km$).

(*a*)

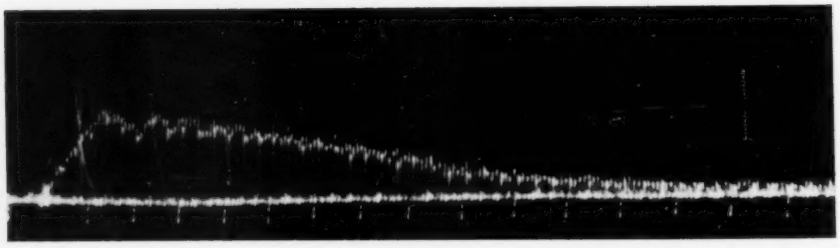

(*b*)

FIG. 7.—*Observed diffraction patterns produced by a meteor which rises to maximum electron density in a trail length* $\lesssim$800 *m* (*a*) *the echo at* O_1 *corresponds to the theoretical curve of Fig.* 6(*g*). (*b*) *the echo at* O_2. (*Reproduced by courtesy of Mr K. R. R. Bowden.*)

A radio link between O_1 and O_2 enables the signals from S_1 and S_2 to be displayed side by side at the same station. A switched pre-amplifier accepts alternate echo pulses from S_1 and S_2, and the signals pass through the same receiving and amplifying channels to a switched beam oscilloscope (Fig. 2). Alternate echo pulses from the Jodrell Bank and distant receiver thus appear at 150 c/s on the upper and lower traces respectively. The slow time base of 0·4 sec duration is triggered by the first pulse of predetermined amplitude to be received from either station. Ranges are recorded on a separate cathode ray tube. A full description of the recording system, without the beam switching, has been given previously (Greenhow, 1954).

(*c*) *Aerial system.*—An array of 4 Yagi aerials inclined at 45° to the horizontal is used for transmission, giving a beamwidth of $\pm 25°$ to the first zero of the main beam. Identical horizontally-polarized receiving aerials consisting of a single dipole and reflector are used at both stations. The transmitting beam looks eastward over the distant receiver. Thus when a meteor trail is in the process of formation the echo will appear first on the Jodrell Bank receiver, followed a short time later by the echo at the distant station. The first echo to appear is always from a point higher up the trail than the later echo (Fig 1).

(*d*) *Calibration.*—We are not directly concerned with the absolute sensitivities of the two receiving systems, as we only require to measure the relative values of α from the ratio of echo amplitudes at O_1 and O_2. A method which automatically takes account of all losses in the system is to compare echo rates at the two receivers. For equal sensitivities the rates at O_1 and O_2 should be equal, irrespective of trail length and whether echoes are coincident or not.

A second and more direct system of calibration is to observe pairs of echoes with zero time displacements. When this occurs the meteor trail is orientated in such a way that S_1 and S_2 coincide, and the ratio of echo amplitudes at O_1 and O_2 gives the precise ratio in sensitivities in the direction of the trail. The mean value of amplitude ratio for these echoes, after using the first method of correction, is $1{\cdot}01 \pm 0{\cdot}04$. Thus two separate methods of normalizing equipment sensitivities give results which agree closely.

(*e*) *Errors in amplitude ratio.*—Echo amplitude is proportional to $G_T^{1/2}G_R^{1/2}/R^{3/2}$ for given α and λ. Differences in G_T and R for echoes observed at the two stations are negligible, and errors due to differences in receiver polar diagrams are predominant. To reduce this effect to a minimum, identical broad-beam aerials are used for reception. As the transmitting aerial and timing measurements restrict echoes to the central parts of the dipole and reflector mainbeam where $G_R^{1/2}$ varies very slowly, we are chiefly concerned with differences in the vertical polar diagrams caused by the effects of ground reflections. At both receiving sites the ground in front of the aerial is level to within $\pm\lambda/8$ over the first Fresnel zone. As a further precaution measurements have been restricted to echoes between elevations of 25° and 50°, where the rate of change of gain with E is small for an aerial at a height of $\lambda/2$.

To test the vertical polar diagrams at the two stations the distributions of echoing points in elevation have been measured, and are illustrated in Fig. 3. The distributions are similar, showing that there are no appreciable systematic differences between the receiving systems. A point to point comparison of the polar diagrams is given by an inspection of echo pairs with zero time displacements (Section 2(*d*)). The amplitude ratios of individual echo pairs are found to vary

by only ±30 per cent from unity, this figure including the spread in results due to all sources of error.

A rate count shows that we may expect approximately one echo pair in every fifty to be a random coincidence of two entirely separate meteors. 97 per cent of these coincidences can be eliminated from range and timing measurements at the two stations, and echo pairs of this type have therefore been rejected.

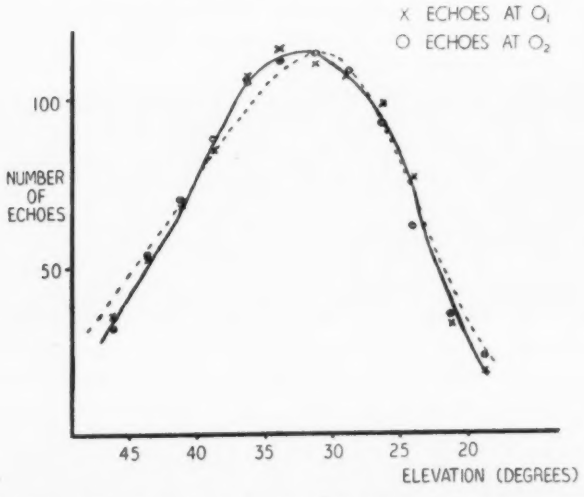

FIG. 3.—*Distribution of echoing points in elevation at the two receiving stations, showing similarity of vertical polar diagrams.*
– – – – *theoretical distribution.*

3. *Measurement of the mean ionization curve*

(*a*) *Coincidence rate.*—With a station separation of 20 km it might be expected that some echoes would appear only at one receiver, because of the finite trail length. Observation of the number of non-coincidences does not give any information about the shape of the ionization curve, as equal echo rates always result in equal numbers of non-coincident echoes at the two stations. Measurement of the coincidence rate does give some information on the lengths of meteor trails (Manning, Villard and Peterson, 1951), but these workers have not assigned a meaning to these lengths in terms of relative ionization densities.

(*b*) *Distribution of amplitude ratios.*—Information about the shape of the ionization curve is obtained from the ratios of echo amplitude at two spaced stations. For example, with the theoretical ionization curve of Fig. 4 (*a*) (Herlofson, 1948) and a maximum possible height separation of $0{\cdot}7H$, the echo amplitude from S_1 can never exceed twice the amplitude from S_2 (when S_1 and S_2 lie on the part of the curve before α_{max}). On the other hand it is possible for the echo from S_1 to be infinitely greater than that from S_2, if S_1 and S_2 lie below the point of maximum electron density. The shape of the ionization curve can therefore be tested by observation of the ratios in echo amplitudes at the two stations.

(i) *Selection of echoes.*—The smallest echoes recorded are those with amplitudes twice the receiver noise level, and the greatest number are observed with this

amplitude. In order to determine the shape of the ionization curve with reasonable accuracy, therefore, measurements are first restricted to those echoes greater than 10 times receiver noise ($10 \times n$) on one or other of the receivers, and then further restricted to 20 times noise echoes. The minimum detectable signal is assumed to be rather less than $4 \times n$, to allow for the possibility of the triggering mechanism failing to accept a small echo (although in practice the apparatus triggers reliably on $2 \times n$ signals). Measurements are restricted to short duration "decay" echoes, for which $\alpha \propto$ echo amplitude (Section 2 (*a*)). Thus ratios in line density can be measured up to 2·8/1 or 5·5/1 for the smallest echoes in the two groups. The ratio $r = A_1/A_2$ is determined for each pair of echoes, where A_1 and A_2 are the echo amplitudes observed from the upper and lower reflecting points respectively. When echoes occur at only one station, the ratio can only be specified within certain limits depending upon the echo amplitude. This value is always $>5{\cdot}5$ or $<0{\cdot}18$ for the second group, and $>2{\cdot}8$ or $<0{\cdot}36$ for the first group of echoes.

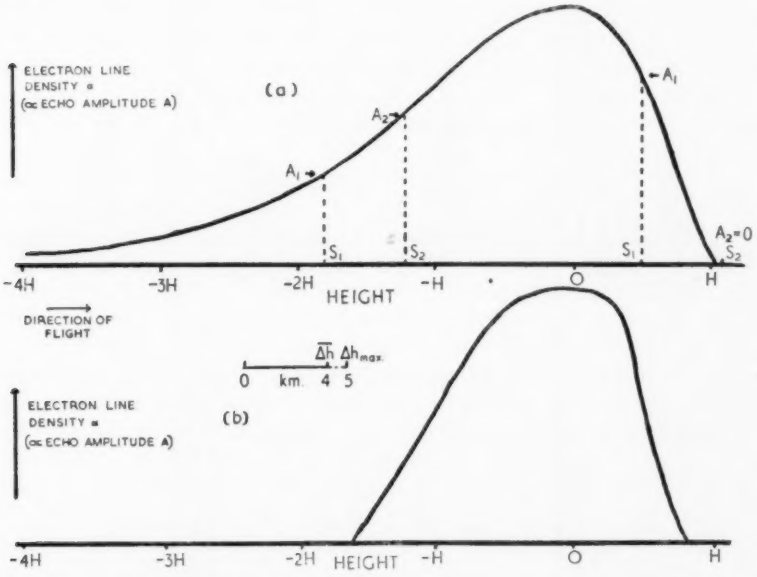

FIG. 4.—(*a*) *Theoretical ionization curve*

$$\frac{\alpha}{\alpha_{\max}} = \frac{9}{4}\frac{p}{p_{\max}}\left(1 - \frac{1}{3}\frac{p}{p_{\max}}\right)^2 \quad \textit{(Herlofson, 1948).}$$

Abscissa expressed in terms of scale height H, where $p/p_{\max} = exp\,[-(h-h_{\max})/H]$. *p and h are atmospheric pressure and height.* $p_{\max}$ *and* $h_{\max}$ *refer to point of maximum ionization.*

(*b*) *Proposed ionization curve for faint meteors.*

In order to simplify the interpretation of the results, it is desirable to consider echo pairs with a fixed separation in height, rather than the full range of Δh from 0 to 5 km. The mean height separation of all echoes with $2 > r > 0{\cdot}5$ is found to be 3·1 km, while for echoes with ratios $4 > r > 2$ and $0{\cdot}5 > r > 0{\cdot}25$ it is 4·1 km. In order to maintain a constant value of Δh for all ratios, therefore, echo pairs with close spacings have been rejected. The median value of Δh for near unity values of r then rises to 4·0 km. Thus we may assume a value $\overline{\Delta h} \sim 0{\cdot}6^{+0{\cdot}07}_{-0{\cdot}15} H$.

The deviations include 75 per cent of the echoes. Although the separation of specular reflecting points for meteors observed at only one station cannot be determined, the small number of echo pairs of sufficient amplitude to enable very high ratios to be measured also show separations of approximately 4 km. Thus we may determine the ratio of electron line densities between pairs of points separated in height by approximately 4 km at various points along the ionization curve.

(ii) *Experimental results.*—Distributions of the amplitude ratio r for the two groups of echoes are given in Fig. 5 (*a*) and (*b*). The histograms are markedly

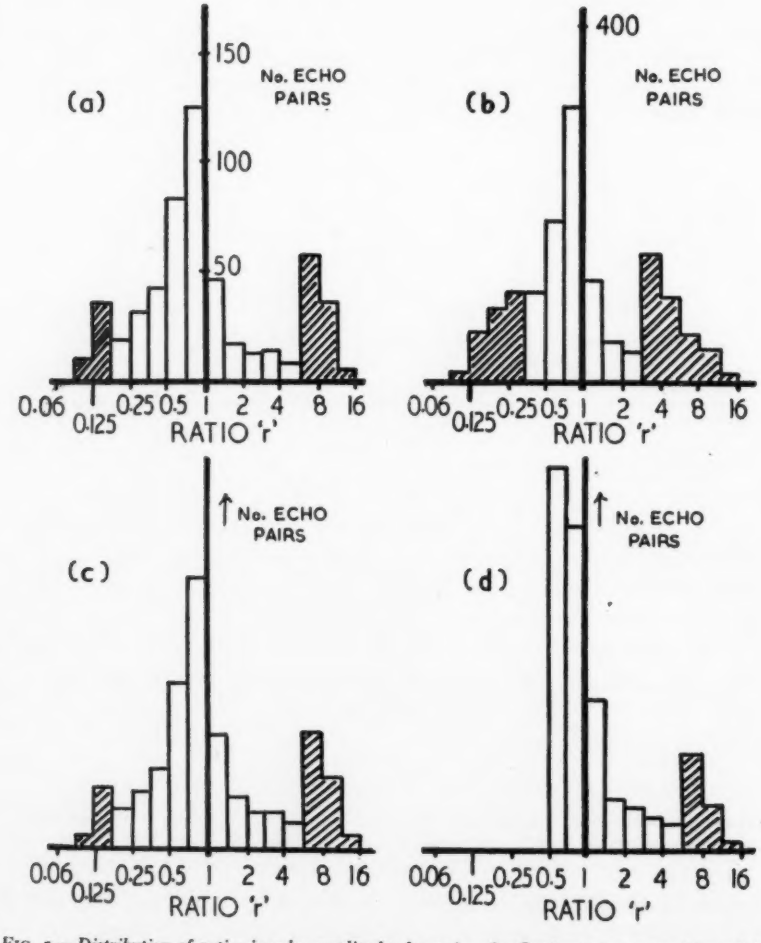

FIG. 5.—*Distribution of ratios in echo amplitudes for pairs of reflecting points spaced by a height difference of 4 km.*

(*a*) *Observed distribution (echoes* $> 5{\cdot}6 \times$ *minimum detectable level).*
(*b*) *Observed distribution (echoes* $> 2{\cdot}8 \times$ *minimum detectable level).*
(*c*) *Theoretical distribution for ionization curve of Fig.* 4 (*b*).
(*d*) *Theoretical distribution for ionization curve of Fig.* 4 (*a*).

asymmetrical as expected, but an unexpected feature is the large number of echo pairs in which the signal from S_2 is greater than 4 or 5 times that from S_1. Ratios as low as 0·1 are observed, indicating increases in electron line density by a factor of 10 over $\Delta h \sim 4$ km, on the part of the ionization curve before α_{max}. On this part of the theoretical curve the amplitude increases with decreasing height in the manner $\exp(h/H)$, and the maximum possible increase in A for $\Delta h \sim 4$ km is only a factor of 1·8. It appears, therefore, that the rate of increase of ionization is much greater than expected, values up to five times the theoretical rate being observed.

On the other hand, the large number of examples in which the echo from S_1 considerably exceeds that from S_2 is in agreement with theory. Thus, casual inspection of observed ratio distributions suggests that ionized meteor trails are shorter than has previously been assumed. In the following paragraph an attempt is made to deduce qualitatively the shape of the observed ionization curve, using the measured amplitude ratios of Fig. 5.

(*c*) *Theoretical ratio distributions.*—The theoretical distribution of amplitude ratios for a meteor trail of given α_{max}, observed in a part of the polar diagram of sensitivity $S = G_T^{1/2} G_R^{1/2} / R^{3/2}$, is simply obtained by sliding a pair of points spaced by 0·6 H along the horizontal axis in Fig. 4(*a*). The histogram showing the frequency of occurrence of different values of A_1/A_2 is plotted and the process is stopped when A_1 and A_2 fall below an arbitrary minimum detectable level. The complete distribution is then obtained by superimposing a large number of such histograms for all values of S and α_{max}, weighting each curve in relation to the collecting area of given sensitivity and the distribution of meteor masses. Sporadic meteors have been used in the present experiments, and the well-established inverse square law distribution of masses is assumed (Kaiser, 1953). The variation of $G_T^{1/2} G_R^{1/2} / R^{3/2}$ is considered by constructing sensitivity contours in the 95 km plane above the earth in the manner discussed by Clegg (1948). In practice S and α_{max} were varied in eight steps of 1·4, 98 per cent of all echoes being included in this sensitivity range of 64 to 1. A random distribution of radiants is assumed. The theoretical ratio distribution is illustrated in Fig. 5(*d*), and this may be compared with the experimental observations. The theoretical distribution is asymmetrical, with quite a high probability of the echo lower down the trail being greater than 5·5 times the upper echo. On the other hand, when the echoing points are above α_{max}, there should only be 50 echoes with $r < 0{\cdot}36$ in Fig. 5(*b*) (after allowing for experimental errors), whereas 273 are observed; and 20 with $r < 0{\cdot}36$ in Fig. 5(*a*), whereas 100 are observed. If the observations are restricted to even larger ratios in Fig. 5(*a*), there should be no echo pairs in which the echo from S_2 exceeds that from S_1 by more than 5·5 to 1, yet this occurs in approximately 10 per cent of the observations.

(*d*) *The mean ionization curve.*—An attempt has been made to fit an ionization curve to the observed ratio distributions, and the resultant curve is shown in Fig. 4(*b*). When the procedure of Section 3(*c*) is repeated using this curve, the theoretical distribution shown in Fig. 5(*c*) is obtained. This is in reasonable agreement with the observations, giving low values of r before α_{max}. This proposed ionization curve is much shorter than the curve of Fig. 4(*a*), the difference mainly arising in the absence of a long exponential rise before the point of maximum ionization. The differences are not so great near α_{max}. It must be emphasized that the curve shown in Fig. 4(*b*) is not necessarily a unique

solution, but it represents the average behaviour of meteors observed with the present equipment.

4. *Additional evidence for anomalous ionization curves.*—So far we have considered only trails with $\alpha \lesssim 10^{12}$ cm^{-1}, using echo amplitude as a measure of electron line density. However, when $\alpha \gtrsim 10^{12}$ cm^{-1}, the electron line density can be determined approximately from the echo duration independently of the equipment parameters (Section 2(*a*)). Thus in Fig. 2(*d*) the echo at the home station is of the short duration "decay" type, and without specifying the precise value of α we can say that it must be less than 10^{12} cm^{-1}. From the rate of decay we deduce that the appropriate value of D is 3×10^5 cm^2 sec^{-1}. At a point whose height is only 2·5 km lower the electron line density has increased to such an extent that a "long duration" echo has developed, with $T > 0{\cdot}3$ sec. Substituting a value of D allowing for the 2·5 km height difference, we find that $\alpha > 10^{13}$ cm^{-1}. Thus the electron line density has increased by more than a factor of 10 in a height difference of 2·5 km. Echo pairs of this type are frequently observed, although they have not been used in the present analysis as they do not satisfy the restrictions placed on echo characteristics. However, they serve to show that very rapid increases in α do occur before α_{max}, without reference to the aerial polar diagrams and other variables.

TABLE I

Number of diffraction maxima observed in meteor echoes at two spaced stations ($V \lesssim 25$ km sec^{-1}). In (a) and (b) the average reflection point is the same for O_1 and O_2, and is approximately at α_{max}. In (d) the average reflecting point is approximately 4 km further along the trail than in (c).

	Number of diffraction maxima	1 max	2 max	3, 4 max	⩾5 max
(*a*)	All echoes at O_1	per cent 52	per cent 21	per cent 18	per cent 9
(*b*)	All echoes at O_2	55	16	19	10
(*c*)	Echoes at O_1 Coincidences with $Vt > 4$ km	35	19	31	15
(*d*)	Echoes at O_2. Coincidences with $Vt > 4$ km	73	13	13	1

5. *Fragmentation.*—Very frequently an echo is observed from the upper reflecting point showing pronounced diffraction fluctuations during trail formation, yet these fluctuations may be much smaller or entirely absent in the echo from the point a few km further down the trail. In Table I the percentage of echoes showing well-marked diffraction patterns are given for all echoes on the two stations, whether coincident or not (*a* and *b*). Only meteors with $V \lesssim 25$ km sec^{-1} are used (estimated from the rate of rise of amplitude), as greater velocity results in a smoothing out of the fluctuations because of the low pulse recurrence rate. At both stations approximately 28 per cent of all echoes show at least three diffraction maxima while 53 per cent show only one. However, if we consider only coincidences with $Vt > 4$ km, the situation is very different. The percentage

of echoes with three or more zones is increased to 46 per cent from the upper reflection point, and reduced to only 14 per cent 4 km further along the trail. Similarly the percentage showing no zone formation is reduced to 35 per cent at O_1, but increased to 73 per cent at O_2.

Table II shows that faster meteors are less affected, as a higher percentage of echoes give good diffraction patterns. These results were obtained using earlier single station observations at a high pulse recurrence rate.

This smoothing of the diffraction pattern can be explained by the progressive fragmentation of meteors proposed by Jacchia (1955) from observations of faint photographic meteors. Thus each fragment will produce its own diffraction pattern, and when the separation of fragments along the trail becomes comparable with a Fresnel zone length the fluctuations will be smoothed out. Differential velocities of the order of 1 km sec^{-1} are required to smooth out all but the first maxima in a path length of 1 km. The first Fresnel zone is comparatively large ($\sim$1 km), and as this is primarily responsible for the main "body" echo the first diffraction maximum will not be seriously affected.

TABLE II

Number of diffraction maxima observed in meteor echoes as a function of meteor velocity.

Number of diffraction maxima	1 max	2 max	3, 4 max	$\geqslant$5 max
$>$60 km sec^{-1}	per cent 22	per cent 23	per cent 29	per cent 27
40–60 km sec^{-1}	28	23	24	25
25–40 km sec^{-1}	44	20	22	14
$<$25 km sec^{-1}	53	19	19	9

6. *Irregular ionization.*—The effect of irregular ionization along a meteor trail is to distort the simple diffraction patterns illustrated in Fig. 6 (*a*), (*b*) and (*c*). The distortion is most noticeable if the irregularity occurs before the centre of the first Fresnel zone, and as an example the result of increasing the electron line density in the 9th zone before S_0 by 50 per cent is shown in Fig. 6 (*d*). Deep diffraction fluctuations are now observed before the meteor reaches the foot of the normal to the trail. These are analogous to the Doppler whistles observed with C.W. techniques as the meteor approaches the observer, although in the present case the meteor trail produces its own reference phase. Because of the small amplitude of these fluctuations they are normally observed only in trails giving very large body echoes, which saturate the receiver. As a selection criterion echoes which rise to saturation as the meteor crosses the first Fresnel zone have been investigated. Of these 51 per cent show deep fluctuations before the specular reflecting point, a further 29 per cent fluctuate slightly, and only 20 per cent show the smooth rise in amplitude expected for a uniformly ionized trail.

An example of this type of echo where the irregularity actually occurred between the normals to the trail from the two observing stations is given in

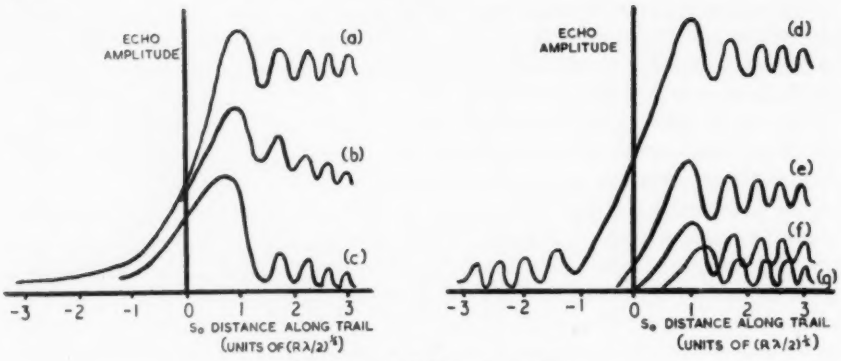

FIG. 6.—*Theoretical diffraction patterns.*

(*a*) *For infinitely long uniformly ionized trail, with zero rate of diffusion.*

(*b*), (*c*) *As in* (*a*) *showing effects of increasing the rates of diffusion* (*Kaiser*, 1953).

(*d*) *Effect of increasing the electron line density in the* 9*th zone before* S_0 *by* 50 *per cent, for trail of* (*a*). (S_0 *is the specular reflecting point.*)

(*e*), (*f*), (*g*) *Effect of sudden commencement of ionization* (*linear rise from zero to maximum electron density in a length* $(R\lambda/2)^{1/2}$). (*e*) *Trail begins* $0{\cdot}4(R\lambda/2)^{1/2}$ *before* S_0, (*f*) *trail begins at* S_0, (*g*) *trail begins* $0{\cdot}4(R\lambda/2)^{1/2}$ *after* S_0.

Fig. 2(*c*). The echo at O_1 rises smoothly as the meteor approaches S_{01}, but at O_2 large diffraction fluctuations are observed before S_{02} is reached.

Occasionally an echo appears only as a small diffracted signal at O_1, whereas at O_2 a normal body echo is obtained (Fig. 7); this effect can only be explained if the first Fresnel zone at S_1 is absent, and the meteor begins to ionize almost instantaneously between S_1 and S_2 with a rise to maximum electron density in a distance $\lesssim(R\lambda/2)^{1/2}$ (800 m). Theoretical examples of the diffraction patterns for trails with abrupt commencements are given in Fig. 6(*e*), (*f*) and (*g*).

A consideration of echo amplitudes and trail length shows that if all trails are of this type 3 per cent of the echo pairs should be of the form illustrated in Fig. 7. Thus we might expect 50 examples of this effect out of a total of 1700 suitable echoes, whereas only 8 were observed. This suggests that between 10 and 22 per cent of all meteor trails reach their maximum ionization almost instantaneously, with an even greater rate of rise than indicated by the ionization curve of Fig. 4(*b*).

7. *Discussion.*—An investigation of echo amplitudes at two spaced stations has shown that the ionization curves of faint +6 to +8 magnitude meteors are much shorter than predicted by theory. In particular the rise to maximum electron line density is more rapid than expected. It must be emphasized however that only a mean ionization curve has been derived, and large variations may exist between individual meteors. For example the experimental observations could be explained by a mixture of long and short trails. Direct evidence that the linear electron density may increase even more rapidly than suggested by the mean curve is given by the transition from short to long duration echoes from points separated by only a few km. Almost instantaneous increases in α from zero to maximum in a trail length less than 800 m have been inferred for a small percentage of meteor trails. Evidence for the fragmentation of meteors and irregular production of ionization has also been presented.

These results may be compared with the photographic observations of faint +3 m meteors (Jacchia, 1949, 1955). In general the light curves are shorter than expected and breaks in the photographic trail produced by the rotating shutter become filled in, leading Jacchia to suggest that the meteors are in the process of fragmentation. In addition a small number of these meteors are observed to reach maximum light almost instantaneously, and others show irregularities in their light curves. Thus the various anomalies observed in the light curves of faint visual meteors, appear to have their analogues in the ionization curves of faint radar meteors.

8. *Acknowledgments.*—The work described in this paper has been carried out at the Jodrell Bank Experimental Station, University of Manchester. The authors wish to thank Professor A. C. B. Lovell, Director of the Station, for his interest in the investigation. They also wish to thank their colleague Dr H. P. Palmer for his cooperation at the distant station.

Jodrell Bank Experimental Station,
University of Manchester:
1957 *March* 28.

References

Clegg, J. A., 1948, *Phil. Mag.*, **39,** 577.
Davies, J. G. and Ellyett, C. D., 1949, *Phil. Mag.*, **40,** 614.
Evans, S., 1954, *M. N.*, **114,** 63.
Greenhow, J. S., 1952, *Proc. Phys. Soc.* B, **65,** 169.
Greenhow, J. S., 1954, *Phil. Mag.*, **45,** 471.
Herlofson, N., 1948, *Phys. Soc. Rep. Prog. Phys.*, **II,** 444.
Hoppe, J., 1937, *Astronom. Nach.*, **262,** 169.
Jacchia, L. G., 1949, Harv. Coll. Obs. & M.I.T. Cent. of Anal. Tech. Rep., No. 3.
Jacchia, L. G., 1955, *Ap. J.*, **121,** 521.
Kaiser, T. R., 1953, *Phil. Mag. Supp.*, **2,** 495.
Kaiser, T. R., 1954, *M.N.*, **114,** 39.
Lovell, A. C. B. and Clegg, J. A., 1948, *Proc. Phys. Soc.*, **60,** 491.
Manning, L. A., Villard, O. G. and Peterson, A. M., 1951, Stanford Tech. Rep., No. 40.
Öpik, E., 1933, Acta. Univ. Tartu. A., 26.
Sparrow, C. M., 1926, *Ap.J.*, **63,** 90.
Whipple, F. L., 1943, *Rev. Mod. Phys.*, **15,** 246.

THE DISTRIBUTION OF THE DIRECTIONS OF PERIHELIA OF LONG-PERIOD COMETS

J. G. Tyror

(Communicated by R. A. Lyttleton)

(Received 1956 October 31)

Summary

The distribution of the directions of perihelia of 448 long-period comets is investigated. Standard statistical tests strongly suggest a departure from randomness in the distribution. It further appears that there is some evidence that the perihelion points exhibit a preference for lying near the galactic plane. It is indicated how the accretion theory of the origin of comets can account for the form of the distribution.

---

1. *Introduction.*—The problem of the origin of comets has engaged the attention of numerous workers over a long period of time. Although much has been discovered about the behaviour of comets, there still remains no generally accepted hypothesis of their origin, each hypothesis presented having some not entirely satisfactory features.

Among recent hypotheses, Lyttleton (**1**) envisages a process of accretion of dust particles by the Sun in the course of passage through interstellar dust clouds. It is shown that this may result in condensations of interstellar matter falling in towards the centre of mass of the solar system along a general direction which must be that of the local relative motion of cloud and solar system. These condensations are identified as comets, many thousands of which may, under suitable conditions, be formed on the passage of the Sun through a single cloud. The hypothesis explains many of the observed features of the behaviour of comets and of the properties of their orbits.

One fact, however, emerges which is peculiar to this type of theory, namely that the comets must have originally come from preferred positions in the sky. The comets formed in any one passage through an interstellar cloud would be expected to have their perihelion points grouped together on the celestial sphere (if allowances for planetary perturbations could be made), which feature could only be seriously departed from if there was some change in the direction of relative motion of cloud and Sun during the passage. The effect of perturbations during the first and succeeding perihelion passages would probably result in the diffusion of the perihelion points of such a family, and also possibly in the loss of many members (by expulsion, break-up, or direct infall to the Sun). However, it may still be possible, at least for families born during recent cloud passages, to detect some traces of perihelion grouping.

The object of the present paper is to examine the distribution of perihelion points of long-period comets to determine whether or not evidence of any such grouping is present. Previous work on this subject was carried out by Pickering (**2**) in 1911 (with comments by Eddington (**3**) and Oppenheim (**4**) in 1924). These writers, who preferred to consider the distribution of aphelion points,

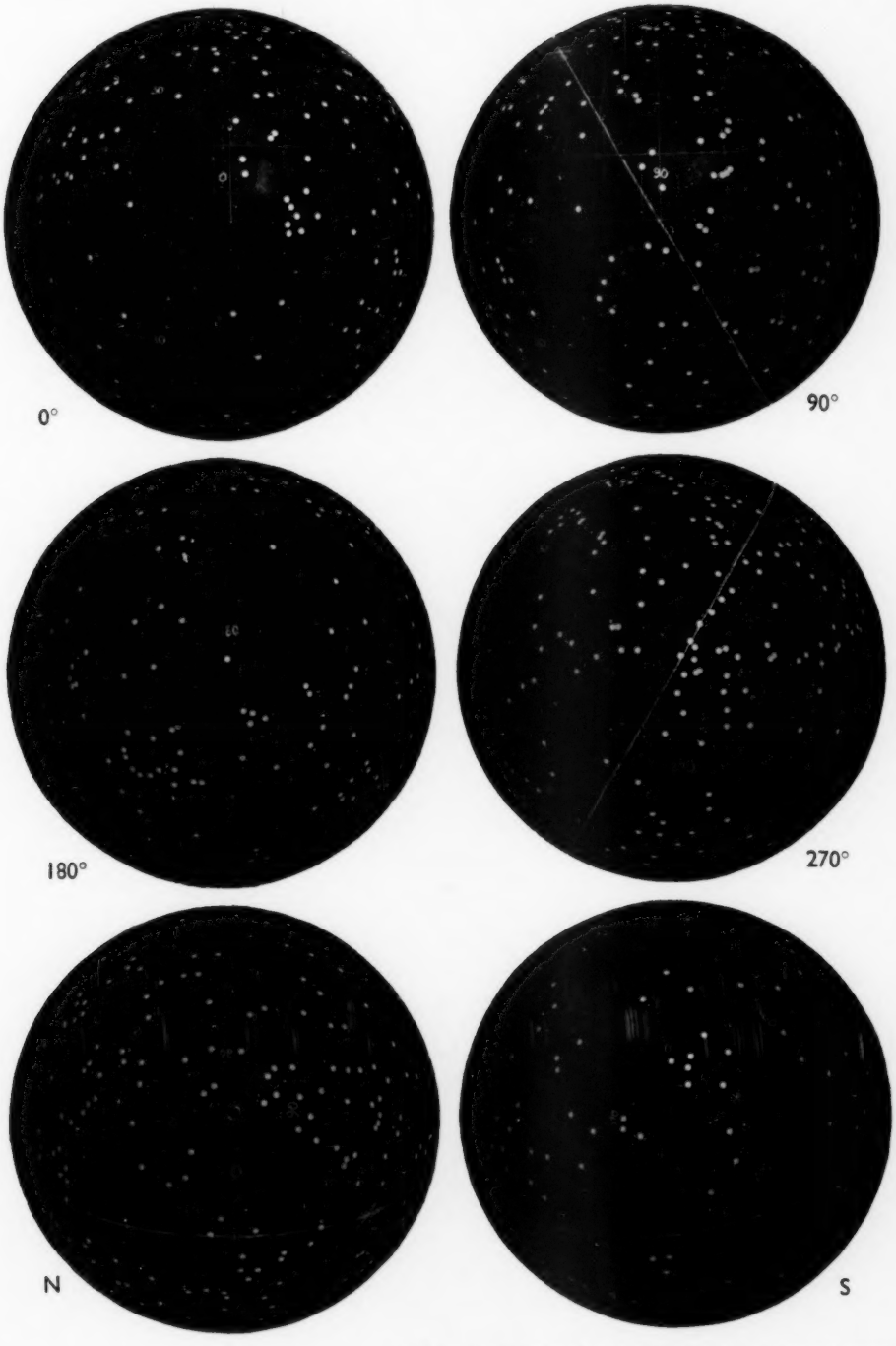

J. G. Tyror, The distribution of the directions of perihelia of long-period comets.

claim to have found some evidence of the grouping of the points, but it has been thought advisable to revise their results in the light of the additional data on cometary orbits made available since their work was completed. Of the number of orbits included in the present investigation, 26 per cent refer to comets discovered since Pickering's work was completed.

Short period and periodic comets are excluded from this survey on the grounds that the large planetary perturbations that must have been experienced by them to bring them to their present orbits may be expected to have eradicated most if not all reliable evidence of any original grouping. In actual fact such perturbations must have affected all orbits to a greater or lesser extent. Hence some effort will be made to isolate and investigate comets that may have suffered only relatively slight perturbations since these will then be expected to give a better indication of the original distributions of cometary orbits.

The data on comet orbits have been taken in the first place from Baldet's tables (**5**) and, for more recent orbits, from the annual list given in *Monthly Notices* of the Royal Astronomical Society. Much of this has been summarized by Porter (**6**).

The available data almost certainly suffer from observational selection, and so care must be exercised in attempting to draw conclusions concerning the general distribution of comets. The nature of the available data has in its turn dictated the methods employed in the analysis. These have been essentially simple for it was not thought worthwhile to attempt delicate techniques on a possibly suspect sample.

2. *Distribution of perihelion points.*—Plate 7 contains a plot (in ecliptic coordinates) of the positions on the celestial sphere of the points of perihelion of 448 comets with periods greater than 200 years up to and including comet 1952 f. Of these

67 have a calculated eccentricity $e > 1$,

263 have an assigned eccentricity $e = 1$,

118 have a calculated eccentricity $e < 1$.

On direct examination several fairly large regions on the sphere are seen to be particularly noticeable for the absence of points, e.g. the so-called Hoek's zone (**7**) centred roughly on $(350°, -30°)$, and the zone centred on $(310°, 55°)$. On the other hand it also appears possible to distinguish definite compact groups of points. This grouping becomes more apparent in Table I (*a*), for the construction of which the surface of the sphere is divided into 432 approximately equal areas and the number of points per area given. Taking these basic units of area in groups of six, the observed frequency of points per area has been compared with that expected on a Poisson distribution. This indicates a preponderance of regions with many points and with few points—a feature typical of the existence of groups. The value of χ^2 associated with the observed distribution corresponds to a probability of less than 0·001. Although differing values of the probability may be expected from different arbitrary subdivisions of the celestial sphere, this figure may be taken as an order of magnitude estimate, and is indicative of a real departure from randomness.

In order to investigate further the distribution given in Table I, a simple sensitive test given by Sterne (**8**) may be used. Essentially this gives information concerning the size of the regions in which occurs the departure from randomness

(*a*) TABLE I.—*Distribution of the perihelion points of* 448 *long-period comets in* (*a*) *ecliptic coordinates,* (*b*) *galactic coordinates.*

β°	180	270	0	90	180
90		2 2 1 1 2 2 1 3 3 2 2 2			
57	1	3 1 2 2 1 3 2 2 3 1 1 1 1 1 1 2 4 4 2 2 1 4 2 2 1 2 1 1			
42		2 1 4 4 1 1 2 4 1 3 3 1 1 2 1 1 1 2 1 2 1 2 1 1 2			
30		1 1 1 2 2 3 4 4 1 1 1 1 1 2 1 3 4 1 2 1 2 2 1 1 1			
20		1 2 1 4 3 2 1 1 2 1 4 3 2 1 1 2 1 2 1 1 1 1 2 1 5 2 1 1 1 1			
10		1 1 1 2 3 1 7 2 3 4 4 1 1 1 3 1 1 2 1 2 1 3 1 2 1 1			
0	1	2 2 1 1 2 1 1 5 3 1 1 4 1 1 1 1 1 1 3 1 1 2 2 1			
10	3	2 1 1 1 1 2 1 1 2 1 1 1 2 1 2 2 2 1 3 3			
20	1	1 1 3 3 1 2 1 1 1 1 2 1 1 1 1 2 1 1 4 3 2			
30		1 2 2 1 2 1 1 2 1 1 1			
42	1	2 1 2 2 1 3 2 2 2 1 1 1 1 1 1			
57		2 2 1 1 1 1 1 1 1 1 1			
90					

(*b*)

b°					
90		2 2 1 1 1 3 1 1 1 1 1			
57	2	1 1 3 1 2 3 2 1 1 1 2 2 3 1 1 1 1 2 1 3 1 1 1 1 1			
42	2	2 4 5 4 1 1 1 2 2 1 1 1 1 5 2 2 2 4 1 4 2 3 1 1 1 1 1			
30	2	3 1 1 2 3 2 3 1 3 1 1 5 1 3 3 1 2 1 2 1 3 2 2 1			
20		2 2 1 1 2 2 1 2 3 1 2 1 1 3 1 3 1 4 3 2 1 1 4 1 2			
10	2	1 1 3 1 1 1 4 4 3 2 1 4 1 1 1 2 1 1 4 2 1 3			
0		1 1 2 3 9 3 2 4 1 1 2 2 2 3 2 2			
10	1	1 1 1 1 1 1 1 2 2 2 1 1 4 1 3 1 2 2 3 2 2 2 4 2 3 3 1 1 2 2			
20		1 2 1 1 1 1 1 1 1 1 3 2 1 4 1 1 1 2 1 1 2 1			
30		1 1 3 2 1 1 2 4 1 3 1 3 1 1 2 1 3 1			
42	1	1 1 1 2 1 2 1 1 2 1 7 2 1 1 1 2 1 1			
57		1 1 1 1 1 1 1 1 1 1 1 1 1 1 1 1 1 1 1			
90					

previously noted. If these are larger than the subdivisions used, a tendency for unit areas containing small numbers of points to lie close together may be expected, and similarly for areas containing large numbers; i.e. there will exist a positive correlation between the numbers of perihelion points in a unit area and the numbers in other areas close by. The probability of a numerical configuration occurring through random causes can therefore be estimated from a correlation diagram such as that given in Fig. 1. Here the number (x) of points

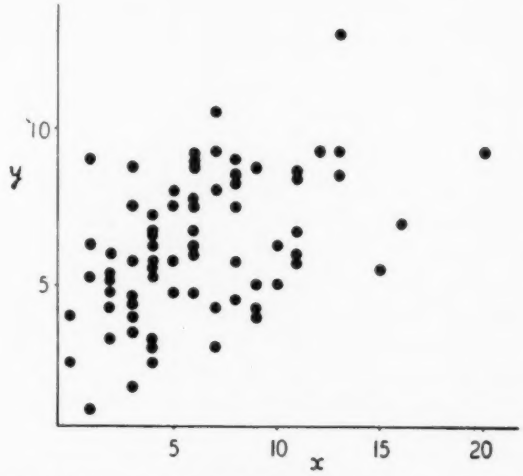

FIG. 1.—*Correlation between number of perihelion points per unit area* (x) *and average number of points in adjacent areas* (y).

per area is plotted against the average number (y) in the four immediately adjacent areas. Thus 72 points appear in the correlation diagram. The probabilities obtained again varied with the choice of sub-division and were $O(10^{-20})$. This value is very low and in spite of the uncertainty involved in using the number of points in a given area in two ways a real departure from randomness is strongly suggested. It may thus be concluded that grouping must exist in regions larger than the unit areas considered.

3. *Plane of preference of perihelion points.*—Coordinates may be assigned to the perihelion points by adopting a right-handed cartesian system with origin at the Sun. The coordinate axes are chosen so that the x-axis and the y-axis lie in the plane of the ecliptic ($\beta=0$) with the x-axis along $\lambda=0$ and the y-axis along $\lambda=\pi/2$, with the z-axis completing the system.

The sample moments of the 1st and 2nd orders are then found to be

$$\bar{x}=-0{\cdot}0069; \quad \bar{y}=-0{\cdot}0446; \quad \bar{z}=+0{\cdot}1316;$$
$$a=\overline{x^2}=+0{\cdot}2993; \quad b=\overline{y^2}=+0{\cdot}3931; \quad c=\overline{z^2}=+0{\cdot}3076;$$
$$f=\overline{yz}=-0{\cdot}00916; \quad g=\overline{xz}=+0{\cdot}02741; \quad h=\overline{xy}=-0{\cdot}00997.$$

From a visual inspection of Plate 7 it appears possible to identify on the celestial sphere a great circle of apparent maximum density of points. This suggests a form for the non-randomness of the distribution noted in the previous section.

Let the direction cosines of the normal to the preferred great circle be (l, m, n). Then

$$\overline{D^2} = \frac{1}{448} \sum_i (lx_i + my_i + nz_i)^2$$

must be a minimum subject to the restriction $l^2 + m^2 + n^2 = 1$ where summation is over all the perihelion points. Thus

$$\left.\begin{aligned} (M - \lambda I) \begin{bmatrix} l \\ m \\ n \end{bmatrix} &= 0 \\ l^2 + m^2 + n^2 &= 1 \end{aligned}\right\}, \tag{1}$$

where

$$M = \begin{bmatrix} a & h & g \\ h & b & f \\ g & f & c \end{bmatrix}.$$

The smallest eigenvalue $\lambda = \lambda_1$ gives the preferred great circle.

The significance or degree of definition of the preferred great circle may be assessed by calculating the value of $\overline{D^2}$ and comparing this with the value of $\overline{D^2} = \frac{1}{3}$ which is obtained from a random distribution of points. Assuming a normal distribution of $\overline{D^2}$ about its mean value of $\frac{1}{3}$, the value of $(\frac{1}{3} - \overline{D^2})$ may be compared with the standard deviation of the distribution about the mean (see Table II). In the case considered here $(\frac{1}{3} - \overline{D^2})$ is found to have a value of more than four times the standard deviation, and the preferred great circle is thus reasonably well defined.

TABLE II

Mean square distance of perihelion points from preferred plane and galactic latitude of normal to the preferred plane

	$\overline{D^2}$	$\frac{1}{3} - \overline{D^2}$	Standard Deviation	g	$l - \cos g$
All comets	0·276	0·057	0·014	78°	0·022
Group corrected comets	0·269	0·063	0·016	67°	0·080
P class	0·226	0·107	0·036	84°·5	0·004
M class	0·262	0·071	0·026	81°·5	0·012

On substituting $\lambda = \lambda_1$ equations (1) solve to give

$$l = +0{\cdot}7674, \qquad m = +0{\cdot}0151, \qquad n = -0{\cdot}6410.$$

This direction may be compared with that of the galactic pole given by

$$L = +0{\cdot}8772, \qquad M = -0{\cdot}0536, \qquad N = -0{\cdot}4772.$$

The angle between these two directions is given by the galactic co-latitude $(\pi/2 - g) = 12°$. If the relation between the direction of the galactic pole and the normal to the preferred great circle were random, the probability of the two lying at an angular distance less than $(\pi/2 - g)$ apart would be $1 - \cos g$. In the case considered here the probability is seen to be $\sim 0{\cdot}02$. The low value of the probability certainly suggests the presence of a galactic influence in the distribution of perihelion points. Consequently the distribution has been obtained in terms of galactic coordinates and is presented in Table I(*b*). The decrease in density of points to the galactic pole is immediately apparent.

The centre of the perihelion points is found to lie in a direction given by

$$\lambda = 261^\circ, \qquad \beta = 71^\circ$$

which it is noted is only some 20° removed from the apex of the Sun's motion at

$$\lambda_s = 271^\circ, \qquad \beta_s = 53^\circ.$$

The significance of the similarity of the two directions depends on the significance of the displacement of the centre of the distribution from the centre of the sphere. The significance of the displacement can be determined by considering each of the first order moments of the distribution as independent with a standard deviation of $\sqrt{(1/3n)}$ and applying a χ^2-test with three degrees of freedom. In the case considered the displacement of the centre of the distribution is found to be significant at the 1 per cent level.

The two effects identified here—a preferred plane and a displaced centre for the distribution—will not, in general, be independent of each other. It may, however, certainly be concluded that they are not different aspects of the same phenomenon. For, by itself, a displaced centre, i.e. the preference of perihelion points to be distributed about a particular point on the celestial sphere, will define an infinite number of equally significant preferred planes, all passing through this particular point. Further, the poles of such planes would be 90° removed from the displaced centre. The actual value found is 49°.

It does not seem possible to correct accurately the preferred plane for the displaced centre. Generally, however, it may be expected that the result of such a correction would be to move the nearer preferred pole towards the position of the displaced centre, i.e. away from the galactic pole.

4. *Observational selection.*—The previous two sections show that there is some evidence that the perihelion points of long-period comets tend to be distributed non-randomly. This tendency may be due either to observational selection, to a real grouping phenomenon, or a combination of both. That observational selection must play a large part in the discovery of comets has long been realized. For example Holetschek (**9**) has shown that a comet stands the best chance of being discovered if its perihelion occurs in opposition and has a perihelion distance q lying in the range $0{\cdot}3 < q < 1{\cdot}2$ a.u. Some writers (**10**), too, have defined "zones of avoidance" having the shape of right circular cones with apex at the Earth and axis the line Earth–Sun and within which, for small semi-angle of cone, discovery of even bright comets is highly improbable. Again a comet is most likely to be discovered at or near perihelion when, generally speaking, it is likely to be close to the Earth, and at its greatest intrinsic brightness.

The last point could well explain the fact that, of the 448 comets considered, 259 have their perihelion points in the Northern Hemisphere where there are, or have been, a preponderance of observing stations. On the other hand this distribution of points between the two hemispheres may be an indication of a real preference for points to lie in the northern half of the sphere. In this case the work and conclusions of Sections 2 and 3 continue to hold good. If, however, observational selection is regarded as explaining any part of the discrepancy in numbers between points in the Northern and Southern Hemispheres then some account must be taken of it.

The effect of this particularly simple form of selection, if it exists, can be surmounted by considering the observed distribution in zones of equatorial

latitude, since the random theoretical distribution can be assumed symmetrical about the polar axis. The distribution in the zones is found to be significantly non-random, and thus it can be claimed that the form of observational selection considered here cannot account for the previously noted departure from randomness of the distribution of perihelion points on the celestial sphere. In zones of equal galactic latitude the departure from randomness is far less marked, again indicating the presence of some galactic preference.

The selection between the two hemispheres may be expected to affect the position of the preferred plane found in the previous section. Suitable corrections are found to move the preferred plane nearer to the galactic plane and also to shift the centre of the distribution closer to the Sun's apex of motion.

Allowances for other types of observational selection are more difficult to make but an attempt has been made by Bourgeoise and Cox (**10**) to consider correlations that may be contained in any cometary list. They conclude that certain statistical features of cometary orbits, such as the general distribution of numbers with q and of the observed mean value $\bar{q}$ with i, are well explained on the basis of observational selection. In particular an ellipsoid of dispersion is obtained for the spatial distribution of perihelion points. The least axis of this ellipsoid is found to lie within 5° of the galactic pole. Earlier work by Oppenheim (**4**) is also corrected with similar results. It thus appears that even when observational selection is taken into account there still remains evidence of the non-random distribution of perihelion points.

5. *Groups of comets.*—Local condensations of points can be observed in many regions of Plate 7, those at (275°, 0), (160°, −25°), (220°, −30°), and (15°, 0) being especially noticeable. On closer examination it appears that in many cases the comets corresponding to adjacent points also exhibit a close similarity in their other orbital elements (with the exception of time phase), a fact first noted some 90 years ago by Hoek (**7, 11**) and later studied in detail by Pickering (**2**). The members of a group are thus comets that not only have come from the same part of the sky, but also in doing so have followed very similar orbits. In this way it is possible to discover 74 such comet groups containing in all some 174 comets, although there is no absolutely clear-cut criterion for deciding whether or not particular comets form a group. The members of a group are usually considered to be the component parts of a larger parent comet and hence it is clearly necessary to consider whether the non-randomness in the distribution of perihelion points can be explained in terms of comet groups.

Consequently the analysis of the previous section has been repeated after replacing each group by a single point at its "centre". Non-randomness is still present and details of the preferred plane for the group-corrected distribution of perihelion points is given in Table II.

Mention has been made of the difficulty of deciding whether or not comets form a possible group, and the inclusion or exclusion of doubtful cases has considerable effect on the result. Corrections similar to those applied in the previous section can bring the preferred plane close to that of the Galaxy. Nevertheless, although there is a small indication of possible galactic concentration, the evidence derived by a consideration of groups must be regarded as inconclusive.

6. *The period of comet orbits.*—Of the elements of the orbit of a comet, it appears that the period is the least likely to be affected by observational selection.

Consequently an investigation of the distribution of the periods of long-period comets may be expected to furnish immediate information about the general distribution of orbits in space. Perturbations by the planets will be likely to manifest themselves most strongly on comets whose orbits have a small angle of inclination to the ecliptic. It is well known, for example, that the short-period (captured) comets exhibit markedly small values of i. Similarly it appears that comets with a period in years given by $\log P < 6$ may also have come to possess them through planetary perturbations.

On the other hand, as Oort (**12**) has pointed out, if comets exist with large values of $\log P$ their orbits must stretch well out into interstellar space and hence be affected by nearby stars. Thus comets with a true period greater than a value given by $\log P = 16$ may certainly be perturbed near aphelion by the Sun's stellar neighbours. Hence there remains the possibility that comets with intermediate values of the period may be relatively unperturbed. It is interesting to note that the distribution of comet frequency with $\log P$ has a weak maximum in this region—at $\log P = 8$.

Consequently the positions of the points of perihelion of the 70 comets with $6{\cdot}8 < \log P < 11{\cdot}0$—which may be termed the P class—are considered separately. The preferred plane for the P class comets is calculated as in Section 3. As for the total distribution discussed in that section, it is noted that the plane of maximum frequency of points lies very near to the galactic plane but closer than does the same plane for the total distribution of perihelion points. In fact it is found that the normal to the preferred plane for the P class comets lies at an angular distance of only $5^{\circ}{\cdot}5$ from the galactic pole (see Table II).

7. *Bright comets.*—A further relatively unperturbed class can be expected to be provided by those comets that have made but few passages through the solar system and in this sense are to be regarded as new. It seems probable that high luminosity is associated in a general way with new comets. The absolute magnitude at any time can be expected to be a function (decreasing with time) of the mass, density and chemical composition of a comet, and hence of its age and number of perihelion passages. Thus on general grounds it seems that what are termed new comets may be expected to be brighter than the average.

The question of how the brightness of comets depends upon distance from the Sun is an extremely complex one. The apparent law of variation of magnitude with distance from Sun and Earth varies from comet to comet and in addition comets are sometimes observed to undergo quite large sudden irregular fluctuations of apparent magnitude. As a result, no precise unique absolute magnitude (defined as the apparent magnitude if at 1 a.u. from the Earth and 1 a.u. from the Sun) can usually be calculated for a comet. Nevertheless, Vsessaviatsky (**13**) has assigned absolute magnitudes to several comets, and his results have been used here to obtain a list of some 79 bright comets, defined as those having an assigned absolute magnitude less than 5·00.

In order to include in the discussion comets for which no absolute magnitudes are given, the list of bright comets is enlarged by including those further comets that were observable for relatively long periods—four months prior to 1875 and five months thereafter. The complete list of so-called bright comets thus totals 127 and will be referred to as the M class. The two separate criteria of brightness adopted here are necessarily of a somewhat arbitrary nature and were chosen to provide a satisfactory number of comets for investigation. It is also

clear, however, that the members of class M were certainly brighter, on the whole, than comets not included in it. As before, details of the preferred plane for points corresponding to the M class are given in Table II. As with the P class it is found that the preferred plane for the M class lies rather closer to the galactic plane than the preferred plane for all observed comets.

8. *Conclusions.*—The danger of drawing too detailed conclusions concerning comets from a discussion of the type considered here must be immediately apparent. In the first place, doubt has often been cast on the reliability and significance of many of the observations made. Owing to the continuous effect of planetary perturbations, the elements of a cometary orbit will change during a single passage and from passage to passage. The data used in this paper refer only to particular osculating orbits that represent the actual paths of comets for limited times. Thus, for example, the given tabulated value of $P = 1\,385\,600$ years for Comet 1826 II will certainly not carry the significance the number of figures appears to indicate.

Again, as has already been stressed, the available data have probably suffered from observational selection. Nevertheless, certain conclusions will be tentatively advanced.

It seems quite clear, for instance, that departure from randomness in the observed distribution of perihelion points of the comets considered is strongly suggested, even when the effects of comet groups and observational selection are considered in an elementary way. When enquiry is made into the nature of the non-randomness it appears that there is evidence indicating a preference for the perihelion points to lie near a particular great plane. Further, the centre of the observed distribution appears to be significantly displaced towards a point on the celestial sphere. The possible identification of the plane and the point with well-known and easily recognizable astronomical features is certainly striking.

The identification of the plane with that of the Galaxy also has been seen to become more apparent when two special sub-classes of the comets are considered. These represent comets with special values of the period (P class) and bright comets (M class), and were selected for special study on the ground that they might well contain a high proportion of relatively unperturbed comets. Some evidence is available in support of this.

It is difficult, then, to resist the suggestion that the comets studied were introduced into the solar system with their orbital principal axes exhibiting a preference for lying near the galactic plane, and that superimposed on this there has been a further tendency for comets to approach the Sun from a direction (given by the position of aphelion) directly opposed to that of the Sun's motion relative to the nearest stars.

9. *Accretion theory.*—It is interesting to attempt to interpret these suggestions in the light of the accretion hypothesis. According to the hypothesis, the position of perihelion indicates the direction from which the comet-producing cloud has approached the Sun. The perihelion positions would therefore be expected to exhibit a tendency for lying near the apex of the Sun's motion relative to the local interstellar clouds. If clouds share in the local general stellar motions this position may be expected to lie near the stellar apex of the stellar motion. As regards possible galactic influence, it may be observed that if cloud distribution or structure possessed any galactic preference then a star would remain longest immersed in a cloud when moving relatively in the galactic plane. Thus if all

directions of relative motion were equally probable the distribution of perihelion points would have a preference for lying near the galactic plane.

Acknowledgments.—The author gratefully acknowledges the encouragement and helpful advice given by Dr R. A. Lyttleton and Professor T. G. Cowling during the preparation of this paper.

A. E. R. E.,
Harwell,
Didcot, Berks:
1956 *October.*

References

(1) Lyttleton, R. A., *M.N.*, **108,** 465, 1948 ; *The Comets and their Origin*, Cambridge, 1953.
(2) Pickering, W. H., *Harvard Annals*, **61,** 1911.
(3) Eddington, A. S., *Obs.*, **36,** 142, 1913.
(4) Oppenheim, S., *Zur Statistik der Kometen und Planeten im Zusammenhung mit der Verteilung der Sterne. Probleme der Astronomie*, Berlin, 1924.
(5) Baldet, F. and de Obaldia, G., *Catalogue Général des Orbites de Comètes de l'an* −466 *a* 1952, Observatoire de Paris, 1952.
(6) Porter, J. G., *Comet and Meteor Streams*, London, 1952.
(7) Hoek, M., *M.N.*, **26,** 1, 1865 and *M.N.*, **26,** 204, 1866.
(8) Sterne, L., *Harvard Circular*, **396,** 1934.
(9) Holetschek, H., *Sitzungsberichte Akad. Wien, Math. Nat.*, **88,** 1099, 1884.
(10) Bourgeoise, P. and Cox, J. F., *B.A.*, **9,** 349, 1933.
(11) Guillemin, A., *The World of Comets*, London, 1877.
(12) Oort, J. H., *B.A.N.*, **11,** 91, 1950.
(13) Vsessviatsky, A., *Moscow A. J.*, **10,** 327, 1933.

A PHOTOELECTRIC STELLAR SPECTROPHOTOMETER, USING A FABRY–PEROT ETALON

J. E. Geake and W. L. Wilcock

(Received 1957 March 7)

Summary

Tests are described of a photoelectric method of investigating stellar spectra, in which a prism monochromator and a Fabry–Perot etalon are used to scan the spectrum simultaneously. The addition of the etalon enables the monochromator to be used with a wider entrance slit for a given wave-length resolution. The etalon is tilted in order to scan in wave-length : this method is simple, but leads to a loss of wave-length resolution which is assessed quantitatively.

---

1. *Introduction.*—We have described elsewhere (**1**) an instrument for the direct photoelectric scanning of astronomical spectra. The light passing the exit slit of a prism monochromator is received by a photomultiplier. This is followed by an amplifier and a pen recorder which draws out the spectral profile directly as the wave-length passed by the monochromator is varied continuously. In order to use our instrument at its maximum resolution of about $\frac{1}{2}$ A a narrow entrance slit (about 25 μ) is needed, and this width is usually several times less than that of the tremor disk of the stellar image. This leads to a considerable waste of light, and also to large fluctuations in the amount of light entering the monochromator as the image moves about under the influence of atmospheric turbulence. The effect of these fluctuations has been removed satisfactorily for most purposes by a compensating system, but some imperfections remain.

It would therefore be advantageous to widen the entrance slit until the whole stellar image is always passed, if this could be done without loss of resolution. It has been shown by Jacquinot and Dufour (**2**) that the addition of a Fabry–Perot etalon to a monochromator enables wider slits to be used for a given resolution, and references to the history of this method are given by Jacquinot and Chabbal (**3**) and by Dunham (**4**). It is the purpose of this paper to describe astronomical tests of such an arrangement which have been carried out with our instrument mounted on the 120 cm telescope at Asiago, Italy, and which we believe to be its first stellar application.

2. *Theory.*—If a Fabry–Perot etalon, having parallel reflecting surfaces with optical separation t, is placed in a parallel beam of white light, it passes a series of wave-lengths which satisfy the relationship

$$\lambda_\theta = \frac{2t}{p}\cos\theta = \lambda_0 \cos\theta \qquad p = 1, 2, 3, \ldots \tag{1}$$

where θ is the angle of incidence on the reflecting surfaces. It therefore acts as a filter with many passbands corresponding to different values of the order of interference p. If all but one of these passbands is suppressed by a preliminary filter the whole arrangement has a single passband : we use our prism monochromator

as this preliminary filter. In order to scan the spectrum the passband of the system must be moved continuously over a range of wave-lengths. For the etalon this may be achieved by varying either t or θ; it is better, for reasons given below, to vary t, but it is so much simpler to vary θ that we chose to do this for our initial tests. The wave-length passed by the etalon is changed at a constant rate, by using a synchronous motor and cam to tilt the etalon so that $\cos\theta$ varies linearly with time. Simultaneously, the wave-length passed by the monochromator is changed, by using another synchronous motor to turn one of its prisms, so that the etalon passband remains in the centre of the monochromator passband.

In our auto-collimating monochromator, the width of the exit slit is made equal to that of the entrance slit, which in turn is fixed by the requirement that the whole stellar image shall be passed. The wave-length range corresponding to this slit width must not be greater than the separation $\Delta\lambda$ between the etalon passbands, which according to (1) is given by:

$$\Delta\lambda = \frac{\lambda_0}{p} = \frac{\lambda_0^2}{2t}, \tag{2}$$

and this fixes the maximum permissible value of t for a given monochromator dispersion and slit width.

The wave-length resolution of this combination of etalon and monochromator is determined by the half-width $\delta\lambda$ of the etalon passband used. Neglecting the effect of the finite slit width, $\delta\lambda$ is given by

$$\delta\lambda = \frac{\lambda_0}{pN} \tag{3}$$

where N is the equivalent number of interfering beams, and depends on the reflectivity and flatness of the surfaces. When the finite slit width is taken into account it is found to cause an increase in the half-width of the passband. This increase, $\delta'\lambda$, is negligible at normal incidence, but becomes increasingly important as the scan proceeds and θ increases: it may be found by differentiating (1), from which

$$\delta'\lambda \sim \lambda_0 \sin\theta\,\delta\theta \sim \lambda_0 \sin\theta \cdot \frac{s}{f} \tag{4}$$

where s is the exit slit width and f is the focal length of the collimating lens immediately before the etalon. By (4) and (1), $\delta'\lambda$ (for θ small) can be expressed in terms of the wave-length range $(\lambda_0 - \lambda_\theta)$ of a scan starting at normal incidence as:

$$\delta'\lambda \sim \frac{2s\lambda_0^{1.2}}{f}(\lambda_0 - \lambda_\theta)^{1/2}. \tag{5}$$

This progressive increase of the instrumental half-width as the scan proceeds is the disadvantage of scanning by tilting the etalon. We were able to use this method because the slit width required to accept the image of a star was small and because we scanned only a small wave-length range. For a larger wave-length range the loss of resolution could be minimized by using a saw-tooth form of scan (**3**).

3. *Instrumental arrangement.*—Fig. 1 shows the etalon mounted experimentally on our monochromator at Asiago, with the covers of its light-tight box removed. The tilting lever, cam follower and cam can be seen under the etalon box. The

angular range of the scan is adjusted by sliding the cam follower along the arm, and then moving the cam and motor assembly correspondingly. This adjusts both the rate and the range of scan, as the cam throw and rate of rotation are fixed. The monochromator must be adjusted to scan in wave-length at the same rate as the etalon, so that their passbands remain coincident. Contacts, operated by the cam, stop the monochromator scan automatically at the end of the etalon scan, and restart it at the beginning of the next scan. In the interval the monochromator is turned back to a pre-set starting wave-length by hand.

The etalon consists of a pair of $1\frac{1}{4}$ in. flats, of which the central 1 cm is used. The reflecting surfaces have 5-layer dielectric coatings; the present flats are of rather poor quality, and their irregularities limit the resolution to about 1/13th of an order. Nickel wire spacers 90 μ in diameter are used, giving an inter-order spacing of 11 A at λ4471. The transmission of the etalon is about 60 per cent at this wave-length.

The etalon may be turned by hand through 90°, so that it can be adjusted to parallelism *in situ* by viewing circular fringes against a screen illuminated by a helium discharge tube.

4. *Tests and performance of the instrument.* (*a*) *Calculated performance and laboratory tests.*—Table I gives values of the half-width in angstrom units, calculated from (5), after scanning 11, 22 and 33 A, starting at normal incidence. A collimating lens with a focal length of 9 cm was used before the etalon and a mean wave-length of 4471 A is assumed.

TABLE I

Angle tilted in degrees	Scan range in A	Half-width in A at end of scan			
		Slit width in μ			
		100	500	1000	1500
4·1	11	0·35	1·8	3·5	5·3
5·7	22	0·50	2·5	5·0	7·5
6·9	33	0·60	3·0	6·0	9·1

These figures are also shown graphically in Fig. 2; lines 1, 2 and 3 represent the calculated half-width after 11, 22 and 33 A of scan respectively. Line M shows, for comparison, the half-width of the monochromator passband without

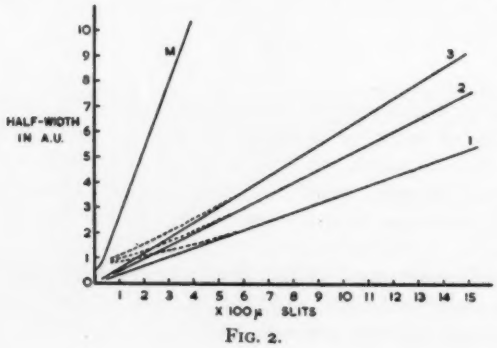

FIG. 2.

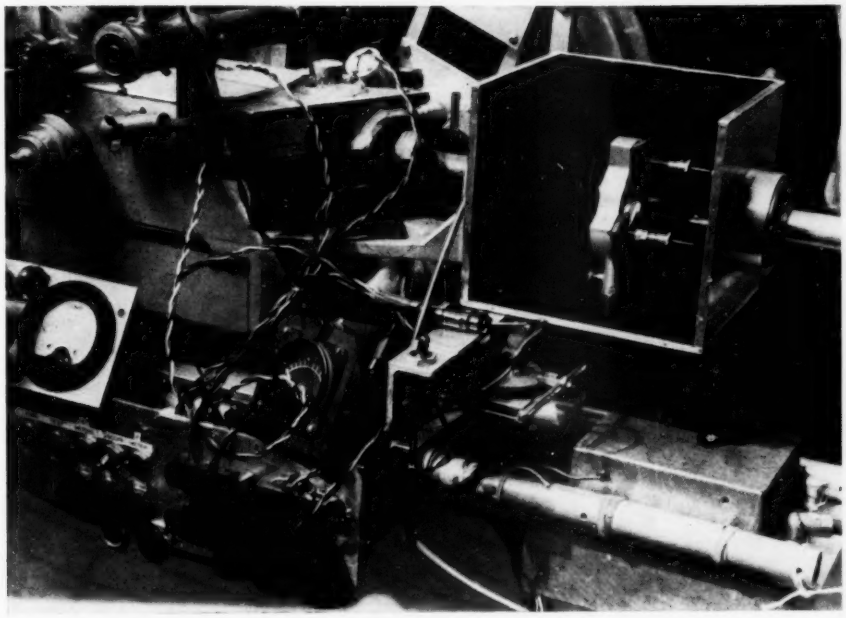

FIG. 1.

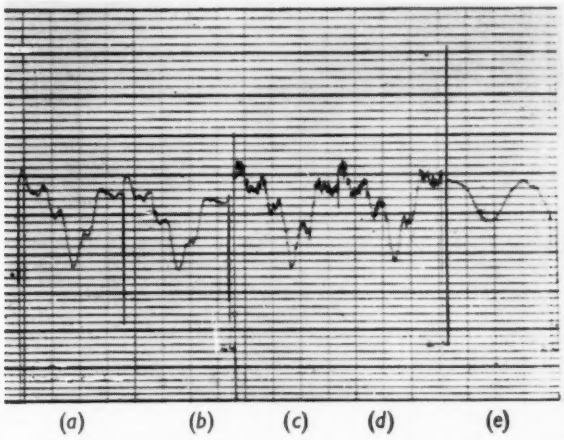

FIG. 3.—*Repeated scans of the* Hγ *absorption line in the spectrum of scattered sunlight.*

Scans (*a*) *and* (*b*): *Etalon, plus monochromator with* 200 μ *slits.*

(*c*) *and* (*d*): *Monochromator alone, with* 50 μ *slits, giving about the same resolution as* (*a*) *and* (*b*), *with the amplifier gain increased by* 3.

(*e*): *Monochromator alone with* 200 μ *slits.*

Each scan took 4 *min; recording time-constant* 1 *sec; range of scan* 20*A.*

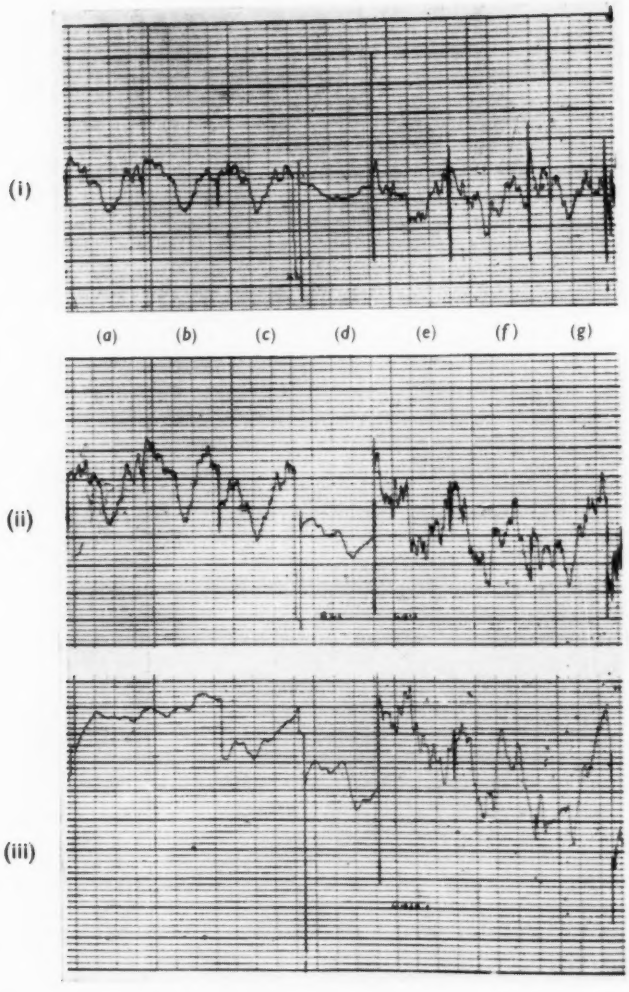

FIG. 4.—*Repeated scans of the* Hγ *absorption line in the spectrum of* o U Ma, *of spectral class* Go.

Trace (*ii*): *output of signal photocell, which scans spectrum.*

Trace (*iii*): *output of comparison photocell, showing variations of total* (*white*) *light, after the entrance slit.*

Trace (i): *the ratio of* (*ii*) *and* (*iii*), *the spectral profile compensated for variations of the total light passing the entrance slits.*

Scans (*a*) *to* (*c*): *Etalon, plus monochromator with* 400 μ *slits.*

(*d*): *Monochromator alone with* 400 μ *slits.*

(*e*) *to* (*g*): *Monochromator alone with* 75 μ *slits, giving about the same resolution as scans* (*a*) *to* (*c*), *with the amplifier gain increased by* 3.

Each scan took 4 *min: recording time-constant* 10 *sec: range of scan* 20 *A.*

J. E. Geake and W. L. Wilcock, A photoelectric stellar spectrophotometer, using a Fabry–Perot etalon.

the etalon. Experimental measurements were in good agreement with these calculated results except at the lower end, where the natural half-width of the etalon passbands (due in this case mainly to irregularities of the etalon plates), becomes important. The actual performance in this region is shown by the dotted lines.

The measurements were carried out by setting the monochromator to pass the $\lambda 4471$ line from a helium discharge tube. The etalon was then tilted to pass this line at several successive orders, starting at normal incidence, and with the spacer adjusted so that the line was passed at normal incidence. The half-widths of the recorded profiles of successive orders were measured, for several values of monochromator slit width. This is equivalent to measuring the half-width after successive intervals of 11 A, with the etalon and monochromator scanning together.

(*b*) *Astronomical tests.*—(i) The Hγ absorption line in the spectrum of scattered sunlight was scanned, and the result is shown in Fig. 3. Scans (*a*) and (*b*) were made by using the etalon and the monochromator with wide slits; scans (*c*) and (*d*) were made without the etalon, but with the monochromator slit width reduced to give the same wave-length resolution. The increased noise fluctuations result from the reduced amount of light passed by the narrower slits. The amplifier gain was increased to keep the recorder deflection about the same. Scan (*e*) shows a scan with the monochromator alone with the same wide slits as were used for the etalon scans.

(ii) Similar test scans were made of the Hγ absorption line in the spectrum of o U Ma, a star of spectral class Go. These are shown in Fig. 4, and illustrate both of the advantages of using the etalon. The wider slits used with the etalon result in a gain in light, in this case by a factor of about 3 in spite of the fact that the transmission of this etalon is only 60 per cent; also, the fluctuations caused by the stellar image moving about on the slit under the influence of atmospheric turbulence are greatly reduced. This is seen by comparing the fluctuations on trace (iii), which is a record of the undispersed light after the entrance slit, for scans with and without the etalon. The fluctuations with the etalon are largely caused by changes in the atmospheric transparency due to haze, as these tests were carried out on a particularly bad night. It is the fluctuations due to obstruction by the slit jaws which are the most difficult to remove by compensation (1), and their absence results in the improved quality of the scans with the etalon.

5. *Acknowledgments.*—The authors are grateful to Professor L. Rosino and the authorities of the University of Padua for permission to use the 120 cm telescope at Asiago, to Mr J. Ring for coating the etalon plates with their dielectric reflecting layers, and to Dr H. J. J. Braddick for his help and advice.

The Physical Laboratories,
University of Manchester:
1957 *March* 6.

References

(1) J. E. Geake and W. L. Wilcock, *M.N.*, **116**, 561, 1956.
(2) P. Jacquinot and C. Dufour, *J. rech. cent. nat. rech. sci.*, Labs. Bellevue (Paris), No. 6, 91, 1948.
(3) P. Jacquinot and R. Chabbal, *J. Opt. Soc. Am.*, **46**, 556, 1956.
(4) T. Dunham, *Vistas in Astronomy*, Ed. Beer, Pergamon Press 1956, Vol. II, p. 1223.

THE NON-RADIAL OSCILLATIONS OF CENTRALLY CONDENSED STARS

John W. Owen

(Communicated by Z. Kopal)

(Received 1957 April 4)

Summary

The second-order differential equation governing the non-radial oscillations of polytropic stellar models has been integrated for values of the polytropic index varying between 3 and 4. It has been shown that the fundamental mode is no longer a member of the discrete frequency spectrum for the polytrope $n=3{\cdot}25$; and that, as n increases, an increasing number of modes on either side of the fundamental mode disappear from the spectrum.

It has been shown analytically that the equation has no solutions compatible with the boundary conditions of the problem for the limiting polytrope $n=5$.

---

1. *Introduction.*—The significance of the problem of non-radial oscillations of stellar models has been adequately discussed in previous works by Rosseland (**1**), Pekeris (**2**), Cowling (**3**) and Kopal (**4**). Rosseland pointed out that a limitation to purely radial oscillations could fail to reveal the possible instability of a particular model for a more general type of disturbance: a consideration of the homogeneous gas sphere emphasizes this point. Kopal has stressed the interests of double-star astronomy in possible free periods of non-radial oscillations. It is well known that any non-vanishing orbital eccentricity (no matter how small) is bound to invoke, through tides, non-radial oscillations (corresponding to the second and higher spherical harmonic distribution) of both components. These are forced oscillations of period equal to that of the binary orbit; and if the latter is sufficiently far removed from any period of free oscillation in which either component can oscillate then the amplitudes of the forced non-radial oscillations can be predicted by the equilibrium theory of tides. If, however, one of the free periods can resonate with the orbital period then the amplitude of the corresponding mode would greatly exceed that of the equilibrium tide. This would give rise in eclipsing binary systems to photometric phenomena which could become not only observable but conspicuous. Such phenomena which could be ascribed to this cause have indeed been pointed out in a number of known systems; but their identification remains uncertain as yet. As the problem at issue is of considerable theoretical as well as practical interest, the aim of the present work will be to throw light on the problem of whether or not resonance between free and forced periods of non-radial oscillation is at all possible, or likely to develop, in self-gravitating gas spheres characterized by a sufficiently high degree of central condensation. In order to attempt to answer this question, our aim will be to establish the specific values of free periods of non-radial oscillations for polytropic gas spheres (of the many other models which could be considered) whose index n lies between 3 and 5, and to compare them with the Keplerian orbital period of binary motion.

In doing this, we propose to regard the amplitudes (and velocities) of oscillating motion to be sufficiently small for their squares and higher powers to be ignored (i.e. to consider the oscillatory problem in its acoustic approximation). The system of differential equations governing such motion is one of fourth order, and was first formulated by Pekeris (**2**). He solved his equations, however, only for the homogeneous gas sphere, and showed this to be unstable with respect to non-radial oscillations. It may be remembered that Emden (**5**) had previously considered the general oscillations of a polytropic gas sphere. He simplified the problem by neglecting changes in the gravitational potential produced by the oscillations, and thereby reduced the differential equation to one of second order; unfortunately, however, he used an over-simplified form of the equation of continuity. This was pointed out by Cowling (**3**) who derived the correct second-order differential equation governing this simplified problem, and also investigated the general nature of its frequency spectrum. He also located the fundamental mode and one overtone for the second-harmonic oscillation of Eddington's "standard model". Kopal (**4**) has extended these results to the third- and fourth-harmonic oscillations, and has located the second overtone in each case. These results obtained by Cowling and Kopal all apply to a model with a ratio of specific heats, γ, of $5/3$ and in this numerical investigation we will confine our attention to models having this value of γ.

2. *Equations of the problem.*—Consider the small adiabatic oscillations of a self-gravitating fluid globe. The motion of any individual particle is assumed to take place adiabatically, γ being the ratio of the specific heats (assumed to be constant throughout the sphere). Viscous forces are neglected. Let the pressure P, the density ρ, and the gravitational potential V at any point of the initially spherical body be assumed to have increments δP, $\delta\rho$ and δV, respectively, due to the disturbance. Let the displacement of the matter from its equilibrium position be represented by $\mathbf{h}$, which has a radial component δr. The Eulerian equations of motion are then

$$\rho\frac{\partial^2\mathbf{h}}{\partial t^2}+\nabla\delta P+\delta\rho\nabla V+\rho\nabla\delta V=0. \tag{1}$$

Cowling (**3**) has shown, by means of a perturbation method, that a neglect of $\nabla\delta V$ in this equation leads to values of the period which differ, in the case of the standard model, by less than 4 per cent from the true periods. The approximation should yield even better results for the higher degrees of central condensation which will be considered in this investigation, and it will therefore be retained throughout the present study.

The equation of continuity is

$$\delta\rho=-\nabla.(\rho\mathbf{h}); \tag{2}$$

and the equation of hydrostatic equilibrium

$$\nabla P=-\rho\nabla V. \tag{3}$$

The condition for adiabatic motion can be expressed by the equation

$$\delta P+\delta r\frac{dP}{dr}=c^2\left(\delta\rho+\delta r\frac{d\rho}{dr}\right), \tag{4}$$

where

$$c^2=\gamma\frac{P}{\rho},$$

c corresponding to the velocity of sound in an ordinary gas.

We now assume that the dependence of the perturbed quantities on the polar coordinates θ and ϕ is given by a surface harmonic of order m; and further suppose that their dependence on time is a simple harmonic one. The period of the motion is taken to be $2\pi/\sigma$. The former assumption provides the relationships

$$\nabla^2\delta P=\frac{1}{r^2}\frac{d}{dr}\left(r^2\frac{d\delta P}{dr}\right)-\frac{m(m+1)}{r^2}\delta P, \tag{5}$$

$$\nabla.\left(\frac{\delta\rho}{\rho}\nabla P\right)=\frac{1}{r^2}\frac{d}{dr}\left(r^2\frac{\delta\rho}{\rho}\frac{dP}{dr}\right); \tag{6}$$

and the latter gives

$$\frac{\partial^2\mathbf{h}}{\partial t^2}=-\sigma^2\mathbf{h}. \tag{7}$$

The foregoing developments have so far been quite general and the equations apply to any initial distribution of density and pressure. In order to obtain specific results, we propose from now on to restrict ourselves to a consideration only of the class of stellar models for which this distribution is polytropic. This means that in equilibrium the density and pressure, at a distance r from the centre, are connected to their central values ρ_c and P_c by the equations

$$P=P_c\theta^{n+1},\quad \rho=\rho_c\theta^n \quad \text{for} \quad 0\leqslant n\leqslant 5;$$

where θ satisfies the Lane–Emden equation

$$\frac{1}{x^2}\frac{d}{dx}\left(x^2\frac{d\theta}{dx}\right)+\theta^n=0 \tag{8}$$

with boundary conditions

$$\theta=1 \quad \text{and} \quad \frac{d\theta}{dx}=0 \quad \text{at} \quad x=0.$$

n is the polytropic index, and x is given by $r=r_0x$ where

$$r_0^2=\frac{(1+n)P_c}{4\pi G\rho_c^2}.$$

The equations can then be simplified considerably if we introduce, following Cowling, the pair of non-dimensional variables z and w given by

$$z=\frac{\delta r}{r_0}\theta^{(1+n)/\gamma}, \qquad w=\frac{\delta P}{P_c}\theta^{-(1+n)/\gamma}. \tag{9}$$

Under these conditions our fundamental equations can be shown (see Cowling (3)) to reduce to

$$\frac{d}{dx}(x^2z)=gw, \tag{10}$$

and

$$\frac{dw}{dx}=fz; \tag{11}$$

where

$$g=\theta^Q\left[\frac{m(m+1)}{\alpha}-\frac{x^2}{\gamma\theta}\right], \qquad f=\theta^{-Q}\left[\alpha+K\frac{\theta'^2}{\theta}\right]$$

$$Q=\frac{2(1+n)}{\gamma}-n, \qquad K=\left(\frac{1+n}{\gamma}-n\right)(1+n), \qquad \alpha=\frac{\rho_c}{P_c}r_0^2\sigma^2.$$

The boundary conditions require a node (no displacement) at the centre, and a loop (no pressure variation) at the free surface of the oscillating globe, i.e.

$$\delta r = 0 \quad \text{at} \quad r = 0,$$
$$\delta P = 0 \quad \text{at} \quad r = r_1,$$

where $\rho(r_1) = 0$. These conditions can only be satisfied for a certain discrete spectrum of values of α. There is, in general, a fundamental mode having no loops or nodes between those at the centre and at the surface. Cowling has shown, by applying Sturm–Liouville theory, that there is an infinite set of oscillations having indefinitely long periods and also an infinite set of indefinitely short period. Cowling referred to these as the gravitational (g-) and the pressure (p-) oscillations respectively. They exhibit an increasing number of nodes and loops in the interior. The number of nodes or loops is denoted by the suffix. Thus the g_1- mode has one node and one loop in the interior.

3. *Method of solution.*—In the location of the eigenvalues of equations (10) and (11) use was made of the Manchester University Electronic Digital Computer, Mark I. We used a trial and error method identical to that used by Kopal (**4**). A number of trial integrations were made; the choice of α being designed to converge on the particular eigenvalue sought. We decided to use the Runge–Kutta method, as described by Gill (**6**), to integrate the equations. This method can be applied to a set of simultaneous first-order equations in which the independent variable does not occur explicitly. We found it convenient to incorporate the Lane–Emden equation (**8**), in the form of two simultaneous equations

$$\frac{d\theta}{dx} = \theta' \quad \text{and} \quad \frac{d\theta'}{dx} = -\frac{2\theta'}{x} - \theta^n, \tag{12}$$

with equations (10) and (11); and to integrate the complete system of equations (10), (11), (12) together with the further equation $dy/dx = 1$. This latter equation allows x to occur explicitly in (10), (11) and (12). The system is to be integrated subject to the initial conditions $w = 0$, $z = 0$, $\theta = 1$, $\theta' = 0$ at $x = 0$.

These equations cannot be integrated as they stand because both w and z are zero at the origin. The fact that w must be zero at the origin can be seen if we consider the series expansions, about the origin, of w and z. Kopal (**4**) has shown that close to the origin

$$w = x^m(a_0 + a_2x^2 + a_4x^4 + \ldots), \tag{13}$$
$$z = x^{m-1}(b_0 + b_2x^2 + b_4x^4 + \ldots), \tag{14}$$

where a_0 and b_0 are related by $\alpha b_0 = m a_0$. We will take $a_0 = \frac{1}{2}\alpha$ and $b_0 = \frac{1}{2}m$, for consistency with previous results.

In order to overcome this difficulty we can either make use of the series expansions about the origin, derived and used by Kopal (**4**), to start the integration; or we can make use of a transformation to a more well-behaved pair of dependent variables. The latter course is clearly the more convenient for our machine. We put

$$w = x^{m-1}w_1 \tag{15}$$

and

$$z = x^{m-2}z_1 \tag{16}$$

and equations (10) and (11) become

$$\frac{dw_1}{dx} = f\frac{z_1}{x} - (m-1)\frac{w_1}{x}, \tag{17}$$

$$\frac{dz_1}{dx} = g\frac{w_1}{x} - m\frac{z_1}{x} \tag{18}$$

with initial conditions

$$\frac{w_1}{x} = \frac{\alpha}{2}, \qquad \frac{z_1}{x} = \frac{m}{2} \quad \text{at} \quad x = 0.$$

Using a more systematic notation the five equations to be integrated are

$$\frac{dy_0}{dx} = 1,$$

$$\frac{dy_1}{dx} = y_2,$$

$$\frac{dy_2}{dx} = -\frac{2y_2}{x} - y_1^n,$$

$$\frac{dy_3}{dx} = f\frac{y_4}{x} - (m-1)\frac{y_3}{x},$$

$$\frac{dy_4}{dx} = g\frac{y_3}{x} - m\frac{y_4}{x}.$$

The initial conditions at $x = 0$ are

$$y_0 = 0, \quad y_1 = 1, \quad \frac{y_2}{x} = -\frac{1}{3}, \quad \frac{y_3}{x} = \frac{\alpha}{2} \quad \text{and} \quad \frac{y_4}{x} = \frac{m}{2}.$$

Due to the general nature of the solutions, a variable step-length was used. The functions tended to vary most rapidly at the two ends of the range of integration and a shorter step-length had to be used there. This could be carried out automatically by the machine to keep a constant accuracy. The eigenvalues were located correct to four decimal places.

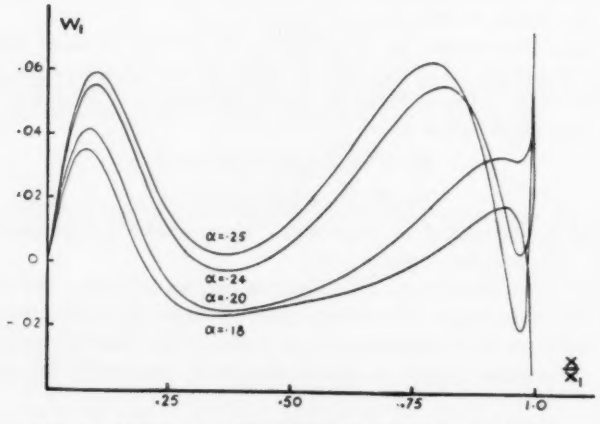

FIG. 1.—*Pattern of machine solutions for the polytrope* $n = 3{\cdot}25$.

The integrations were started with trial values of α. Kopal found that if this value was too large the values of w near x_1 tended to $+\infty$ for the fundamental, the p_2- or the g_2- modes and to $-\infty$ for the p_1- or g_1- modes; while for small values of α the converse was true. The eigenvalue could thus be bracketed, to any desired degree of accuracy, by two values of α.

We first tried to locate the fundamental second-harmonic mode for the polytrope $n=3{\cdot}25$. The initial trial value was taken to be 0·25. In this case w_1 had two zeros close to the boundary and finally tended to $+\infty$ (see Fig. 1). This implied that 0·25 was too small for the p_1- mode and too large for the f-mode. We therefore made a second trial integration with $\alpha=0{\cdot}24$; and found that, although w_1 had no zeros near the boundary and tended to $+\infty$ less rapidly, it had two zeros in the centre of the range. On further reducing α we found that the curve tended to that appropriate to the g_1- mode. Thus for $n=3{\cdot}25$ there is no fundamental second-harmonic mode of oscillation: there is no mode which has no loops in the interior of the star ($0<x<x_1$). This was also found to hold for the polytropes $n=3{\cdot}5$ and $n=3{\cdot}75$. Other small modes were also absent for these models. Fig. 2 shows the development of a minimum in the w_1 curve as n increases from $n=2{\cdot}5$ to $n=3{\cdot}25$.

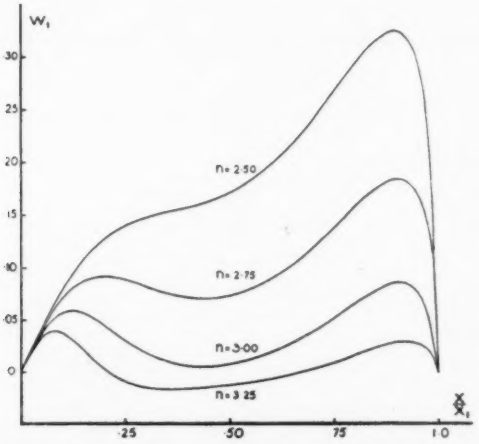

FIG. 2.—*The development of a minimim in the graph of w_1 as n increases from $n=2{\cdot}5$ to $n=3{\cdot}25$.*

4. *The polytrope* $n=5$.—We have seen in the previous section that as n increases an increasing number of modes on either side of the fundamental mode gradually disappear from the characteristic spectrum. It is natural, therefore, to enquire what happens when the degree of central condensation becomes infinite. This is true when the polytropic index reaches the value of 5. In this case it is well known that the solution of the Lane–Emden equation (8) is

$$\theta=(1+\tfrac{1}{3}x^2)^{-1/2}. \tag{19}$$

This polytrope clearly has an infinite radius but its mass remains finite. It is tantamount to a finite gas sphere whose whole mass is condensed to the centre, enveloped by an atmosphere whose mass is infinitesimal for gravitational purposes, i.e. the Roche model. For such a model the perturbation in the gravitational potential produced by the disturbance would be zero; so that the second-order system of equations (10) and (11) represents the rigorous formulation of the problem.

In order to ease the formal analysis of this limiting case it is convenient to make a change of variables $x=\sqrt{3}\tan y$; which has the effect of reducing the

range of integration from $0 \leqslant x \leqslant \infty$ to $0 \leqslant y \leqslant \pi/2$. The Lane–Emden solution (19) is then $\theta = \cos y$ and equations (10) and (11) become

$$\frac{dz}{dy} + \frac{2z}{\cos y \sin y} = Bw, \tag{20}$$

and

$$\frac{dw}{dy} = Az, \tag{21}$$

where

$$A = \sqrt{3}(\cos y)^{-Q-2}\left[\alpha + \frac{K}{3}\sin^2 y \cos^3 y\right], \tag{22}$$

and

$$B = \frac{1}{\sqrt{3}}(\cos y)^{Q}\left[\frac{m(m+1)}{\alpha \sin^2 y} - \frac{3}{\gamma \cos^3 y}\right]. \tag{23}$$

If we eliminate z between (20) and (21), the differential equation governing w assumes the form

$$\frac{d^2w}{dy^2} + p(y)\frac{dw}{dy} + q(y)w = 0, \tag{24}$$

where we have abbreviated

$$p(y) = \frac{d}{dy}\log\frac{\tan^2 y}{A}, \tag{25}$$

and

$$q(y) = -AB. \tag{26}$$

Thus, near the origin

$$p(y) \sim \frac{2}{y} \quad \text{and} \quad q(y) \sim -\frac{m(m+1)}{y^2}. \tag{27}$$

Putting $y_1 = y - \pi/2$, we have near the point $y = \pi/2$,

$$p(y_1) \sim \frac{Q}{y_1} \quad \text{and} \quad q(y_1) \sim -\frac{3\alpha}{\gamma {y_1}^5}. \tag{28}$$

Equation (22) therefore has, in general, a regular singularity at the origin and an irregular singularity at $y = \pi/2$. This means that there can be no solution of (24) which satisfies the boundary condition that w must be zero at $y = \pi/2$. This statement follows from a much more general existence theorem (7). We will state here only the particular form of the theorem which applies in the above instance.

If n_1 and n_2 are the orders of the poles which $p(z)$ and $q(z)$ have respectively at the point z_0, which is an irregular singularity of the equation

$$\frac{d^2v}{dz^2} + p(z)\frac{dv}{dz} + q(z)v = 0, \tag{29}$$

then a necessary condition for the existence of a regular analytic solution of this equation, at $z = z_0$, is that n_1 and n_2 should satisfy the relationship $n_2 \leqslant n_1 + 1$.

There are two exceptional cases for which the above proof does not hold. If $\alpha = 0$ or $\gamma = \infty$, then $q(y)$ would have a pole of order only two at $y = \pi/2$. The equation (24) would then have a regular singularity at both $y = 0$ and $y = \pi/2$. Neither of these cases is, however, of great physical significance as far as real

stars are concerned. The former requires an infinite period for the oscillation, and this means that the star is in a state of neutral equilibrium: while the latter means that the fluid is an incompressible one.

This proof applies equally well to the case $m=0$. The polytrope $n=5$ is thus incapable of performing either radial or non-radial oscillations of finite period.

TABLE I

Polytrope	Oscillation	$m=2$	$m=3$
3·25	p_1	0·3129	0·3372
	f	None	None
	g_1	0·1400	0·1704
	g_2	0·0816	0·1198
3·5	p_2	0·3573	0·3870
	p_1	None	None
	f	None	None
	g_1	None	None
	g_2	0·0874	0·1174
3·75	p_3	0·3795	0·4095
	p_2	None	None
	p_1	None	None
	f	None	None
	g_1	None	None
	g_2	None	None
	g_3	0·0618	None
	g_4	0·0442	0·0697

5. *Results and conclusions.*—The most important result which has transpired from our numerical work is the gradual disappearance of low modes of non-radial oscillation with increasing degree of central condensation of the respective configuration. For $n>3$ the polytropic family of models is seen no longer to be in a position to oscillate non-radially in the fundamental mode (i.e. in one for which the variations remain of the same sign throughout the interior), and with increasing degree of central condensation (i.e. as $n\to 5$), an increasing number of adjacent "pressure" and "gravitational" overtones vanish from the discrete characteristic spectrum of free periods until, for $n=5$ (Roche model), the corresponding configuration loses completely the ability to oscillate non-radially in any free period at all. For $n<5$, the discrete frequency spectrum of free periods consists essentially of high modes of pressure oscillations (whose periods are very short), and correspondingly high modes of gravitational oscillations (whose periods are very long). The fact that an infinite number of indefinitely long periods of oscillation are consistent with the boundary conditions of our problem has been inferred by Cowling (3) from the Sturm–Liouville character of our equations of motion, for very small values of α; the present results supply quantitative evidence as to the structure of characteristic periods corresponding to the low-frequency tail of the characteristic spectrum. The density of this spectrum makes it, moreover, very probable that the periods of some of its members may come very close indeed to the period of the binary orbit and resonate with it. On the

other hand, high modes of oscillation for which resonance becomes possible are characterized by so many nodes between the centre and the surface that their damping is likely to be severe, restricting the amplitude which they may eventually attain.

As a result, it seems at present impossible to predict the height of the partial tides to which a close coincidence of the orbital period with one of the permissible free oscillations can give rise. The mere possibility, however, that this can happen should underline the need for a dynamical theory of stellar tides which is so far completely lacking, and whose development represents an important requirement of the theory of close binary systems.

6. *Acknowledgments.*—The writer would like to thank Professor Z. Kopal for his invaluable help and criticism at all stages of the preparation of this paper, and also for suggesting the problem. The writer is also indebted to Mr R. A. Brooker, of the Computing Machine Laboratory, for the instruction given in the programming of the electronic computer.

The work was carried out with the aid of grants from the University of Manchester, and from the Wallasey Education Committee; the writer would therefore like to record his indebtedness to both of these bodies.

Department of Astronomy,
University of Manchester:
1957 *March.*

References

(1) S. Rosseland, *Univ. Obs. Oslo Publ.* **2**, 1932.
(2) C. L. Pekeris, *Ap. J.*, **88**, 187, 1938.
(3) T. G. Cowling, *M.N.*, **101**, 367, 1941.
(4) Z. Kopal, *Ap. J.*, **109**, 509, 1949.
(5) R. Emden, *Gaskugeln* (B. G. Teubner, 1907).
(6) S. Gill, *Proc. Camb. Phil. Soc.*, **47**, 96, 1951.
(7) E. L. Ince, *Ordinary Differential Equations*, 417, 1927.

TRANSITION PROBABILITIES FOR FORBIDDEN LINES OF Fe III AND Fe V

R. H. Garstang

(Communicated by the Director of the University of London Observatory)

(Received 1957 March 4)

Summary

Transition probabilities have been computed for magnetic dipole and electric quadrupole radiation for all transitions between levels of the $3d^4$ configuration of Fe v and the $3d^6$ configuration of Fe III.

---

1. *Introduction.*—Many gaseous nebulae and peculiar stars have spectra showing emission lines due to forbidden transitions between the lower energy levels of atoms in the first three rows of the Periodic Table. A detailed study of these stars and nebulae presupposes a knowledge of the transition probabilities of the forbidden lines. Forbidden lines cannot be studied in the laboratory, and their transition probabilities must be obtained from quantum theory. Much work has been done on the calculation of transition probabilities of forbidden lines (for a general review see (**9**)), and for atoms in the first two rows of the Periodic Table the available data are relatively complete, although further improvement in the accuracy of the calculations may eventually be possible. The chief gap in our knowledge of forbidden line strengths of astrophysical importance is in the elements of the first long period. The atoms from scandium to nickel, and many of their ions, have low-lying metastable levels arising from configurations of the types d^n, $d^{n-1}s$ and $d^{n-2}s^2$. So far as the writer is aware, the only detailed study of the transition probabilities of the forbidden lines of atoms with incomplete *d*-shells is that of Pasternack (**15**) on the $3d^2$ configuration in [Fe VII] and on the $3d^3$ configurations in [Cr IV], [Mn V] and [Fe VI]. The great labour involved in calculations of this type renders a study of all the atoms in the first long period impracticable. Iron is the most important of these atoms: iron lines of many different stages of ionization are present in celestial spectra. The lines of other atoms are usually much fainter, and for purposes of identification and qualitative discussion transition probabilities for iron will serve for other atoms with the same electron configurations. With these considerations in mind calculations have been performed on the $3d^4$ configuration in Fe v and on the $3d^6$ configuration in Fe III. The results are reported in the present paper. The d^4 and complementary d^6 configurations contain several terms of a kind, and throughout this paper these are distinguished by using Racah's seniority numbers as subscript prefixes, e.g. ${}_2^3\mathrm{F}$, ${}_4^3\mathrm{F}$.

2. *Method of calculation.*—The first step in the calculation of forbidden line strengths is the setting up of the line strength matrices in LS-coupling. Shortley (**18**) gave explicit formulae for magnetic dipole line strengths in LS-coupling, valid for all configurations, and the numerical values required in the present work are obtained by substituting the appropriate quantum numbers in his formulae.

He showed that transitions only occur (in LS-coupling) between the levels of each term, and not between two terms. The only new point to be noticed is that this rule still applies even if there are several terms of a kind in a configuration. For electric quadrupole radiation the methods introduced into the theory of atomic spectra by Racah can conveniently be utilized. A detailed discussion has already been published (**10**), together with the numerical results for the d^4 configuration studied in the present paper. The d^4 results apply also to the d^6 configuration except that all the phases are reversed (**18**).

The second step in the calculations is the setting up of the energy matrices for the electrostatic and spin–orbit interactions. Throughout the calculations configuration interaction was neglected. This is probably very satisfactory for Fe V, where the $3d^3 4s$ configuration is well separated from the $3d^4$ configuration. The approximation is less satisfactory for Fe III, where there is some overlap between the $3d^5 4s$ and $3d^6$ configurations, but in the interests of simplicity the $3d^5 4s$ configuration was neglected. The electrostatic energy matrix for the d^4 (and d^6) configuration has been given by Racah (**16**) and by Trees and Harvey (**32**). The spin–orbit matrix for the d^4 (and d^6) configuration was calculated* using formulae of Racah (**16, 17**). This calculation was independently checked by D. E. Osterbrock. Trees has shown (e.g. (**31**)) that the addition of a term $\alpha L(L+1)$ to the diagonal elements of the electrostatic energy matrix substantially improves the fit of the theory to spectroscopic energy levels. A term of this kind was included in our calculations.

The next step in the calculations is the adoption of numerical values for the parameters occurring in the energy matrices. In accordance with normal practice the parameters are determined so as to obtain as good agreement as possible between the eigenvalues of the energy matrices and spectroscopic energy levels. It is not possible to treat all the centres of gravity of the terms as independent parameters (as has been done for simpler atoms) because of the occurrence of non-zero off-diagonal elements in the electrostatic energy matrix. The theoretical formulae were therefore retained. The electrostatic matrices involve three parameters, A, B, C, together with a fourth parameter α from the $\alpha L(L+1)$ correction. The spin–orbit matrix involves one parameter, ζ_d. The ion Fe III has been studied in detail by Trees (**30, 31**). There appears little prospect of improving on his results, so that his parameters can be adopted without alteration. For Fe V only the lowest five terms (seventeen energy levels) have been observed. The four parameters A, B, C and α were determined to give the best fit to the five observed terms. This method was checked by several trials on Fe III; it was found that while the use of four parameters and five terms was not as good as the use of four parameters and all fourteen observed terms in Fe III, it was much better than using three parameters A, B, C and five terms. The spin–orbit parameter (ζ_d) was estimated by trial and error to give the best possible fit of the theoretical and experimental term intervals. The final values of the parameters are listed in Table I.

Using the adopted parameters the combined electrostatic and spin–orbit matrices were set up numerically, the sign of ζ_d being changed to get the spin–orbit matrix for d^6 from that for d^4. These matrices were diagonalized numerically by successive partial diagonalization, dealing with the large off-diagonal terms individually, and using perturbation theory when all the off-diagonal elements

* The writer has deposited in the Library of the Society copies of the spin–orbit matrix for the d^4 configuration.

TABLE I

Adopted Parameters

Parameter	Fe III	Fe V
A	19969	24303
B	953	1144
C	3652	4459
α	67	85
ζ_d	429	510

had become small. This method, which has recently come into prominence and has been used by many authors, is in fact due to Jacobi, and has been used in the classical problem of the secular variations of the elements of the planetary orbits (**4**). The final energy levels are given in Table II, together with the observed values (**14**). The transformation matrices were then used in the standard manner to transform the line strengths for both magnetic dipole and electric quadrupole radiation from LS-coupling to intermediate coupling.

The electric quadrupole line strengths obtained by the above procedure are multiples of the square of the radial integral

$$s_q = \int_0^\infty r^2 P^2(3d)\, dr.$$

The evaluation of this integral requires a knowledge of the $3d$ radial wave functions for Fe III and Fe V. Professor D. R. Hartree has recently developed methods of estimating wave functions (with exchange) for atoms in the first long period. Using his wave functions, Professor Hartree estimates that for Fe III, $s_q = 1{\cdot}28$, and for Fe V, $s_q = 0{\cdot}94$. These estimates have been used in the present paper.

The final stage in the calculations is the conversion of the line strengths, obtained in atomic units, into transition probabilities.

3. *Results.*—The final values of the transition probabilities for all possible transitions downwards from all levels up to $^1F_3$ are listed in Table III. For the nine highest energy levels, which are of little astrophysical importance, it has not been thought justifiable to publish in full the transition probabilities of the 170 possible transitions from and between these levels.* For these levels, multiplet transition probabilities have been computed by summing the individual values over the lower levels and averaging over the upper levels:

$$A_{nm} = \frac{1}{(2L_n+1)(2S_n+1)} \sum_{J_n J_m} (2J_n+1) A(L_n S_n J_n \rightarrow L_m S_m J_m),$$

where $E_n > E_m$. The multiplet transition probabilities are listed in Table IV.

All quintet–singlet transitions (except ^5D–^1_4G) have been omitted from Tables III and IV. For each atom there are 22 such transitions predicted as having finite strengths. The calculated values are very small, hardly greater than the rounding-off errors in the calculations, and no real significance can be attached to the values.

It is virtually impossible to assess the accuracy of calculations of this nature. One criterion, unfortunately not a sensitive one, is the agreement of observed and calculated energy levels. Inspection of Table II shows that this agreement is quite good for the terms as a whole, and excellent for the term intervals. An approach to the problem of assessing the accuracy of calculations of this type is

* The writer has deposited in the Library of the Society copies of the detailed results for all transitions for which the probabilities have not been published in full in this paper.

TABLE II

Observed and calculated energy levels

Term	J	Fe V Observed		Fe V Calculated		Fe III Observed		Fe III Calculated	
^6D	0	0		−38		1027		952	
	1	145	145	103	141	932	−95	854	−98
	2	419	274	377	274	739	−193	652	−202
	3	804	385	768	391	436	−303	340	−312
	4	1285	481	1261	493	0	−436	−103	−443
^3P	0	24054		24034		21209		21912	
	1	24973	919	24870	836	20688	−521	21376	−536
	2	26466	1493	26328	1458	19405	−1283	20070	−1306
^3H	4	24937		24811		20482		20520	
	5	25229	292	25120	309	20301	−181	20360	−160
	6	25527	298	25463	343	20051	−250	20144	−216
^3F	2	26765		26822		21857		22081	
	3	26846	81	26909	87	21700	−157	21910	−171
	4	26973	127	27058	149	21462	−238	21678	−232
^3G	3	29820		29831		25142		24871	
	4	30150	330	30193	362	24941	−201	24693	−178
	5	30429	279	30489	296	24559	−382	24293	−400
^3D	1	...		37070		30726		30119	
	2	...		36932	−138	30716	−10	30144	25
	3	...		36822	−110	30858	142	30268	124
^1I	6	...		37500		30356		30427	
^1G	4	...		37712		30886		30623	
^1S	0	...		41808		34812		34090	
^1D	2	...		44950		35804		36732	
^1F	3	...		52050		42897		42655	
^3F	2	...		61242		50185		50231	
	3	...		61271	29	50295	110	50311	80
	4	...		61150	−121	50276	−19	50266	−45
^3P	0	...		61981		49148		49298	
	1	...		61464	−517	49577	429	49715	417
	2	...		60484	−980	50412	835	50571	856
^1G	4	...		69916		57222		57390	
^1D	2	...		92241		...		76019	
^1S	0	...		118975		...		98065	

TABLE III

Transition probabilities of [Fe III] *and* [Fe V]

All entries in this Table are probabilities of spontaneous emission from the upper to the lower of the levels mentioned in column 1. The relative positions of the two levels involved in any particular line should be ascertained by reference to Table II. Units: reciprocal seconds. The letters 'v.s.' denote a line with a theoretical finite strength, which is however too weak for transition probabilities to be calculated by the methods of this paper.

Transition		Fe V		Fe III	
		A_m	A_q	A_m	A_q
^5D–^5D	0–1	$1{\cdot}6\times10^{-4}$	...	$1{\cdot}4\times10^{-4}$	...
	0–2	...	$7{\cdot}2\times10^{-11}$	...	$1{\cdot}0\times10^{-10}$
	1–2	$1{\cdot}2\times10^{-3}$	$6{\cdot}5\times10^{-12}$	$6{\cdot}7\times10^{-4}$	$3{\cdot}5\times10^{-12}$
	1–3	...	$6{\cdot}0\times10^{-10}$	...	$5{\cdot}5\times10^{-10}$
	2–3	$2{\cdot}6\times10^{-3}$	$7{\cdot}7\times10^{-11}$	$1{\cdot}8\times10^{-3}$	$6{\cdot}0\times10^{-11}$
	2–4	...	$1{\cdot}1\times10^{-9}$	...	$1{\cdot}7\times10^{-9}$
	3–4	$3{\cdot}0\times10^{-3}$	$2{\cdot}6\times10^{-10}$	$2{\cdot}8\times10^{-3}$	$3{\cdot}7\times10^{-10}$
^5D–^3P	1–0	1·3	...	0·67	...
	2–0	...	$2{\cdot}8\times10^{-4}$	...	$2{\cdot}4\times10^{-4}$
	0–1	0·13	...	0·091	...
	1–1	9×10^{-5}	$1{\cdot}2\times10^{-4}$	8×10^{-5}	7×10^{-5}
	2–1	1·1	$1{\cdot}1\times10^{-4}$	0·53	$7{\cdot}5\times10^{-5}$
	3–1	...	$4{\cdot}1\times10^{-5}$	...	$3{\cdot}2\times10^{-5}$
	0–2	...	$4{\cdot}1\times10^{-5}$	...	$1{\cdot}5\times10^{-5}$
	1–2	0·036	$3{\cdot}1\times10^{-5}$	0·038	$1{\cdot}3\times10^{-5}$
	2–2	$1{\cdot}9\times10^{-4}$	$1{\cdot}3\times10^{-5}$	$1{\cdot}1\times10^{-4}$	$3{\cdot}5\times10^{-6}$
	3–2	0·71	$1{\cdot}3\times10^{-4}$	0·40	$6{\cdot}5\times10^{-5}$
	4–2	...	$1{\cdot}5\times10^{-5}$	...	$7{\cdot}1\times10^{-6}$
^3_4P–^3_4P	0–1	0·014	...	$7{\cdot}5\times10^{-3}$	...
	0–2	...	$6{\cdot}1\times10^{-9}$	...	$8{\cdot}4\times10^{-9}$
	1–2	0·045	$1{\cdot}3\times10^{-9}$	0·047	$1{\cdot}6\times10^{-9}$
^5D–^3H	2–4	...	v.s.	...	$1{\cdot}6\times10^{-6}$
	3–4	4×10^{-4}	v.s.	$8{\cdot}6\times10^{-4}$	$2{\cdot}7\times10^{-6}$
	4–4	$1{\cdot}1\times10^{-3}$	$5{\cdot}8\times10^{-7}$	$4{\cdot}8\times10^{-3}$	v.s.
	3–5	...	$1{\cdot}0\times10^{-6}$	...	$2{\cdot}8\times10^{-6}$
	4–5	1×10^{-5}	v.s.	v.s.	$3{\cdot}3\times10^{-6}$
	4–6	...	$8{\cdot}5\times10^{-6}$	...	$4{\cdot}7\times10^{-6}$
^3_4P–^3H	2–4	...	$2{\cdot}5\times10^{-10}$	...	$1{\cdot}3\times10^{-10}$
^3H–^3H	4–5	$6{\cdot}5\times10^{-4}$	$6{\cdot}9\times10^{-14}$	$1{\cdot}9\times10^{-4}$	$5{\cdot}3\times10^{-13}$
	4–6	...	$1{\cdot}0\times10^{-12}$	...	$3{\cdot}2\times10^{-13}$
	5–6	$5{\cdot}8\times10^{-4}$	$4{\cdot}1\times10^{-15}$	$4{\cdot}1\times10^{-4}$	$2{\cdot}5\times10^{-12}$

TABLE III (*continued*)

Transition		Fe V		Fe III	
		A_m	A_q	A_m	A_q
^5D–^3_4F	0–2	...	$2{\cdot}2\times10^{-5}$	...	$9{\cdot}3\times10^{-6}$
	1–2	0·10	$2{\cdot}6\times10^{-5}$	0·049	$1{\cdot}3\times10^{-5}$
	2–2	0·20	v.s.	0·10	v.s.
	3–2	0·047	$9{\cdot}0\times10^{-6}$	0·026	$8{\cdot}5\times10^{-6}$
	4–2	...	$1{\cdot}5\times10^{-6}$	...	$2{\cdot}1\times10^{-6}$
	1–3	...	$8{\cdot}6\times10^{-6}$	...	$1{\cdot}1\times10^{-5}$
	2–3	0·16	$1{\cdot}8\times10^{-5}$	0·087	$2{\cdot}4\times10^{-5}$
	3–3	0·40	$2{\cdot}0\times10^{-5}$	0·27	$6{\cdot}5\times10^{-6}$
	4–3	0·066	$2{\cdot}6\times10^{-5}$	0·038	$2{\cdot}7\times10^{-5}$
	2–4	...	$8{\cdot}6\times10^{-7}$	...	$7{\cdot}6\times10^{-6}$
	3–4	0·16	$1{\cdot}5\times10^{-5}$	0·081	$2{\cdot}4\times10^{-5}$
	4–4	0·74	$1{\cdot}3\times10^{-4}$	0·44	$6{\cdot}8\times10^{-5}$
^3_4P–^3_4F	0–2	...	$1{\cdot}9\times10^{-7}$	...	$2{\cdot}5\times10^{-10}$
	1–2	$9{\cdot}4\times10^{-6}$	$2{\cdot}7\times10^{-8}$	$3{\cdot}0\times10^{-7}$	$3{\cdot}8\times10^{-9}$
	2–2	$3{\cdot}6\times10^{-7}$	$7{\cdot}3\times10^{-13}$	$2{\cdot}0\times10^{-5}$	$1{\cdot}5\times10^{-8}$
	1–3	...	$3{\cdot}8\times10^{-8}$	...	$3{\cdot}8\times10^{-9}$
	2–3	$1{\cdot}5\times10^{-7}$	$9{\cdot}0\times10^{-12}$	$2{\cdot}9\times10^{-6}$	$7{\cdot}9\times10^{-8}$
	2–4	...	$7{\cdot}7\times10^{-11}$	...	$2{\cdot}0\times10^{-7}$
^3H–^3_4F	4–2	...	$6{\cdot}7\times10^{-8}$	...	$2{\cdot}8\times10^{-8}$
	4–3	$1{\cdot}1\times10^{-3}$	$8{\cdot}2\times10^{-9}$	$7{\cdot}3\times10^{-4}$	$1{\cdot}0\times10^{-8}$
	5–3	...	$4{\cdot}5\times10^{-8}$	...	$1{\cdot}8\times10^{-8}$
	4–4	$4{\cdot}1\times10^{-3}$	$2{\cdot}2\times10^{-10}$	$1{\cdot}3\times10^{-3}$	$1{\cdot}0\times10^{-9}$
	5–4	$5{\cdot}8\times10^{-4}$	$5{\cdot}3\times10^{-9}$	$5{\cdot}9\times10^{-4}$	$7{\cdot}0\times10^{-9}$
	6–4	...	$2{\cdot}5\times10^{-8}$	...	$2{\cdot}0\times10^{-8}$
^3_4F–^3_4F	2–3	$1{\cdot}3\times10^{-5}$	$1{\cdot}7\times10^{-15}$	$1{\cdot}3\times10^{-4}$	$2{\cdot}9\times10^{-15}$
	2–4	...	$2{\cdot}4\times10^{-15}$	...	$1{\cdot}6\times10^{-12}$
	3–4	$4{\cdot}1\times10^{-5}$	$1{\cdot}1\times10^{-14}$	$3{\cdot}4\times10^{-4}$	$1{\cdot}1\times10^{-13}$
^5D–^3G	1–3	...	$2{\cdot}9\times10^{-5}$	...	$1{\cdot}2\times10^{-5}$
	2–3	$7{\cdot}0\times10^{-3}$	$5{\cdot}8\times10^{-5}$	$2{\cdot}7\times10^{-3}$	$2{\cdot}3\times10^{-5}$
	3–3	0·017	$9{\cdot}1\times10^{-6}$	$8{\cdot}0\times10^{-3}$	$2{\cdot}1\times10^{-5}$
	4–3	$2{\cdot}6\times10^{-3}$	v.s.	$7{\cdot}9\times10^{-4}$	$5{\cdot}9\times10^{-6}$
	2–4	...	$4{\cdot}7\times10^{-5}$	...	$2{\cdot}4\times10^{-5}$
	3–4	$7{\cdot}8\times10^{-3}$	$1{\cdot}1\times10^{-4}$	$3{\cdot}7\times10^{-3}$	$4{\cdot}9\times10^{-5}$
	4–4	0·032	$3{\cdot}6\times10^{-6}$	0·019	$4{\cdot}7\times10^{-5}$
	3–5	...	$5{\cdot}0\times10^{-5}$	...	$2{\cdot}8\times10^{-5}$
	4–5	$3{\cdot}5\times10^{-4}$	$1{\cdot}2\times10^{-4}$	$2{\cdot}4\times10^{-4}$	$9{\cdot}3\times10^{-5}$
^3_4P–^3G	1–3	...	$3{\cdot}8\times10^{-8}$	...	$1{\cdot}7\times10^{-8}$
	2–3	$4{\cdot}6\times10^{-6}$	$5{\cdot}9\times10^{-9}$	v.s.	$1{\cdot}3\times10^{-8}$
	2–4	...	$4{\cdot}7\times10^{-9}$	...	$1{\cdot}7\times10^{-7}$
^3H–^3G	4–3	0·036	$5{\cdot}9\times10^{-5}$	0·044	$7{\cdot}4\times10^{-5}$
	5–3	...	$2{\cdot}3\times10^{-6}$	...	$1{\cdot}5\times10^{-5}$
	4–4	0·033	$7{\cdot}6\times10^{-6}$	0·025	$1{\cdot}1\times10^{-5}$
	5–4	$3{\cdot}9\times10^{-4}$	$5{\cdot}6\times10^{-5}$	$1{\cdot}5\times10^{-4}$	$6{\cdot}3\times10^{-5}$
	6–4	...	$1{\cdot}7\times10^{-6}$	...	$1{\cdot}5\times10^{-5}$
	4–5	$1{\cdot}2\times10^{-3}$	$8{\cdot}5\times10^{-8}$	$2{\cdot}7\times10^{-4}$	$1{\cdot}7\times10^{-7}$
	5–5	0·041	$5{\cdot}2\times10^{-6}$	0·029	$8{\cdot}0\times10^{-6}$
	6–5	0·041	$6{\cdot}1\times10^{-5}$	0·042	$6{\cdot}9\times10^{-5}$

TABLE III (*continued*)

Transition		Fe V		Fe III	
		A_m	A_q	A_m	A_q
$^3_4$F–^{3}G	2–3	0·030	$4·4\times10^{-7}$	0·025	$1·1\times10^{-6}$
	3–3	0·037	$8·1\times10^{-8}$	0·039	$4·6\times10^{-7}$
	4–3	$2·2\times10^{-4}$	$5·5\times10^{-8}$	$1·5\times10^{-3}$	$7·8\times10^{-7}$
	2–4	...	$4·4\times10^{-8}$	...	$2·4\times10^{-7}$
	3–4	$7·3\times10^{-4}$	$5·8\times10^{-7}$	$3·2\times10^{-6}$	$7·0\times10^{-7}$
	4–4	0·027	$4·5\times10^{-8}$	0·037	$1·2\times10^{-7}$
	3–5	...	$3·0\times10^{-8}$	...	$1·6\times10^{-7}$
	4–5	0·037	$9·2\times10^{-7}$	0·023	$8·5\times10^{-7}$
^{3}G–^{3}G	3–4	$9·2\times10^{-4}$	$2·9\times10^{-13}$	$2·6\times10^{-4}$	$5·5\times10^{-13}$
	3–5	...	$1·3\times10^{-12}$	...	$1·8\times10^{-11}$
	4–5	$4·4\times10^{-4}$	$2·4\times10^{-13}$	$1·4\times10^{-3}$	$1·5\times10^{-11}$
^{5}D–^{3}D	0–1	0·22	...	0·13	...
	1–1	0·19	$2·1\times10^{-4}$	0·15	$1·5\times10^{-4}$
	2–1	$1·9\times10^{-3}$	$4·2\times10^{-5}$	$1·3\times10^{-3}$	$3·3\times10^{-5}$
	3–1	...	$4·4\times10^{-5}$	...	$4·1\times10^{-5}$
	0–2	...	$5·7\times10^{-5}$	...	$3·8\times10^{-5}$
	1–2	0·20	v.s.	0·095	v.s.
	2–2	0·18	$2·4\times10^{-4}$	0·11	$2·2\times10^{-4}$
	3–2	0·11	$1·7\times10^{-5}$	0·027	$1·7\times10^{-5}$
	4–2	...	$1·9\times10^{-4}$	...	$1·7\times10^{-4}$
	1–3	...	$2·6\times10^{-5}$	...	$2·1\times10^{-5}$
	2–3	0·097	v.s.	0·044	v.s.
	3–3	0·089	$3·4\times10^{-4}$	0·047	$3·0\times10^{-4}$
	4–3	0·37	$7·1\times10^{-4}$	0·23	$5·8\times10^{-4}$
$^3_4$P–^{3}D	0–1	0·049	...	0·023	...
	1–1	0·12	$2·2\times10^{-4}$	0·085	$1·5\times10^{-4}$
	2–1	0·036	$2·2\times10^{-5}$	0·019	$1·2\times10^{-4}$
	0–2	...	$1·6\times10^{-4}$	...	$4·5\times10^{-5}$
	1–2	$7·8\times10^{-4}$	$3·1\times10^{-5}$	$2·6\times10^{-4}$	$1·4\times10^{-5}$
	2–2	0·052	$7·0\times10^{-5}$	0·066	$2·7\times10^{-4}$
	1–3	...	$9·4\times10^{-5}$	...	$6·7\times10^{-5}$
	2–3	0·056	$8·3\times10^{-5}$	0·063	$2·8\times10^{-4}$
^{3}H–^{3}D	4–2	...	$6·4\times10^{-5}$	...	$2·1\times10^{-4}$
	4–3	$5·8\times10^{-5}$	$5·7\times10^{-5}$	$1·0\times10^{-4}$	$5·5\times10^{-6}$
	5–3	...	$1·1\times10^{-4}$	...	$1·6\times10^{-4}$
$^3_4$F–^{3}D	2–1	0·014	$1·7\times10^{-3}$	$3·7\times10^{-3}$	$1·6\times10^{-3}$
	3–1	...	$3·4\times10^{-4}$	...	$1·4\times10^{-3}$
	2–2	0·017	$6·8\times10^{-4}$	$2·0\times10^{-3}$	$7·2\times10^{-4}$
	3–2	$1·6\times10^{-3}$	$1·4\times10^{-3}$	$1·2\times10^{-3}$	$1·0\times10^{-3}$
	4–2	...	$2·0\times10^{-4}$	...	$1·0\times10^{-3}$
	2–3	$5·6\times10^{-5}$	$4·3\times10^{-5}$	$1·3\times10^{-3}$	$5·6\times10^{-5}$
	3–3	$6·4\times10^{-3}$	$4·9\times10^{-4}$	$3·8\times10^{-3}$	$5·7\times10^{-4}$
	4–3	$6·9\times10^{-3}$	$1·9\times10^{-3}$	$6·6\times10^{-3}$	$1·9\times10^{-3}$
^{3}G–^{3}D	3–1	...	$6·5\times10^{-4}$	...	$2·2\times10^{-4}$
	3–2	$9·4\times10^{-5}$	$4·0\times10^{-5}$	$4·9\times10^{-6}$	$6·5\times10^{-5}$
	4–2	...	$3·7\times10^{-4}$	...	$2·2\times10^{-4}$
	3–3	$1·8\times10^{-6}$	$1·3\times10^{-7}$	v.s.	$7·1\times10^{-6}$
	4–3	$8·3\times10^{-6}$	$1·4\times10^{-5}$	$5·2\times10^{-5}$	$8·0\times10^{-5}$
	5–3	...	$2·5\times10^{-4}$	...	$4·3\times10^{-4}$

TABLE III (*continued*)

Transition		Fe V		Fe III	
		A_m	A_q	A_m	A_q
^3D–^3D	2–1	$1{\cdot}0\times10^{-4}$	$2{\cdot}3\times10^{-14}$	$3{\cdot}9\times10^{-8}$	$5{\cdot}3\times10^{-20}$
	3–1	...	$9{\cdot}6\times10^{-15}$	...	$2{\cdot}5\times10^{-15}$
	3–2	$3{\cdot}3\times10^{-5}$	$1{\cdot}6\times10^{-15}$	$5{\cdot}0\times10^{-5}$	$2{\cdot}6\times10^{-14}$
^3H–^1I	4–6	...	$1{\cdot}1\times10^{-6}$	...	$1{\cdot}2\times10^{-6}$
	5–6	0·11	v.s.	0·058	$5{\cdot}9\times10^{-7}$
	6–6	0·14	$2{\cdot}1\times10^{-6}$	0·089	$1{\cdot}8\times10^{-6}$
^3_4F–^1I	4–6	...	$2{\cdot}5\times10^{-6}$	...	$2{\cdot}3\times10^{-6}$
^3G–^1I	4–6	...	$3{\cdot}4\times10^{-7}$	...	$2{\cdot}3\times10^{-9}$
	5–6	$2{\cdot}8\times10^{-4}$	$8{\cdot}7\times10^{-7}$	$2{\cdot}0\times10^{-4}$	$5{\cdot}4\times10^{-7}$
^5D–^1_4G	2–4	...	v.s.	...	v.s.
	3–4	7×10^{-4}	v.s.	$3{\cdot}0\times10^{-4}$	v.s.
	4–4	$4{\cdot}6\times10^{-3}$	v.s.	$2{\cdot}2\times10^{-3}$	v.s.
^3_4P–^1_4G	2–4	...	$3{\cdot}2\times10^{-7}$	...	$1{\cdot}5\times10^{-6}$
^3H–^1_4G	4–4	0·18	$8{\cdot}4\times10^{-6}$	0·081	$7{\cdot}8\times10^{-6}$
	5–4	0·25	$2{\cdot}3\times10^{-5}$	0·20	$8{\cdot}4\times10^{-6}$
	6–4	...	$1{\cdot}6\times10^{-5}$	...	$1{\cdot}7\times10^{-5}$
^3_4F–^1_4G	2–4	...	$1{\cdot}6\times10^{-7}$	...	$4{\cdot}7\times10^{-8}$
	3–4	0·15	$1{\cdot}3\times10^{-7}$	0·12	$8{\cdot}1\times10^{-7}$
	4–4	0·32	$1{\cdot}1\times10^{-6}$	0·23	$1{\cdot}3\times10^{-7}$
^3G–^1_4G	3–4	0·042	$1{\cdot}4\times10^{-6}$	$1{\cdot}7\times10^{-4}$	$4{\cdot}6\times10^{-7}$
	4–4	$6{\cdot}4\times10^{-3}$	$1{\cdot}6\times10^{-8}$	$3{\cdot}3\times10^{-4}$	$2{\cdot}7\times10^{-7}$
	5–4	0·026	$1{\cdot}6\times10^{-7}$	$4{\cdot}3\times10^{-4}$	$5{\cdot}3\times10^{-8}$
^3D–^1_4G	2–4	...	$7{\cdot}6\times10^{-13}$	...	$3{\cdot}4\times10^{-16}$
	3–4	$3{\cdot}6\times10^{-8}$	$1{\cdot}5\times10^{-11}$	$1{\cdot}3\times10^{-12}$	$1{\cdot}1\times10^{-15}$
^1I–^1_4G	6–4	...	$1{\cdot}7\times10^{-12}$	...	$3{\cdot}0\times10^{-10}$
^3_4P–^1_4S	1–0	1·7	...	1·5	...
	2–0	...	$7{\cdot}7\times10^{-5}$	...	$2{\cdot}0\times10^{-4}$
^3_4F–^1_4S	2–0	...	$8{\cdot}8\times10^{-6}$	...	$5{\cdot}3\times10^{-6}$
^3D–^1_4S	1–0	$3{\cdot}3\times10^{-5}$	...	$4{\cdot}2\times10^{-5}$	...
	2–0	...	$7{\cdot}8\times10^{-7}$	...	$6{\cdot}7\times10^{-7}$
^3_4P–^1_4D	0–2	...	$8{\cdot}1\times10^{-5}$	...	$4{\cdot}9\times10^{-5}$
	1–2	0·062	$9{\cdot}6\times10^{-5}$	0·033	$3{\cdot}7\times10^{-5}$
	2–2	0·18	$3{\cdot}1\times10^{-6}$	0·096	$3{\cdot}1\times10^{-6}$
^3H–^1_4D	4–2	...	$3{\cdot}3\times10^{-4}$	...	$8{\cdot}2\times10^{-5}$
^3F–^1_4D	2–2	0·21	$7{\cdot}9\times10^{-6}$	0·12	$2{\cdot}0\times10^{-6}$
	3–2	0·42	$3{\cdot}1\times10^{-4}$	0·22	$9{\cdot}8\times10^{-5}$
	4–2	...	$2{\cdot}1\times10^{-5}$	...	$1{\cdot}2\times10^{-7}$

TABLE III (*continued*)

Transitions		Fe V		Fe III	
		A_m	A_q	A_m	A_q
^3G–^1_4D	3–2	$9{\cdot}5\times10^{-3}$	$2{\cdot}6\times10^{-5}$	$2{\cdot}5\times10^{-3}$	$2{\cdot}0\times10^{-5}$
	4–2	...	$1{\cdot}4\times10^{-5}$	...	$3{\cdot}0\times10^{-5}$
^3D–^1_4D	1–2	0·080	$1{\cdot}1\times10^{-6}$	0·021	$2{\cdot}7\times10^{-7}$
	2–2	0·017	$2{\cdot}5\times10^{-6}$	$3{\cdot}7\times10^{-3}$	$5{\cdot}6\times10^{-7}$
	3–2	0·090	$6{\cdot}5\times10^{-6}$	0·020	$9{\cdot}9\times10^{-7}$
^1_4G–^1_4D	4–2	...	$2{\cdot}0\times10^{-4}$	...	$5{\cdot}3\times10^{-5}$
^1_4S–^1_4D	0–2	...	$1{\cdot}9\times10^{-6}$	...	$1{\cdot}1\times10^{-8}$
^3_4P–^1F	1–3	...	$1{\cdot}4\times10^{-4}$	...	$1{\cdot}5\times10^{-4}$
	2–3	$1{\cdot}0\times10^{-3}$	$4{\cdot}7\times10^{-6}$	$5{\cdot}4\times10^{-4}$	$2{\cdot}0\times10^{-6}$
^3H–^1F	4–3	$4{\cdot}0\times10^{-3}$	$1{\cdot}5\times10^{-3}$	$3{\cdot}5\times10^{-3}$	$8{\cdot}9\times10^{-4}$
	5–3	...	$1{\cdot}8\times10^{-3}$	...	$2{\cdot}8\times10^{-3}$
^3_4F–^1F	2–3	$2{\cdot}0\times10^{-4}$	$1{\cdot}2\times10^{-3}$	$4{\cdot}4\times10^{-4}$	$1{\cdot}0\times10^{-3}$
	3–3	$5{\cdot}1\times10^{-3}$	$7{\cdot}8\times10^{-4}$	$1{\cdot}9\times10^{-3}$	$1{\cdot}3\times10^{-3}$
	4–3	0·012	$1{\cdot}2\times10^{-3}$	$5{\cdot}6\times10^{-3}$	$4{\cdot}8\times10^{-4}$
^3G–^1F	3–3	0·12	$7{\cdot}2\times10^{-4}$	0·050	$2{\cdot}0\times10^{-4}$
	4–3	0·17	$1{\cdot}0\times10^{-4}$	0·098	$7{\cdot}1\times10^{-4}$
	5–3	...	$6{\cdot}3\times10^{-4}$	...	$2{\cdot}2\times10^{-4}$
^3D–^1F	1–3	...	$1{\cdot}3\times10^{-5}$	...	$8{\cdot}2\times10^{-6}$
	2–3	0·070	$9{\cdot}9\times10^{-5}$	0·034	$7{\cdot}1\times10^{-5}$
	3–3	0·15	$4{\cdot}0\times10^{-5}$	0·061	$1{\cdot}7\times10^{-5}$
^1_4G–^1F	4–3	v.s.	$4{\cdot}8\times10^{-3}$	v.s.	$3{\cdot}7\times10^{-3}$
^1_4D–^1F	2–3	v.s.	$3{\cdot}2\times10^{-4}$	v.s.	$5{\cdot}9\times10^{-4}$

TABLE IV

Transition probabilities for multiplets

Multiplet	Fe V		Fe III	
	A_m	A_q	A_m	A_q
^5D–^3_2F	0·16	$5{\cdot}9\times10^{-3}$	0·077	$4{\cdot}4\times10^{-3}$
^3_4P–^3_2F	v.s.	0·22	v.s.	0·18
^3H–^3_2F	$2{\cdot}7\times10^{-3}$	1·8	$1{\cdot}2\times10^{-3}$	1·3
^3_4F–^3_2F	0·15	0·89	0·096	0·66
^3G–^3_2F	0·27	0·83	0·15	0·57
^3D–^3_2F	0·26	0·015	0·097	$9{\cdot}0\times10^{-3}$
^1I–^3_2F	...	$6{\cdot}0\times10^{-6}$	...	$1{\cdot}2\times10^{-5}$
^1_4G–^3_2F	0·022	$1{\cdot}0\times10^{-3}$	$6{\cdot}0\times10^{-3}$	$7{\cdot}0\times10^{-4}$
^1_4S–^3_2F	...	$1{\cdot}1\times10^{-5}$	...	$1{\cdot}2\times10^{-5}$
^1_4D–^3_2F	0·035	$1{\cdot}2\times10^{-4}$	0·016	$1{\cdot}1\times10^{-4}$
^1F–^3_2F	0·081	$8{\cdot}7\times10^{-6}$	0·048	$5{\cdot}9\times10^{-6}$

TABLE IV (*continued*)

Multiplet	Fe V		Fe III	
	A_m	A_q	A_m	A_q
$^5D-^3P$	0·62	0·014	0·36	0·010
$^3P-^3P$	0·035	1·0	0·022	0·82
$^3H-^3P$	...	$7·2\times10^{-5}$	...	$7·8\times10^{-4}$
$^3F-^3P$	v.s.	0·13	v.s.	0·11
$^3G-^3P$	v.s.	$3·1\times10^{-3}$	v.s.	$1·7\times10^{-3}$
$^3D-^3P$	0·19	0·51	0·097	0·30
$^1G-^3P$	...	$4·2\times10^{-4}$	...	$3·3\times10^{-4}$
$^1S-^3P$	0·043	$8·9\times10^{-5}$	0·026	$6·1\times10^{-5}$
$^1D-^3P$	0·14	$2·9\times10^{-4}$	0·11	$2·4\times10^{-4}$
$^1F-^3P$	$1·1\times10^{-5}$	$1·1\times10^{-5}$	$7·2\times10^{-6}$	$4·4\times10^{-6}$
$^3F-^1P$	*	*	*	*
$^3P-^1G$	...	$1·6\times10^{-3}$	...	$1·6\times10^{-3}$
$^3H-^1G$	0·37	$6·6\times10^{-3}$	0·14	$3·8\times10^{-3}$
$^3F-^1G$	0·42	$2·0\times10^{-3}$	0·19	$9·9\times10^{-4}$
$^3G-^1G$	0·44	$4·7\times10^{-3}$	0·39	$4·5\times10^{-3}$
$^3D-^1G$	$1·7\times10^{-3}$	$2·3\times10^{-3}$	$7·5\times10^{-4}$	$1·5\times10^{-3}$
$^1I-^1G$	...	1·9	...	1·4
$^1G-^1G$	v.s.	0·20	$4·6\times10^{-4}$	0·13
$^1D-^1G$	...	0·025	...	0·021
$^1F-^1G$	$1·7\times10^{-3}$	0·071	$1·1\times10^{-3}$	0·044
$^3F-^1G$	0·076	$2·3\times10^{-5}$	0·040	$1·6\times10^{-5}$
$^3P-^1G$	...	$4·3\times10^{-6}$	...	$1·7\times10^{-6}$
$^3P-^1D$	0·086	0·027	0·055	0·027
$^3H-^1D$	...	0·091	...	0·11
$^3F-^1D$	v.s.	0·15	$2·7\times10^{-3}$	0·15
$^3G-^1D$	v.s.	0·13	v.s.	$1·4\times10^{-3}$
$^3D-^1D$	1·1	0·056	0·61	0·036
$^1G-^1D$	...	15·9	...	11·4
$^1S-^1D$	...	1·4	...	0·96
$^1D-^1D$	$7·0\times10^{-3}$	4·3	v.s.	3·5
$^1F-^1D$	$3·3\times10^{-3}$	0·71	$1·7\times10^{-3}$	0·50
$^3F-^1D$	0·20	$3·5\times10^{-3}$	0·10	$3·5\times10^{-3}$
$^3P-^1D$	0·11	$6·7\times10^{-4}$	0·061	$5·7\times10^{-4}$
$^1G-^1D$	...	0·37	...	0·29
$^3P-^1S$	0·44	0·020	0·12	0·021
$^3F-^1S$	...	0·11	...	0·090
$^3D-^1S$	v.s.	0·43	v.s.	0·29
$^1D-^1S$	...	33·0	...	25·9
$^3F-^1S$	...	$1·4\times10^{-3}$	...	$6·6\times10^{-4}$
$^3P-^1S$	3·3	0·032	1·9	0·023
$^1D-^1S$	...	3·2	...	2·3

* Transition probabilities cannot be quoted for the $^3F-^3P$ multiplet because the two terms overlap. The transition probabilities of the individual lines are all small, not greater than 10^{-6} sec^{-1}, and are unlikely to be of any importance.

to repeat the calculations for various reasonable values of the parameters, and examine the changes in the transition probabilities. This approach is not practicable, however, as the labour involved would be prohibitive. Previous experience with simpler atoms suggests that the strengths of the stronger lines should be accurate to better than ±50 per cent, but the weaker lines may be uncertain by larger amounts.

4. *Relative intensities in multiplets.*—It is interesting to examine Table III and the data on which Table IV is based to see whether any general rules are suggested regarding relative intensities in multiplets. Among the triplet–triplet transitions are several in which electric quadrupole radiation is stronger than magnetic dipole radiation, the former being permitted in LS-coupling for these transitions, the latter arising only through departures from LS-coupling. In these cases transitions with $\Delta L = \Delta J$ are the strongest. This is as expected by the usual formulae for relative intensities in electric quadrupole multiplets. For the remaining triplet–triplet transitions and for triplet–quintet transitions magnetic dipole radiation predominates, and in these cases there appears to be no rule by which the strongest transitions can be predicted. For the singlet–triplet transitions ($\Delta S = +1$) the combinations ($\Delta L = -1$, $\Delta J = 0$), ($\Delta L = 0$, $\Delta J = +1$) and ($\Delta L = +1$, $\Delta J = +1$) give the strongest lines, but there are a few exceptions to these rules. There is no obvious theoretical reason why any particular rules should hold; the intensities depend on the precise nature of the departures from LS-coupling in the configuration concerned.

In his paper on η Carinae (**28**) Thackeray pointed out that for his observed [Fe II] transitions between terms of the same multiplicity $\Delta J = \Delta L$ gives the strongest lines. This suggests that most of these transitions are due predominately to electric quadrupole radiation.

5. *Comparison with observations.*—[Fe III] lines were first identified by Edlén and Swings (**7**) following their analysis of the Fe III spectrum (**8**). They showed that five strong lines of previously unknown origin in RY Scuti (**11**) could be ascribed to the ^{5}D–^{3}F multiplet of [Fe III]. The strongest line was present in a number of other objects. [Fe III] and [Fe V] were tentatively identified by Dufay and Bloch (**5**) in Nova DQ Herculis 1934. The first star found to have strong [Fe V] lines was AX Persei, studied by Swings and Struve (**22, 23**). Many objects are now known with either or both [Fe III] and [Fe V]; among them are RY Scuti (**8, 11, 19, 26**), BF Cygni (**1, 12, 23, 24, 27**), AX Persei (**22, 23**), RR Telescopii (**28, 29**), η Carinae (**28, 29**), FR Scuti (**3**), MWC 17 (**20**), MWC 349 (**21**), Z Andromedae (**13**), R Aquarii (**20**), the Orion Nebula (**25, 33**) and NGC 7027 (**2**). [Fe III] and [Fe V] have also been observed, usually blended, in various novae, and other peculiar stars and nebulae show the one or two strongest lines of these ions.

The most extensive data available for comparison with the theory are for the ^{5}D–$^3_4$F multiplet of [Fe III]. Much of the available data for this multiplet are collected in Table V. The theoretical intensity is on a scale on which λ4658 is taken as 100, and it is further supposed that a Boltzmann distribution is valid between the three levels $^3_4$F$_2$, $^3_4$F$_3$, $^3_4$F$_4$. The observed intensities are quoted directly, no attempt being made to place them on a common scale. The general agreement between theoretical and observed intensities is remarkably good, and may be interpreted as confirming the theoretical intensities. It also suggests that there are no very substantial departures from the Boltzmann distribution

TABLE V

Intensities of [Fe III] *multiplet* ^5D–^3_4F *in celestial spectra*

J ^5D	J ^3_4F	λ	Theory	1	2	3	4	5	6	7	8	9	10
0	2	4800	0·0012				1						
1	2	4778	6	0		0·83	1–2				0·7		
2	2	4734	13	1	4	bl	3	1	0·5	5	0·6	2	P
3	2	4667	3	0			bl		1	5	0·4		
4	2	4574	0·0003	0?							0·3		
1	3	4814	0·0019				bl				bl		
2	3	4769	15	1	4	1·2	2		0·5	2	0·8	1·5	
3	3	4702	48	3	14	6·8	5	2	2	10	0·8	7	P
4	3	4607	7	0	9		0?			8	0·5		0·5
2	4	4824	0·0017							6			
3	4	4755	18	1	6	2·5	3		1		0·9	2	0·4
4	4	4658	100	5	20	13·4	8	5	6	15	1·5	14	1·6

1. RY Scuti (**19**)
2. RY Scuti (**26**)
3. BF Cygni, 1950 July 15 (**1**)
4. BF Cygni (**23**)
5. FR Scuti (**3**)
6. RR Telescopii (**28**)
7. Nova Herculis 1934 (**6**)
8. Orion Nebula (**33**)
9. Orion Nebula (**25**)
10. NGC 7027 (**2**)

in the ^3F term. Lines of the ^5D–^3_4P multiplet of [Fe III] and of the ^5D–^3_4F and ^5D–^3_4P multiplets of [Fe V] are observed in various objects, and the theoretical and observed relative intensities are in general agreement. Special mention must be made of observations of the spectrum of RR Telescopii in 1956. Dr A. D. Thackeray kindly sent to the writer prints of an excellent plate showing the [Fe V] spectrum in great strength: all the strong predicted lines of the ^5D–^3_4P and ^5D–^3_4F multiplets are present with approximately correct relative intensities.

Several other points should be noted:

(*a*) The low transition probabilities of the ^5D–^3H and ^5D–^3G multiplets provide a reasonable explanation of the weakness or absence of these multiplets in the various celestial spectra (e.g. (**22**)).

(*b*) The absence of the ^5D–^3D multiplet of [Fe III] in BF Cygni (**24**), the Orion Nebula (**8**) and other objects cannot be explained by low transition probabilities, the values of the latter being comparable with those for observed multiplets.

(*c*) The identifications of λ4800 in BF Cygni (**23**) as the $^5D_0$–$^3_4F_2$ transition of [Fe III] and of λ3736 in AX Persei (**23**) as the $^5D_0$–$^3_4F_2$ transition of [Fe V] are not supported by the theoretical probabilities of these transitions.

(*d*) The identification of λ5057 in various objects as the $^5D_1$–$^3_4P_1$ transition of [Fe III] is not confirmed.

(*e*) The identification of λ4986 and λ5033 in RY Scuti (**19**) as lines of the ^5D–^3H multiplet of [Fe III] seems unlikely in view of the low probabilities of these transitions.

Acknowledgments.—The writer is greatly indebted to Dr D. E. Osterbrock for checking the spin–orbit matrix and for several valuable discussions while we both were at Yerkes Observatory. Thanks are due to Professor D. R. Hartree

for providing estimates of the radial quadrupole integrals and to Dr A. D. Thackeray for sending prints of the spectrum of RR Tel. The persistent requests of Dr L. H. Aller and Dr P. Swings for information on the transition probabilities of forbidden iron lines have been a source of much encouragement during the performance of these very laborious calculations.

University of London Observatory,
Mill Hill Park, London, N.W.7:
1957 *February* 28.

References

(1) L. H. Aller, *Pub. Dom. Astrophys. Obs.*, **9**, 321, 1954.
(2) L. H. Aller, I. S. Bowen and R. Minkowski, *Ap. J.*, **122**, 62, 1955.
(3) W. P. Bidelman and C. B. Stephenson, *P.A.S.P.*, **68**, 152, 1956.
(4) C. V. L. Charlier, *Mechanik des Himmels*, Band 1, 378, 1902.
(5) J. Dufay and M. Bloch, *Ann. d'Astrophys.*, **3**, 1, 1940.
(6) J. Dufay and M. Bloch, *Ann. d'Astrophys.*, **10**, 29, 1947.
(7) B. Edlén and P. Swings, *The Observatory*, **62**, 234, 1939.
(8) B. Edlén and P. Swings, *Ap. J.*, **95**, 532, 1942.
(9) R. H. Garstang, *Vistas in Astronomy*, Pergamon Press, London, Vol. 1, p. 268, 1955.
(10) R. H. Garstang, *Proc. Camb. Phil. Soc.*, **53**, 214, 1957.
(11) P. W. Merrill, *Ap. J.*, **67**, 179, 1928.
(12) P. W. Merrill, *Ap. J.*, **98**, 334, 1943.
(13) P. W. Merrill, *Ap. J.*, **107**, 317, 1948.
(14) Charlotte E. Moore, *Nat. Bur. Standards Circular* 467, Vol. II, 1952.
(15) S. Pasternack, *Ap. J.*, **92**, 129, 1940.
(16) G. Racah, *Phys. Rev.*, **62**, 438, 1942.
(17) G. Racah, *Phys. Rev.*, **63**, 367, 1943.
(18) G. H. Shortley, *Phys. Rev.*, **57**, 225, 1940.
(19) P. Swings and O. Struve, *Ap. J.*, **91**, 546, 1940.
(20) P. Swings and O. Struve, *Ap. J.*, **93**, 349, 1941.
(21) P. Swings and O. Struve, *Ap. J.*, **95**, 159, 1942.
(22) P. Swings and O. Struve, *Ap. J.*, **96**, 254, 1942.
(23) P. Swings and O. Struve, *Ap. J.*, **97**, 194, 1943.
(24) P. Swings and O. Struve, *Ap. J.*, **101**, 224, 1945.
(25) Tcheng Mao-Lin and J. Dufay, *Ann. d'Astrophys.*, **7**, 143, 1944.
(26) Tcheng Mao-Lin and M. Bloch, *Ann. d'Astrophys.*, **15**, 12, 1952.
(27) Tcheng Mao-Lin and M. Bloch, *Ann. d'Astrophys.*, **17**, 6, 1954.
(28) A. D. Thackeray, *M.N.*, **113**, 211, 1953.
(29) A. D. Thackeray, *M.N.*, **115**, 236, 1955.
(30) R. E. Trees, *Phys. Rev.*, **82**, 683, 1951.
(31) R. E. Trees, *Phys. Rev.*, **85**, 382, 1952.
(32) R. E. Trees and Marion M. Harvey, *J. Research Nat. Bur. Standards*, **49**, 397, 1952.
(33) A. B. Wyse, *Ap. J.*, **95**, 356, 1942.

PHOTOELECTRIC PHOTOMETRY OF GALACTIC CEPHEIDS

Olin J. Eggen, S. C. B. Gascoigne and E. J. Burr*

(Received 1957 January 28)

Summary

Photoelectric light curves have been observed in two colours for 26 galactic cepheids, and these, together with another four variables observed only near maximum and minimum and the 33 reported on in a previous paper, bring the total to 63 for which photoelectrically determined light curves are available. This number includes all the known, nearer cepheids. The relations between shape of light curve, amplitude and period length are re-examined and it is shown that the magnitudes used by Blaauw and Morgan in their discussion of the zero-point of the period-luminosity relation are too faint by $0^m.17$, relative to the International P_E-system.

---

1. *Introduction.*—A previous application of photoelectric photometry to cepheid variables (Eggen 1951) showed that little reliance could be placed on much of the photographic photometry of these stars except for the determination of periods. The photoelectrically-determined light curves indicated, among other things, a division of the classical cepheids into three sub-groups, but the need for more observations was clearly indicated. A second programme was accordingly commenced in 1951 by Eggen with the 9-inch Mt Stromlo refractor and continued by him with the 12-inch Lick refractor, and by Gascoigne and Burr with the 9-inch refractor and the 30-inch reflector at Mt Stromlo. In this programme emphasis was placed (i) on the brighter cepheids, since these would presumably be the least reddened by galactic absorption; (ii) on those of the longest periods, for comparison with similar cepheids in other galaxies; and (iii) on cepheids that might be expected to show population type II characteristics. The new programme has resulted in reasonably complete light curves for 26 cepheids which, together with an additional four variables observed only near maximum and minimum light, bring the total number for which photoelectrically determined light curves are available to 63. This number includes most of the known nearer cepheids.

The details of the observational procedure are discussed in Section 2 and the individual observations are set out in Table II and plotted in Figs. 1 to 4. The maxima and minima colours and magnitudes and other data relating to all 63 cepheids on this and the preceding programme are collected in Table IV. In Section 3 we discuss the correlations between shape of light curve, period length, and the light and colour amplitudes, and it is shown that the variables with asymmetric light curves have greater amplitudes, in general, than those with symmetric light curves. We also conclude that, because the magnitudes used were in the mean too faint, the zero-point of the period–luminosity relation derived by Blaauw and Morgan (1954) needs a correction of $-0^m.17$.

* Formerly at Lick Observatory, now at the Royal Greenwich Observatory.

2. *Observations.*—All of the colours and magnitudes in this paper are on the $(P, V)_E$-system which has previously been fully described (Eggen 1955); for convenience, $(P-V)_E$ has been abbreviated to C_E in the figures for this paper. The observations by Gascoigne and Burr were made with a 1P21 photomultiplier and photometer, on loan from the Lick Observatory, that are almost identical

TABLE I

Comparison stars for cepheid variables observed by Gascoigne and Burr

Comp.	Name	V_E	*A.D.*	$(P-V)_E$	*A.D.*	*n*
HR 1917	β Dor	5·33	±0·01	0·93	±0·005	4
HD 69066	RS Pup	6·88	·03	0·67	·01	7
HR 3445	RZ Vel, T Vel	3·78	·02	0·565	·015	5
HD 93306	VY Car	7·57	·03	0·95	·01	7
HR 3914	*l* Car	5·51	·02	1·21	·01	6
HD 108500	R Cru, T Cru	6·82	·02	0·54	·01	7
HD 109761	R Mus, S Mus	7·39	·02	0·81	·01	7
HD 161852	W Sgr, X Sgr, RY Sco	6·60	·02	0·25	·02	7
HR 7130	κ Pav	5·97	±0·03	0·90	±0·01	6

with those used by Eggen; their filters were 2 mm of Schott GG 11 for the yellow region and 1 mm of BG 12 with 1 mm of Chance OY 10 for the blue, the latter glass being used to exclude the ultra-violet region. The observational procedure used by Eggen has been previously described (1955). Gascoigne and Burr compared the cepheids with the stars listed in Table I; the magnitudes and colours of these stars were determined through observations of some bright stars and stars in Harvard *E*-Regions Nos. 3, 6 and 9, which had been observed at the Cape Observatory (1953), and the reduction to the $(P, V)_E$-system was made with the relations previously published (Eggen 1955).

TABLE II

Observations of cepheid variables; those designated by an asterisk were made by Gascoigne and Burr, the remainder by Eggen

SW Tauri $4^h\ 19^m{\cdot}3$, $+3°\ 54'$
Max = JD 2419730·3536 + $1^d{\cdot}5836468$ E

JD	Phase	*V*	*P*—*V*
	p	m	m
2434418·743	0·041	9·73	0·455
4334·944	0·126	9·38	0·36
3178·947	0·167	9·36	0·35
	0·146	9·37	0·355
2882·840	0·189	9·28	0·30
4369·889	0·192	9·36	0·345
2882·869	0·208	9·22	0·34
	0·196	9·29	0·33
2882·986	0·281	9·21	0·31
2887·736	0·281	9·38	0·32
2887·751	0·290	9·36	0·32
	0·284	9·32	0·315

SW Tauri (*continued*)

JD	Phase	*V*	*P*—*V*
	p	m	m
2887·809	0·327	9·35	0·365
2860·899	0·335	9·36	0·365
	0·331	9·36	0·365
3180·967	0·443	9·67	0·545
4425·736	0·457	9·71	0·545
	0·450	9·69	0·545
4341·934	0·540	9·78	0·60
3190·933	0·736	9·89	0·705
2883·759	0·770	9·93	0·705
	0·753	9·91	0·705
4424·710	0·809	10·10	0·705
2883·838	0·819	10·00	0·725
	0·814	10·05	0·715

SW Tauri (*continued*)

JD	Phase	V	$P-V$
	p	m	m
2883·865	0·900	10·06	0·69
3206·853	0·996	9·89	0·57

RX Aurigae $4^h\,54^m\cdot5$, $+39°.49'$
Max = JD 2420651·543 + $11^d\cdot623731$ E

JD	Phase	V	$P-V$
	p	m	m
2433216·917	0·010	7·34	0·68
4425·840	0·015	7·40	0·71
4460·705	0·015	7·39	0·68
	0·013	7·38	0·69
4428·809	0·185	7·41	0·75
4335·049	0·204	7·45	0·825
4369·941	0·206	7·44	0·805
	0·198	7·43	0·79
2882·976	0·281	7·50	0·83
2883·952	0·365	7·55	0·915
4337·016	0·374	7·58	0·895
	0·370	7·56	0·905
2861·005	0·391	7·64	0·935
4418·844	0·413	7·70	0·95
	0·402	7·67	0·94
2885·995	0·541	7·94	1·01
2944·903	0·609	8·06	1·00
4341·986	0·801	7·81	0·905
3181·031	0·923	7·63	0·795
4424·901	0·934	7·63	0·785
	0·928	7·63	0·79

SV Persei $4^h\,42^m\cdot8$, $+42°\,07'$
Max = JD 2419055·345 + $11^d\cdot128877$ E

JD	Phase	V_E	$(P-V)_E$
	p	m	m
2434424·783	0·041	8·65	0·80
2944·896	0·064	8·65	0·81
	0·052	8·65	0·805
3178·962	0·096	8·70	0·85
4425·769	0·135	8·74	0·915
4337·012	0·154	8·76	0·915
	0·144	8·75	0·915
3181·021	0·281	8·95	1·00
2947·791	0·324	9·00	1·00
4418·816	0·460	9·31	0·99
2860·865	0·513	9·33	1·02

SV Persei (*continued*)

JD	Phase	V_E	$P-V_E$
	p	m	m
2883·938	0·587	9·30	0·995
4341·958	0·599	9·30	1·02
	0·593	9·30	1·01
2885·979	0·770	8·99	0·865
2887·947	0·947	8·54	0·67
4335·042	0·977	8·55	0·72

β Doradus $5^h\,32^m\cdot7$, $-62°\,33'$
Max = JD 2426013·93 + $9^d\cdot842603$

JD	Phase	V	$P-V$
	p	m	m
2434705·147*	0·020	3·48	0·58
4420·080*	0·058	3·54	0·60
4449·958*	0·093	3·55	0·63
4834·016*	0·113	3·58	0·64
4451·009*	0·200	3·69	0·71
4844·952*	0·224	3·70	0·75
4422·044*	0·257	3·79	0·75
4451·957*	0·296	3·83	0·81
4826·083*	0·307	3·86	0·80
	0·302	3·84	0·805
4855·936*	0·340	3·91	0·82
4433·031*	0·373	3·93	0·89
4442·963*	0·383	3·97	0·89
	0·378	3·95	0·89
4462·974*	0·416	4·00	0·84
4434·050*	0·477	4·05	0·86
4700·158*	0·513	4·04	0·84
4463·994*	0·519	4·02	0·89
4847·942*	0·528	4·00	0·88
	0·520	4·02	0·87
4828·917*	0·596	3·93	0·76
4820·003*	0·689	3·78	0·67
4829·985*	0·704	3·75	0·66
4840·981*	0·821	3·58	0·65
4438·008*	0·879	3·56	0·54
4419·030*	0·951	3·39	0·46
4438·960*	0·976	3·40	0·52

RT Aurigae $6^h\,22^m\cdot1$, $+30°\,33'$
Max = JD 2420957·466 + $3^d\cdot728261$

JD	Phase	V_E	$(P-V)_E$
	p	m	m
2434342·049	0·034	5·08	0·31
4427·819	0·039	5·07	0·31
	0·036	5·08	0·31

RT Aurigae (*continued*)

JD	Phase	V_E	$(P-V)_E$
	p	m	m
3249·892	0·094	5·18	0·38
2825·012	0·132	5·21	0·41
3238·899	0·145	5·22	0·43
4335·062	0·160	5·27	0·465
4424·865	0·247	5·39	0·505
2833·028	0·282	5·41	0·515
2944·931	0·297	5·44	0·55
2822·007	0·326	5·47	0·57
3285·906	0·465	5·59	0·64
4425·856	0·513	5·70	0·675
2848·962	0·556	5·74	0·65
4459·728	0·598	5·72	0·665
3020·741	0·630	5·75	0·675
4418·885	0·643	5·75	0·68
2882·903	0·659	5·77	0·655
2841·975	0·682	5·77	0·675
3437·052	0·694	5·79	0·685
	0·688	5·78	0·68
2860·984	0·780	5·77	0·655
3233·920	0·810	5·74	0·595
4460·760	0·875	5·41	0·43
2883·896	0·926	5·26	0·365

AH Velorum $8^h\,08^m{\cdot}9$, $-46°\,21'$
Max = JD 2426145·708 + $4^d{\cdot}227172$ E

JD	Phase	V_E	$(P-V)_E$
	p	m	m
2433775·892	0·033	5·49	0·385
3776·889	0·269	5·66	0·49
4454·110*	0·476	5·85	0·50
3777·909	0·510	5·83	0·50
5841·212*	0·615	5·76	0·52
3778·901	0·745	5·75	0·485
3783·993	0·950	5·47	0·41

RS Puppis $8^h\,09^m{\cdot}2$, $-34°\,17'$
Max = JD 2427083·613 + $41^d{\cdot}414$ E

JD	Phase	V	$P-V$
	p	m	m
2435160·025*	0·017	6·58	1·22
4828·931*	0·022	6·63	1·22
	0·020	6·60	1·22
4829·996*	0·047	6·64	1·27
4871·987*	0·061	6·64	1·28
4872·972*	0·085	6·68	1·34
3796·896	0·102	6·74	1·32
4833·046*	0·121	6·75	1·33
	0·111	6·74	1·325

RS Puppis (*continued*)

JD	Phase	V	$P-V$
	p	m	m
4834·026*	0·145	6·82	1·36
4840·051*	0·290	7·02	1·48
4840·991*	0·313	7·05	1·50
4469·100*	0·330	7·07	1·51
3764·979	0·331	7·05	1·52
	0·330	7·06	1·515
4470·087*	0·357	7·06	1·55
4844·035*	0·386	7·16	1·59
4844·978*	0·409	7·16	1·57
4472·083*	0·405	7·19	1·53
	0·407	7·18	1·55
4847·985*	0·482	7·32	1·57
3775·915	0·595	7·53	1·61
3776·906	0·619	7·57	1·60
3777·943	0·644	7·59	1·63
3778·917	0·668	7·53	1·57
4855·979*	0·675	7·58	1·61
	0·672	7·56	1·59
4859·003*	0·748	7·34	1·45
4820·014*	0·806	6·84	1·19
4451·988*	0·920	6·45	1·05
4826·087*	0·953	6·49	1·08
4867·964*	0·964	6·55	1·10
	0·958	6·52	1·09

RZ Velorum $8^h\,33^m{\cdot}6$, $-43°\,46'$
Max = JD 2421057·710 + $20^d{\cdot}39645$ E

JD	Phase	V	$P-V$
	p	m	m
2433765·135	0·021	6·49	0·66
4826·115*	0·039	6·48	0·64
	0·030	6·485	0·65
4867·977*	0·092	6·57	0·78
4848·002*	0·112	6·65	0·80
4808·151*	0·159	6·74	0·88
4830·022*	0·231	6·84	1·03
4871·996*	0·289	6·91	1·12
4873·008*	0·338	7·07	1·18
4833·062*	0·380	7·10	1·24
4834·056*	0·429	7·21	1·25
3776·006	0·554	7·48	1·38
3796·910	0·579	7·51	1·39
3776·992	0·603	7·52	1·38
3778·040	0·654	7·61	1·40
3779·010	0·702	7·62	1·28
4820·036*	0·741	7·51	1·25
4844·081*	0·920	7·25	1·02
4844·997*	0·965	6·45	0·59

T Velorum $8^h\,34^m.4$, $-47°\,00'$
Max = JD 2426274·432 + 4^d·639769

JD	Phase	V	P–V
	p	m	m
2434872·001*	0·017	7·71	0·62
3797·005	0·018	7·67	0·605
	0·018	7·69	0·61
4826·107*	0·125	7·81	0·73
4840·058*	0·132	7·88	0·73
	0·128	7·84	0·73
4867·984*	0·151	7·84	0·75
4844·985*	0·194	7·93	0·78
4859·015*	0·218	7·97	0·77
4872·995*	0·231	7·97	0·83
	0·224	7·97	0·80
3778·070	0·245	7·99	0·785
4808·158*	0·257	8·02	0·80
	0·251	8·00	0·79
3796·915	0·305	8·10	0·85
3779·015	0·448	8·15	0·88
3765·140	0·455	8·16	0·875
	0·452	8·16	0·88
4855·991*	0·566	8·28	0·91
4833·069*	0·626	8·28	0·95
3776·010	0·800	8·25	0·87
4820·022*	0·814	8·09	0·75
4834·035*	0·834	8·07	0·74
4847·992*	0·842	8·01	0·75
	0·838	8·04	0·745
4830·003*	0·965	7·69	0·60
4844·069*	0·996	7·68	0·63

SW Velorum $08^h\,40^m.4$, $-47°\,02'$
Max = JD 2434872·95 + 23^d·473 E

JD	Phase	V	P–V
	p	m	m
2434872·999*	0·002	7·55	0·66
4830·007*	0·171	7·80	0·95
4808·170*	0·240	7·88	1·02
4833·072*	0·301	7·95	1·14
4834·040*	0·342	7·99	1·16
4840·063*	0·599	8·46	1·47
4844·988*	0·809	8·70	1·37
5481·238*	0·914	8·70	1·22
4847·995*	0·937	8·49	1·12
4872·004*	0·960	8·09	0·91

l Carinae $9^h\,42^m.5$, $-62°\,03'$
Max = JD 2427089·82 + 35^d·5323 E

JD	Phase	V	P–V
	p	m	m
2434872·010*	0·017	3·34	0·89
4873·030*	0·046	3·28	0·89
3775·986	0·171	3·44	1·04
4557·960*	0·179	3·40	1·04
	0·175	3·42	1·04
3776·988	0·200	3·44	1·09
4808·116*	0·219	3·47	1·09
	0·210	3·46	1·09
3778·035	0·229	3·49	1·12
3779·003	0·256	3·52	1·175
4845·004*	0·257	3·52	1·18
	0·256	3·52	1·18
4527·064*	0·309	3·60	1·20
3852·859	0·335	3·63	1·29
4848·016*	0·342	3·63	1·29
	0·338	3·63	1·29
3784·010	0·397	3·69	1·32
3855·877	0·420	3·75	1·335
4818·067*	0·499	3·84	1·35
4820·043*	0·555	3·91	1·38
4469·187*	0·681	3·99	1·35
4826·201*	0·722	4·01	1·32
3797·015	0·764	4·02	1·305
4472·166*	0·764	3·99	1·36
	0·764	4·00	1·33
4830·028*	0·835	4·00	1·29
3765·097	0·865	3·97	1·25
4867·989*	0·904	3·84	1·14
4833·084*	0·922	3·76	1·08
4087·153*	0·929	3·75	1·125
	0·926	3·76	1·10

VY Carinae $10^h\,40^m.6$, $-57°\,02'$
Max = JD 2434529·90 + 18^d·9370 E

JD	Phase	V	P–V
	p	m	m
2434833·099*	0·011	6·90	0·74
4928·072*	0·026	6·89	0·71
	0·018	6·90	0·725

VY Carinae (*continued*)

JD	Phase	V	$P-V$
	p	m	m
4834·136*	0·066	7·03	0·86
4873·018*	0·119	7·06	0·90
3851·900	0·197	7·27	1·06
3777·015	0·243	7·31	1·07
3796·920	0·294	7·44	1·11
3779·025	0·349	7·49	1·185
4557·981*	0·483	7·79	1·19
4845·018*	0·640	7·90	1·25
4560·989*	0·642	7·94	1·21
4920·971*	0·651	7·88	1·21
	0·644	7·91	1·22
4543·988*	0·744	7·76	1·10
4848·023*	0·799	7·65	1·03
4527·076*	0·851	7·64	0·96
4472·178*	0·952	6·87	0·67

S Muscae $12^h\,07^m\cdot4$, $-69°\,36'$

Max = JD 2419541·800 + $9^d\cdot658688$ E

JD	Phase	V	$P-V$
	p	m	m
2434833·142*	0·169	5·91	0·63
4544·030*	0·237	5·93	0·63
4921·003*	0·266	5·93	0·70
4950·000*	0·268	5·97	0·66
4834·163*	0·275	6·00	0·70
	0·270	5·97	0·69
4873·066*	0·303	6·03	0·70
4950·979*	0·370	6·14	0·72
4845·093*	0·407	6·15	0·75
4903·060*	0·408	6·14	0·75
	0·408	6·14	0·75
4527·110*	0·485	6·21	0·79
4952·949*	0·574	6·35	0·84
4953·943*	0·676	6·41	0·83
3852·943	0·686	6·40	0·82
4558·031*	0·686	6·45	0·83
	0·683	6·42	0·83
4848·086*	0·717	6·45	0·79
3776·118	0·723	6·40	0·78
	0·720	6·42	0·785
4926·043*	0·788	6·37	0·75
3777·095	0·833	6·20	0·67
4927·009*	0·888	6·13	0·68
4917·985*	0·954	5·98	0·59
3855·888	0·991	5·96	0·60
4561·019*	0·996	5·95	0·58
	0·994	5·96	0·59

T Crucis $12^h\,15^m\cdot9$, $-61°\,44'$

Max = JD 2427578·96 + $6^d\cdot733178$ E

JD	Phase	V	$P-V$
	p	m	m
2434925·008*	0·022	6·36	0·67
4845·069*	0·150	6·41	0·74
4925·949*	0·162	6·43	0·76
4952·969*	0·175	6·43	0·75
	0·162	6·43	0·75
3855·891	0·239	6·45	0·79
4873·045*	0·305	6·52	0·83
4953·934*	0·318	6·54	0·85
4927·017*	0·321	6·52	0·82
	0·315	6·53	0·83
4833·119*	0·375	6·57	0·89
3776·183	0·401	6·56	0·875
4920·992*	0·426	6·63	0·88
4544·015*	0·438	6·62	0·90
	0·432	6·62	0·89
4558·020*	0·518	6·70	0·95
4834·158*	0·529	6·69	0·93
	0·524	6·70	0·94
3777·186	0·550	6·69	0·935
4848·054*	0·593	6·72	0·92
4949·992*	0·733	6·80	0·92
3852·950	0·803	6·66	0·84
4950·967*	0·878	6·56	0·73
4527·096*	0·925	6·48	0·70
4561·003*	0·961	6·40	0·66
4917·999*	0·981	6·36	0·68
	0·971	6·38	0·67

R Crucis $12^h\,18^m\cdot1$, $-61°\,04'$

Max = JD 2419432·010 + $5^d\cdot825589$ E

JD	Phase	V	$P-V$
	p	m	m
2434544·007*	0·072	6·42	0·47
4527·091*	0·168	6·57	0·55
4848·058*	0·265	6·64	0·67
4917·994*	0·270	6·67	0·67
3776·185	0·270	6·66	0·665
4952·963*	0·272	6·69	0·68
	0·269	6·66	0·67
3776·986	0·408	6·80	0·765
4953·928*	0·438	6·81	0·78
4925·015*	0·475	6·89	0·80
4558·015*	0·476	6·88	0·78
	0·476	6·88	0·79

T Velorum $8^h\,34^m.4$, $-47°\,00'$
Max = JD 2426274·432 + 4^d·639769

JD	Phase	*V*	*P*–*V*
	p	m	m
2434872·001*	0·017	7·71	0·62
3797·005	0·018	7·67	0·605
	0·018	7·69	0·61
4826·107*	0·125	7·81	0·73
4840·058*	0·132	7·88	0·73
	0·128	7·84	0·73
4867·984*	0·151	7·84	0·75
4844·985*	0·194	7·93	0·78
4859·015*	0·218	7·97	0·77
4872·995*	0·231	7·97	0·83
	0·224	7·97	0·80
3778·070	0·245	7·99	0·785
4808·158*	0·257	8·02	0·80
	0·251	8·00	0·79
3796·915	0·305	8·10	0·85
3779·015	0·448	8·15	0·88
3765·140	0·455	8·16	0·875
	0·452	8·16	0·88
4855·991*	0·566	8·28	0·91
4833·069*	0·626	8·28	0·95
3776·010	0·800	8·25	0·87
4820·022*	0·814	8·09	0·75
4834·035*	0·834	8·07	0·74
4847·992*	0·842	8·01	0·75
	0·838	8·04	0·745
4830·003*	0·965	7·69	0·60
4844·069*	0·996	7·68	0·63

SW Velorum $08^h\,40^m.4$, $-47°\,02'$
Max = JD 2434872·95 + 23^d·473 E

JD	Phase	*V*	*P*–*V*
	p	m	m
2434872·999*	0·002	7·55	0·66
4830·007*	0·171	7·80	0·95
4808·170*	0·240	7·88	1·02
4833·072*	0·301	7·95	1·14
4834·040*	0·342	7·99	1·16
4840·063*	0·599	8·46	1·47
4844·988*	0·809	8·70	1·37
5481·238*	0·914	8·70	1·22
4847·995*	0·937	8·49	1·12
4872·004*	0·960	8·09	0·91

l Carinae $9^h\,42^m.5$, $-62°\,03'$
Max = JD 2427089·82 + 35^d·5323 E

JD	Phase	*V*	*P*–*V*
	p	m	m
2434872·010*	0·017	3·34	0·89
4873·030*	0·046	3·28	0·89
3775·986	0·171	3·44	1·04
4557·960*	0·179	3·40	1·04
	0·175	3·42	1·04
3776·988	0·200	3·44	1·09
4808·116*	0·219	3·47	1·09
	0·210	3·46	1·09
3778·035	0·229	3·49	1·12
3779·003	0·256	3·52	1·175
4845·004*	0·257	3·52	1·18
	0·256	3·52	1·18
4527·064*	0·309	3·60	1·20
3852·859	0·335	3·63	1·29
4848·016*	0·342	3·63	1·29
	0·338	3·63	1·29
3784·010	0·397	3·69	1·32
3855·877	0·420	3·75	1·335
4818·067*	0·499	3·84	1·35
4820·043*	0·555	3·91	1·38
4469·187*	0·681	3·99	1·35
4826·201*	0·722	4·01	1·32
3797·015	0·764	4·02	1·305
4472·166*	0·764	3·99	1·36
	0·764	4·00	1·33
4830·028*	0·835	4·00	1·29
3765·097	0·865	3·97	1·25
4867·989*	0·904	3·84	1·14
4833·084*	0·922	3·76	1·08
4087·153*	0·929	3·75	1·125
	0·926	3·76	1·10

VY Carinae $10^h\,40^m.6$, $-57°\,02'$
Max = JD 2434529·90 + 18^d·9370 E

JD	Phase	*V*	*P*–*V*
	p	m	m
2434833·099*	0·011	6·90	0·74
4928·072*	0·026	6·89	0·71
	0·018	6·90	0·725

VY Carinae (*continued*)

JD	Phase	V	$P-V$
	p	m	m
4834·136*	0·066	7·03	0·86
4873·018*	0·119	7·06	0·90
3851·900	0·197	7·27	1·06
3777·015	0·243	7·31	1·07
3796·920	0·294	7·44	1·11
3779·025	0·349	7·49	1·185
4557·981*	0·483	7·79	1·19
4845·018*	0·640	7·90	1·25
4560·989*	0·642	7·94	1·21
4920·971*	0·651	7·88	1·21
	0·644	7·91	1·22
4543·988*	0·744	7·76	1·10
4848·023*	0·799	7·65	1·03
4527·076*	0·851	7·64	0·96
4472·178*	0·952	6·87	0·67

S Muscae $12^h\,07^m\cdot4$, $-69°\,36'$

Max = JD 2419541·800 + $9^d\cdot658688$ E

JD	Phase	V	$P-V$
	p	m	m
2434833·142*	0·169	5·91	0·63
4544·030*	0·237	5·93	0·63
4921·003*	0·266	5·93	0·70
4950·000*	0·268	5·97	0·66
4834·163*	0·275	6·00	0·70
	0·270	5·97	0·69
4873·066*	0·303	6·03	0·70
4950·979*	0·370	6·14	0·72
4845·093*	0·407	6·15	0·75
4903·060*	0·408	6·14	0·75
	0·408	6·14	0·75
4527·110*	0·485	6·21	0·79
4952·949*	0·574	6·35	0·84
4953·943*	0·676	6·41	0·83
3852·943	0·686	6·40	0·82
4558·031*	0·686	6·45	0·83
	0·683	6·42	0·83
4848·086*	0·717	6·45	0·79
3776·118	0·723	6·40	0·78
	0·720	6·42	0·785
4926·043*	0·788	6·37	0·75
3777·095	0·833	6·20	0·67
4927·009*	0·888	6·13	0·68
4917·985*	0·954	5·98	0·59
3855·888	0·991	5·96	0·60
4561·019*	0·996	5·95	0·58
	0·994	5·96	0·59

T Crucis $12^h\,15^m\cdot9$, $-61°\,44'$

Max = JD 2427578·96 + $6^d\cdot733178$ E

JD	Phase	V	$P-V$
	p	m	m
2434925·008*	0·022	6·36	0·67
4845·069*	0·150	6·41	0·74
4925·949*	0·162	6·43	0·76
4952·969*	0·175	6·43	0·75
	0·162	6·43	0·75
3855·891	0·239	6·45	0·79
4873·045*	0·305	6·52	0·83
4953·934*	0·318	6·54	0·85
4927·017*	0·321	6·52	0·82
	0·315	6·53	0·83
4833·119*	0·375	6·57	0·89
3776·183	0·401	6·56	0·875
4920·992*	0·426	6·63	0·88
4544·015*	0·438	6·62	0·90
	0·432	6·62	0·89
4558·020*	0·518	6·70	0·95
4834·158*	0·529	6·69	0·93
	0·524	6·70	0·94
3777·186	0·550	6·69	0·935
4848·054*	0·593	6·72	0·92
4949·992*	0·733	6·80	0·92
3852·950	0·803	6·66	0·84
4950·967*	0·878	6·56	0·73
4527·096*	0·925	6·48	0·70
4561·003*	0·961	6·40	0·66
4917·999*	0·981	6·36	0·68
	0·971	6·38	0·67

R Crucis $12^h\,18^m\cdot1$, $-61°\,04'$

Max = JD 2419432·010 + $5^d\cdot825589$ E

JD	Phase	V	$P-V$
	p	m	m
2434544·007*	0·072	6·42	0·47
4527·091*	0·168	6·57	0·55
4848·058*	0·265	6·64	0·67
4917·994*	0·270	6·67	0·67
3776·185	0·270	6·66	0·665
4952·963*	0·272	6·69	0·68
	0·269	6·66	0·67
3776·986	0·408	6·80	0·765
4953·928*	0·438	6·81	0·78
4925·015*	0·475	6·89	0·80
4558·015*	0·476	6·88	0·78
	0·476	6·88	0·79

R Crucis (*continued*)

JD	Phase	*V*	(*P*–*V*)
	p	m	m
4873·053*	0·555	7·00	0·83
4825·947*	0·635	7·07	0·87
4833·129*	0·702	7·13	0·89
4845·062*	0·750	7·22	0·88
4949·984*	0·761	7·21	0·89
	0·756	7·22	0·885
4920·987*	0·783	7·16	0·83
3825·955	0·809	7·09	0·76
4927·020*	0·819	7·08	0·81
	0·814	7·08	0·785
4834·148*	0·877	6·88	0·67
4950·963*	0·929	6·68	0·56
3855·885	0·952	6·58	0·51
4561·008*	0·990	6·39	0·44
4928·059*	0·997	6·40	0·43
	0·994	6·40	0·435

R Muscae $12^h\,36^m\cdot0$, $-68°\,52'$
Max = JD 2426496·288 + $7^d\cdot510211$ E

JD	Phase	*V*	*P*–*V*
	p	m	m
2434952·952	0·022	5·95	0·43
4848·093*	0·060	6·00	0·49
4833·147*	0·070	6·02	0·47
	0·065	6·01	0·48
4953·947*	0·155	6·13	0·57
4834·166*	0·206	6·19	0·61
4527·115*	0·321	6·19	0·63
3776·198	0·335	6·22	0·625
	0·328	6·20	0·63
4917·977*	0·365	6·31	0·71
4903·042*	0·377	6·33	0·72
4873·089*	0·388	6·35	0·74
	0·377	6·33	0·725
4558·035*	0·438	6·50	0·79
4926·040*	0·439	6·48	0·77
	0·438	6·49	0·78
3777·238	0·473	6·48	0·78
3852·963	0·556	6·59	0·86
4927·006*	0·568	6·60	0·87
4544·024*	0·573	6·62	0·87
	0·566	6·60	0·87

R Muscae (*continued*)

JD	Phase	*V*	*P*–*V*
	p	m	m
4950·008*	0·630	6·70	0·86
4845·097*	0·661	6·74	0·87
4950·983*	0·760	6·71	0·76
4921·008*	0·769	6·66	0·79
	0·764	6·68	0·775
4561·024*	0·836	6·47	0·64
5200·154*	0·938	6·01	0·43
3855·890	0·946	6·06	0·42
	0·942	6·04	0·425

W Virginis $13^h\,20^m\cdot9$, $-02°\,52'$
Max = JD 2420472·543 + $17^d\cdot271671$ E

JD	Phase	*V*	*P*–*V*
	p	m	m
2433063·771	0·010	10·30	0·50
3082·767	0·110	9·94	0·385
2944·976	0·132	9·79	0·40
3083·762	0·168	9·73	0·345
2948·042	0·310	9·47	0·47
3069·726	0·355	9·47	0·48
3087·743	0·398	9·42	0·55
3089·726	0·513	9·60	0·61
3090·729	0·571	9·66	0·655
3091·722	0·629	9·76	0·725
3040·819	0·682	10·05	0·805
3092·740	0·688	10·11	0·80
	0·685	10·08	0·80
3059·740	0·777	10·51	0·83
3060·795	0·838	10·60	0·85
3062·741	0·951	10·49	0·635

AL Virginis $14^h\,05^m\cdot8$, $-12°\,50'$
Max = JD 2430202·60 + $10^d\cdot30438$ E

JD	Phase	*V*	*P*–*V*
	p	m	m
2433095·740	0·063	9·22	0·44
3096·736	0·160	9·34	0·54
3027·855	0·476	9·69	0·705
3089·733	0·480	9·82	0·69
	0·478	9·76	0·70
3059·785	0·574	9·82	0·565
3090·735	0·578	9·76	0·545
	0·576	9·79	0·555
3060·795	0·672	9·76	0·48
3091·729	0·674	9·69	0·46
	0·673	9·72	0·47

AL Virginis (*continued*)

JD	Phase	V	P–V
	p	m	m
3081·743	0·705	9·65	0·46
2948·063	0·732	9·57	0·42
3040·826	0·734	9·59	0·405
	0·733	9·58	0·41
3061·753	0·765	9·55	0·40
3092·750	0·773	9·36	0·355
	0·769	9·46	0·38
3062·750	0·862	9·21	0·295
3093·736	0·869	9·12	0·255
	0·866	9·16	0·275
3063·781	0·962	9·12	0·30

RU Camelopardalis $17^h\ 10^m{\cdot}9$, $+69°\ 51'$
Max = JD 2423153·88 + $22^d{\cdot}1725$ E

JD	Phase	V	P–V
	p	m	m
2432887·883	0·012	8·28	0·90
2822·012	0·042	8·26	0·89
2825·017	0·177	8·26	0·92
2848·969	0·257	8·28	0·10
3027·972	0·331	8·36	1·185
3009·972	0·519	8·80	1·34
2833·031	0·539	8·83	1·355
2944·965	0·587	8·88	1·36
2860·922	0·796	9·05	1·235
2884·008	0·838	8·76	1·21
2885·899	0·923	8·53	1·00
2821·017	0·997	8·38	0·925

X Sgr $17^h\ 41^m{\cdot}3$, $-27°\ 48'$
Max = JD 2403169·58 + $7^d{\cdot}01216$ E

JD	Phase	V	P–V
	p	m	m
2434921·144*	0·072	4·20	0·47
5012·997*	0·171	4·24	0·55
4873·109*	0·222	4·32	0·60
5308·039*	0·247	4·30	0·61
4544·149*	0·309	4·43	0·62
4558·176*	0·309	4·43	0·61
5013·967*	0·309	4·38	0·63
	0·309	4·41	0·62
4951·038*	0·335	4·43	0·63
5014·948*	0·449	4·51	0·74
4903·083*	0·496	4·54	0·74
4868·254*	0·529	4·67	0·75
4602·038*	0·564	4·67	0·77
5002·987*	0·600	4·73	0·82
4959·951*	0·606	4·74	0·79
	0·603	4·74	0·805

X Sgr (*continued*)

JD	Phase	V	P–V
	p	m	m
4918·045*	0·630	4·78	0·79
4925·065*	0·631	4·76	0·83
	0·630	4·77	0·81
4869·102*	0·650	4·75	0·81
4848·115*	0·657	4·77	0·81
	0·654	4·76	0·81
4603·051*	0·709	4·82	0·80
4561·124*	0·730	4·81	0·81

BL Herculis $17^h\ 56^m{\cdot}8$, $19°\ 15'$
Max = JD 2415196·499 + $1^d{\cdot}307472$ E

JD	Phase	V	P–V
	p	m	m
2433093·764	0·450	10·42	0·42
4195·965	0·452	10·34	0·45
	0·451	10·38	0·435
3059·951	0·589	10·47	0·46
3092·809	0·720	10·56	0·37
3062·944	0·878	10·18	0·245
4193·934	0·898	10·16	0·24
	0·888	10·17	0·24
4567·908	0·926	9·91	0·165
3091·803	0·950	9·82	0·105
3095·764	0·980	9·75	0·11
	0·965	9·78	0·11
3116·757	0·036	9·87	0·11
4570·828	0·160	10·00	0·285
4251·812	0·165	10·08	0·215
4213·910	0·176	10·13	0·24
	0·167	10·07	0·25
3094·767	0·217	10·02	0·255
4549·971	0·208	10·03	0·265
4574·809	0·205	10·02	0·25
	0·210	10·02	0·26
3073·938	0·286	10·12	0·275
3098·792	0·296	10·20	0·28
	0·291	10·16	0·28
3066·947	0·350	10·30	0·345
3123·728	0·367	10·38	0·34
	0·358	10·34	0·34

W Sgr $17^h\,58^m.6$, $-29°\,35'$
Max = JD 2403198·30 + 7^d·59466 E

JD	Phase	V	P–V
	p	m	m
2434868·258*	0·030	4·25	0·45
5012·992*	0·087	4·23	0·48
4959·944*	0·102	4·30	0·49
4603·055*	0·110	4·31	0·51
	0·106	4·30	0·50
4869·111*	0·142	4·35	0·55
4558·190*	0·203	4·47	0·60
5013·974*	0·216	4·48	0·58
	0·210	4·48	0·59
5014·956*	0·346	4·45	0·64
4544·144*	0·353	4·47	0·61
	0·350	4·46	0·625
4848·118*	0·378	4·50	0·67
4925·060*	0·509	4·78	0·82
4918·040*	0·585	4·86	0·84
4561·138*	0·591	4·87	0·85
	0·588	4·86	0·845
4903·102*	0·618	4·87	0·86
4873·102*	0·668	4·98	0·90
5002·980*	0·769	4·92	0·88
4951·043*	0·930	4·62	0·59
5308·055*	0·938	4·59	0·60
	0·934	4·60	0·595
4602·048*	0·977	4·39	0·53
4921·150*	0·994	4·35	0·46

BB Herculis $18^h\,41^m.3$, $+12°\,14'$
Max = JD 2426244·630 + 7^d·50720 E

JD	Phase	V	P–V
	p	m	m
2433098·813	0·015	9·74	0·69
3091·840	0·086	9·76	0·765
3122·757	0·204	9·90	0·875
3093·816	0·349	9·99	0·825
3116·767	0·406	9·95	0·95
3094·868	0·489	10·11	1·075
3087·889	0·560	10·28	1·07
3095·785	0·611	10·30	1·135
4574·885	0·636	10·38	1·09
	0·624	10·34	1·11
3096·764	0·742	10·39	1·115
3119·771	0·806	10·24	1·07

κ Pavonis $18^h\,46^m.6$, $-67°\,22'$
Max = JD 2426436·5 + 9^d·0738 E

JD	Phase	V	P–V
	p	m	m
2433777·295	0·010	4·06	0·375
4848·128*	0·024	3·98	0·42
	0·017	4·02	0·40
4921·119*	0·077	4·07	0·46
3923·903	0·167	4·33	0·59
5013·013*	0·195	4·34	0·68
5004·002*	0·204	4·37	0·64
	0·200	4·36	0·66
3852·177	0·262	4·44	0·735
5013·984*	0·302	4·52	0·76
3898·042	0·317	4·57	0·75
	0·310	4·54	0·755
4959·978*	0·350	4·62	0·78
4951·001*	0·361	4·60	0·79
3853·167	0·372	4·69	0·79
	0·361	4·64	0·79
4561·166*	0·398	4·71	0·77
3917·017	0·408	4·71	0·80
5014·962*	0·410	4·71	0·81
	0·405	4·71	0·79
3980·920	0·451	4·71	0·80
4925·108*	0·507	4·74	0·75
3856·170	0·703	4·57	0·485
3946·913	0·703	4·51	0·50
5308·021*	0·707	4·49	0·51
	0·704	4·52	0·50
3928·906	0·718	4·53	0·485
4918·143*	0·740	4·45	0·47
4982·004*	0·778	4·33	0·40
3983·917	0·781	4·29	0·425
	0·780	4·31	0·41
4910·090*	0·852	4·00	0·32
3948·913	0·924	3·97	0·335
4920·244*	0·971	3·94	0·38
5002·031*	0·985	3·96	0·37
	0·978	3·95	0·375

V496 Aquilae $19^h\,03^m.0$, $-07°\,36'$
Max = JD 2428719·90 + 6^d·8069 E

JD	Phase	V	P–V
	p	m	m
2434567·844	0·120	7·59	0·965
74·816	0·144	7·60	1·02

V496 Aquilae (*continued*)

JD	Phase	V	$P-V$
	p	m	m
75·868	0·299	7·68	1·10
70·837	0·560	7·86	1·19
65·878	0·831	7·73	1·065
52·962	0·934	7·66	0·975
66·847	0·974	7·59	0·99

AU Pegasi $21^h\ 19^m{\cdot}4$, $+17°\ 51'$
Max = JD 2428729·76 + $2^d{\cdot}3978$ E

JD	Phase	V	$P-V$
	p	m	m
2433153·893	0·080	9·05	0·73

AU Pegasi (*continued*)

JD	Phase	V	$P-V$
	p	m	m
58·762	0·111	9·04	0·69
	0·113	9·08	0·675
	0·112	9·06	0·68
22·861	0·138	9·06	0·68
51·778	0·198	8·96	0·64
80·701	0·260	9·04	0·65
25·854	0·385	8·99	0·68
54·858	0·483	9·00	0·765
23·854	0·552	9·06	0·815
26·844	0·799	9·23	0·845
79·705	0·845	9·29	0·825
19·872	0·892	9·30	0·84
48·809	0·960	9·22	0·815

Individual observations of magnitudes and colours of the cepheids are collected in Table II where those obtained by Gascoigne and Burr are designated by an asterisk. The light and colour curves are plotted in Figs. 1 to 4, where open circles indicate observations by Gascoigne and Burr, filled circles those by Eggen, and half-filled circles those means in Table II that are formed from observations by all three observers; the crosses in the curves for RU Camelopardalis in Fig. 3 indicate the photoelectric observations made by Lenouvel and Jehoulet (1953). The light elements have been taken from the *General Catalogue of Variable Stars* (Kukarkin and Parenago 1948) or, when the results of the present discussion indicated that revision was necessary, from Table III. For κ Pavonis we have used the period of $9^d{\cdot}0738$ that is indicated by a combination of our 1951 and 1953–54 observations.

TABLE III

Revised elements for seven cepheid variables

W Sgr :	max	= JD 2403198·42 + $7{\cdot}59476^d$ E
S Mus:	rising median	= JD 2434926·89 + $9{\cdot}6598^d$ E
SV Per :	max	= JD 2419055·040 + $11{\cdot}12880^d$ E
VY Car :	max	= JD 2434529·90 + $19{\cdot}9370^d$ E
RZ Vel :	max	= JD 2434844·96 + $20{\cdot}39739^d$ E
SW Vel :	max	= JD 2434872·95 + $23{\cdot}473^d$ E − $3{\cdot}75.10^{-8}$ E^2
RS Pup :	max	= JD 2434823·23 + $41{\cdot}38535^d$ E

There is a substantial overlap between the cepheids observed by Eggen and those observed by Gascoigne and Burr, from which it can be seen that the agreement is satisfactory. Eggen found S Muscae to be $0^m{\cdot}05$ brighter at minimum than did Gascoigne and Burr and he also observed the post-maximum branch of κ Pavonis consistently fainter. In the second case at least it seems probable that this difference reflects a real variation in the light curve, but we have drawn only the mean curve in the figure.

Improved light elements are suggested for seven stars in Table III and the data relative to four of these are shown graphically in Fig. 5. In the figure, the earlier results originated almost entirely from the Harvard College Observatory (Gaposchkin and Payne-Gaposchkin 1946); the points for RZ Velorum are

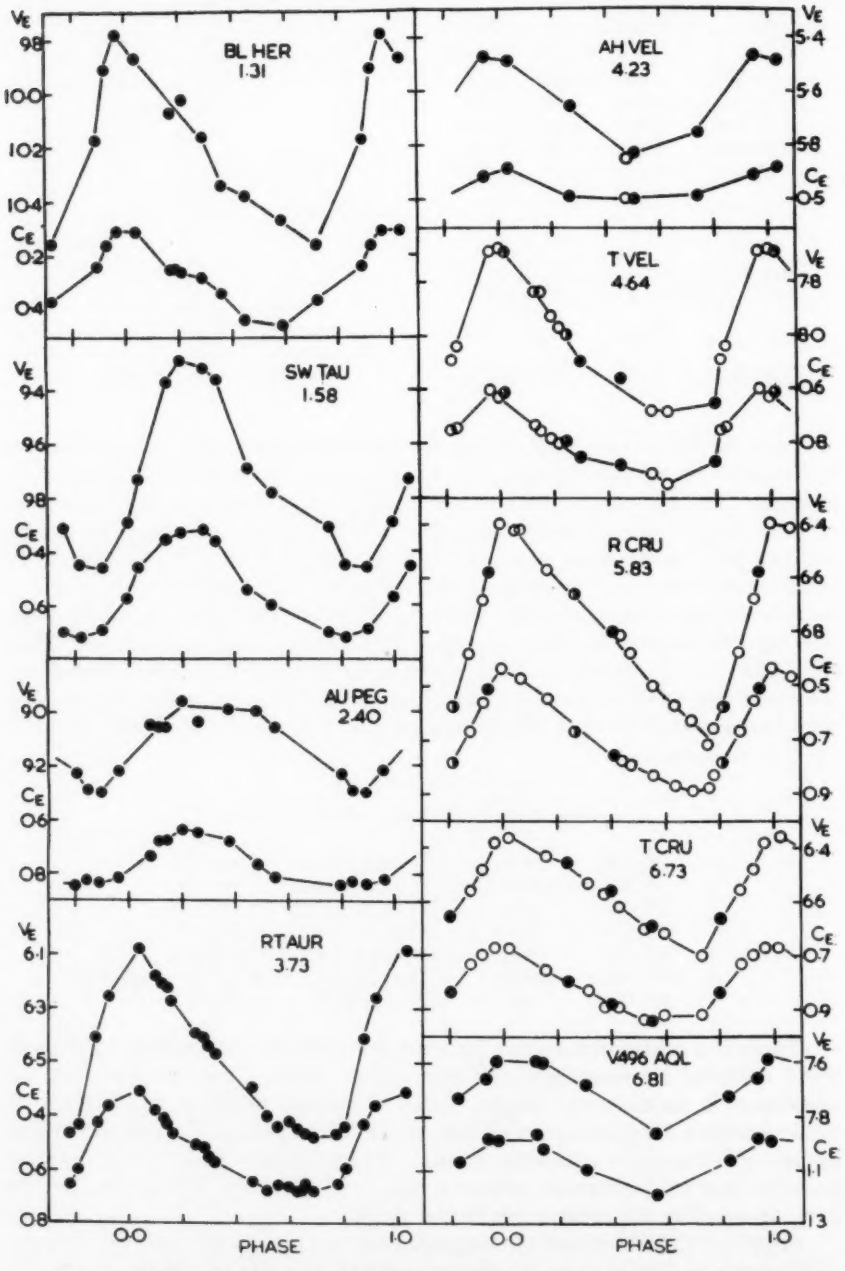

FIG. 1.—*Light and colour curves for individual cepheids. Filled circles represent observations by Eggen, open circles by Gascoigne and Burr, and half-filled circles indicate those means in Table II that are formed from observations by all three observers.*

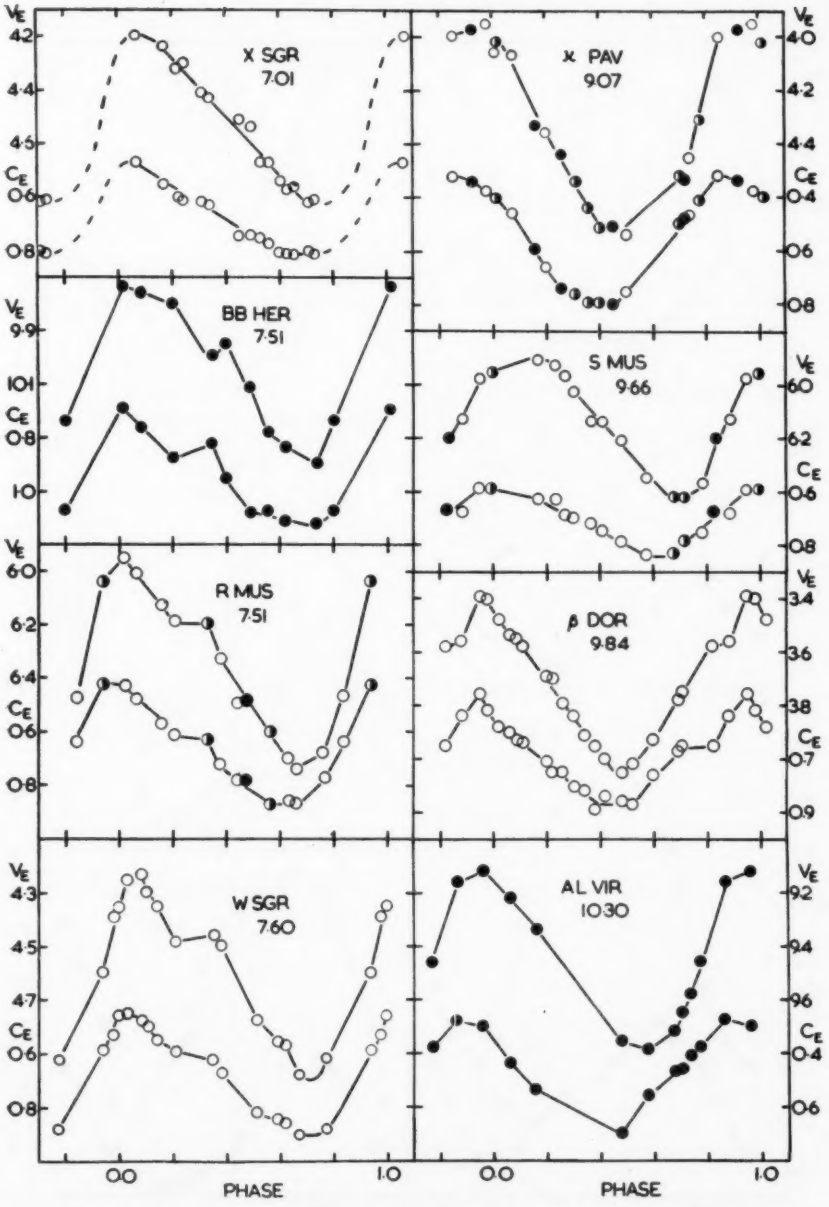

FIG. 2.—*Light and colour curves for individual cepheids. Filled circles represent observations by Eggen, open circles by Gascoigne and Burr, and half-filled circles indicate those means in Table II that are formed from observations by all three observers.*

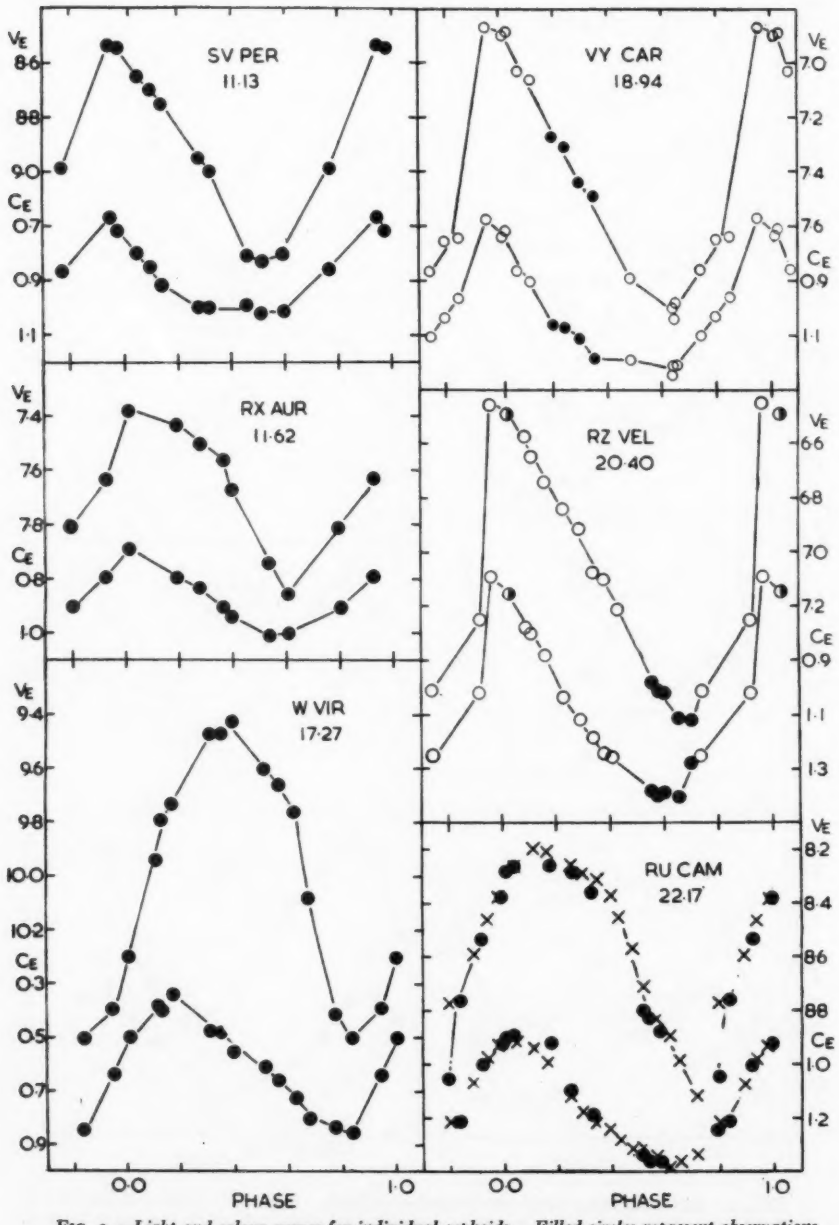

FIG. 3.—*Light and colour curves for individual cepheids. Filled circles represent observations by Eggen, open circles by Gascoigne and Burr, and half-filled circles indicate those means in Table II that are formed from observations by all three observers.*

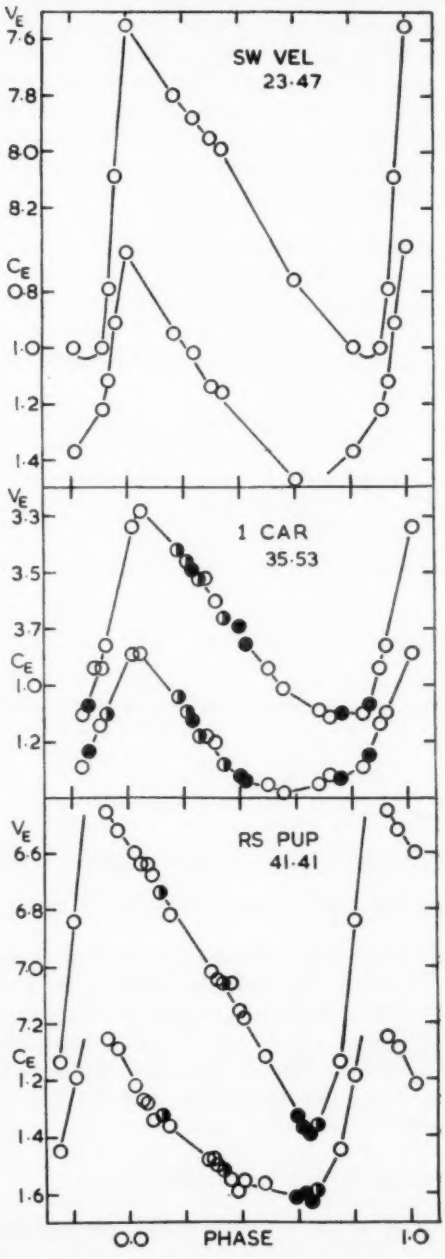

FIG. 4.—*Light and colour curves for individual cepheids. Filled circles represent observations by Eggen, open circles by Gascoigne and Burr, and half-filled circles indicate those means in Table II that are formed from observations by all three observers.*

from a discussion by Oosterhoff (1936). Our observations of this latter star do not support the term in E^2 in the light elements suggested by Oosterhoff, and, indeed, there is little reason to suppose that its period has changed in the last 40 years. The change in the period of SW Velorum, however, continues to be large and regular as found by Oosterhoff (1936), but we find a somewhat smaller secular term than his. The period of RS Puppis has apparently not altered since the curious phase change noted by Gaposchkin and Payne-Gaposchkin (1946) and shown schematically in Fig. 5.

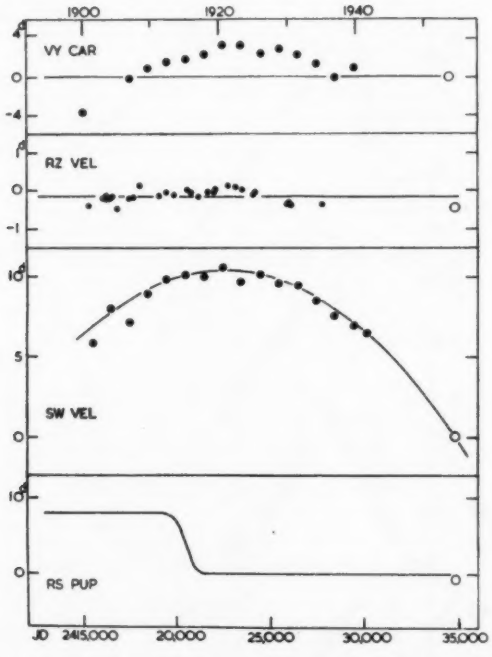

FIG. 5.—*Period variations for RZ Velorum, VY Carinae, SW Velorum and RS Puppis.*

For most of the stars in Fig. 5 the period variations—when they exist—are small and regular. There are four cepheids, however, for which these variations are large and erratic—κ Pavonis (Parenago 1946), AL Virginis (Payne Gaposchkin 1938), W Virginis (Nielsen 1954) and RU Camelopardalis (Lenouvel and Jehoulet 1953); all these have been so fully discussed as to merit no more than brief mention here. For κ Pavonis we can add the following two points to Parenago's (1946) table:

$$E = 1576,\ O-C = +3^{d}\cdot 86 \text{ (Eggen)},$$

$$E = 1692,\ O-C = +1^{d}\cdot 98 \text{ (Gascoigne and Burr)}.$$

Both W Virginis and AL Virginis are recognized members of population type II and evidence will be presented later to indicate that κ Pavonis and RU Camelopardalis may also be members of that population.

The 63 observed variables, including those discussed previously (Eggen 1951), are listed in Table IV together with the following information: Column (1) name: (2) logarithm of the period in days; (3) maximum colour; (4) minimum colour; (5) colour amplitude; (6) maximum visual magnitude; (7) minimum visual magnitude; (8) light amplitude; (9) a classification according to the shape of the light curve, where II indicates a probable member of population type II; (10) radial velocity amplitude in kilometres per second; (11) source of the value in (10). The magnitudes and colours for the 33 variables given in the previous publication (Eggen 1951) have been re-reduced from the original observations to the $(P, V)_E$-system; additional observations made since 1951 have been secured for most of these stars. Since the magnitudes and colours for δ Cephei obtained with the 12-inch refractor may have been affected by the light of the visual companion, the values of V_E and $(P-V)_E$ in Table IV were obtained by conversion from the six-colour observations by Stebbins (1945).

TABLE IV

Photometric data for 63 galactic cepheids

		$(P-V)_E$			V_E					
(1)	(2)	(3)	(4)	(5)	(6)	(7)	(8)	(9)	(10)	(11)
Name	log P	max	min	amp	max	min	amp	Cl.	Vel.	Ref.
BL Her	0·116	0·10	0·46	0·36	9·78	10·56	0·78	II	27	3
SW Tau	0·200	0·32	0·72	0·40	9·29	10·06	0·77	II	38	3
SU Cas*	0·290	0·49	0·64	0·15	5·75	6·13	0·38	?	22	3
AU Peg	0·379	0·64	0·84	0·20	8·98	9·30	0·32	C	...	...
DT Cyg	0·398	0·36	0·51	0·15	5·62	5·92	0·30	C	17	2
SZ Tau	0·498	0·62	0·80	0·18	6·34	6·68	0·34	C	22	2
SS Sct	0·565	0·66	0·92	0·26	7·82	8·30	0·48	B	26	3
RT Aur	0·572	0·30	0·68	0·38	5·05	5·78	0·73	A	33	3
SU Cyg	0·585	0·30	0·55	0·25	6·45	7·06	0·61	A	47	3
α UMi	0·599	0·45	0·50	0·05	1·96	2·06	0·10	C	6	2
ST Tau*	0·605	0·52:	0·92	0·40:	7·75:	8·50	0·75:	?	38	3
AH Vel	0·626	0·39	0·50	0·11	5·47	5·84	0·37	C	17	6
Y Lac	0·635	0·44	0·75	0·31	8·77	9·45	0·68	A	39	3
V Vel*	0·640	0·51	0·77	0·26	7·26	7·80	0·54	?	...	...
T Vul	0·647	0·36	0·67	0·31	5·43	6·09	0·66	A	35	2
FF Aql	0·650	0·57	0·69	0·12	5·17	5·53	0·36	C	16	2
T Vel	0·667	0·61	0·94	0·33	7·68	8·28	0·60	B	39	6
V350 Sgr	0·712	0·60	0·93	0·33	6·90	7·66	0·76	A	39	3
BG Lac	0·727	0·63	0·94	0·31	8·46	9·02	0·56	B	34	3
δ Cep	0·730	0·34	0·72	0·38	3·46	4·28	0·82	A	39	2
Y Sgr	0·761	0·53	0·91	0·38	5·37	6·10	0·73	A	40	2
R Cru	0·765	0·44	0·89	0·45	6·40	7·21	0·81	A	34	6
FM Aql	0·786	0·96	1·32	0·36	7·82	8·51	0·69	B	35	3
X Vul	0·801	1·03	1·47	0·44	8·36	9·15	0·79	A	47	3
RR Lac	0·808	0·55	0·96	0·41	8·38	9·24	0·86	A	26	3
XX Sgr	0·808	0·79	1·17	0·38	8·30	9·02	0·72	B	57	3
T Cru	0·828	0·67	0·94	0·27	6·36	6·79	0·43	A	34	6
U Sgr	0·829	0·75	1·15	0·40	6·25	6·92	0·67	B	38	3
V496 Aql	0·833	0·98	1·19	0·21	7·59	7·86	0·27	C	14	6
U Aql	0·846	0·68	1·08	0·40	6·05	6·80	0·75	B	42	2

TABLE IV (*continued*)

		$(P-V)_E$			V_E					
(1)	(2)	(3)	(4)	(5)	(6)	(7)	(8)	(9)	(10)	(11)
Name	log P	max	min	amp	max	min	amp	Cl.	Vel.	Ref.
X Sgr	0·846	0·45 :	0·81	0·36 :	4·16 :	4·84	0·68 :	A	32	6
η Aql	0·856	0·48	0·91	0·43	3·50	4·27	0·77	B	40	2
BB Her	0·876	0·69	1·12	0·43	9·72	10·39	0·67	II	24	3
R Mus	0·876	0·42	0·87	0·45	5·94	6·74	0·80	B	43	6
W Sgr	0·880	0·45	0·90	0·45	4·22	5·00	0·78	B	44	6
RX Cam	0·898	0·90	1·32	0·42	7·20	8·03	0·83	B	48	3
S Sge	0·920	0·51	0·93	0·42	5·25	6·03	0·78	B	36	4
κ Pav	0·958	0·32	0·80	0·48	3·96	4·73	0·77	II	32	6
FN Aql	0·977	0·91	1·23	0·32	7·95	8·66	0·71	C	40	3
YZ Sgr	0·980	0·74	1·09	0·35	6·83	7·58	0·75	C	34	3
S Mus	0·985	0·59	0·84	0·25	5·90	6·42	0·52	C	29	6
β Dor	0·993	0·46	0·87	0·41	3·39	4·05	0·66	C	36	6
ζ Gem	1·006	0·59	0·90	0·31	3·68	4·15	0·47	C	28	2
AL Vir	1·013	0·28	0·70	0·42	9·12	9·79	0·67	II	35	3
Z Lac	1·037	0·74	1·27	0·53	7·87	8·77	0·90	C	44	3
SV Per	1·046	0·67 :	1·02	0·35 :	8·54 :	9·33	0·79 :	C	36	3
RX Aur	1·065	0·69	1·01	0·32	7·38	8·06	0·68	C	27	3
TT Aql	1·138	0·81	1·46	0·65	6·38	7·50	1·12	AB	52	3
RW Cas	1·170	0·77	1·40	0·63	8·72	9·76	1·04	AB	53	3
X Cyg	1·215	0·70	1·36	0·66	5·76	6·82	1·06	B	56	2
Y Oph	1·234	1·07	1·36	0·29	5·91	6·38	0·47	C	18	1
SZ Aql	1·234	0·88	1·56	0·68	7·84	9·03	1·19	B	64	3
W Vir	1·237	0·34	0·85	0·51	9·44	10·60	1·16	II	67	3
VY Car	1·278	0·67	1·22	0·55	6·87	7·91	1·04	A(C)	...	...
RY Sco*	1·308	1·1 :	1·4 :	0·3 :	7·4 :	8·15	0·75 :	?	37	6
RZ Vel	1·310	0·58	1·40	0·82	6·44	7·62	1·18	B	57	6
WZ Sgr	1·339	0·86	1·54	0·68	7·26	8·34	1·08	A	62	3
RU Cam	1·345	0·90	1·37	0·47	8·20	9·10	0·90	II	20	7
SW Vel	1·371	0·66	1·46	0·80	7·55	8·75	1·20	A	...	...
T Mon	1·431	0·79	1·36	0·57	5·60	6·45	0·85	A	54	5
l Car	1·550	0·89	1·38	0·49	3·28	4·00	0·72	A	40	6
RS Pup	1·617	1·03 :	1·62	0·59 :	6·42 :	7·59	1·17 :	A	58	3
SV Vul	1·654	0·94	1·66	0·72	6·64	7·77	1·13	AB	53	5

* Observed only at maximum and minimum.

The sources given in Column (11) for the radial velocity data in Column (10) are as follows :—

1. Abt, H. A., 1954, *P.A.S.P.*, **66**, 65.
2. Quoted by Eggen, O. J., 1951, *Ap. J.*, **113**, 367.
3. Joy, A. H., 1937, *Ap. J.*, **86**, 363.
4. Herbig, G. H. and Moore, J. H., 1952, *Ap. J.*, **116**, 348.
5. Sanford, R. F., 1956, *Ap. J.*, **123**, 201.
6. Stibbs, D. W. N., 1955, *M.N.*, **115**, 363.
7. Jehoulet, D., 1953, *C.R.*, **236**, 663.

In addition to RU Camelopardalis mentioned above, observations comparable with ours have been published for only one other cepheid in Table IV. Harris (1953) has observed the bright variable ζ Geminorum and the results, when

reduced to the $(P, V)_E$-system, show the following agreement with ours:

	$(P-V)_{max}$	$(P-V)_{min}$	V_{max}	V_{min}
Harris	$0^m.59$	$0^m.89$	$3^m.67$	$4^m.16$
Present	0 .59	0 .90	3 .68	4 .15

3. *Discussion.*—The study of the relations between the various observationally determined parameters of cepheid variables has received much attention, but the subject is complicated and clear-cut results have been difficult to establish. The two most important results are those of Hertzsprung (1926), who showed that, for cepheid light-curves with humps, the phase of the hump decreases as the length of the period increases, and of Parenago and Kukarkin (1936), who found that most of the characteristics of the classical cepheids undergo discontinuous changes at a period of about 10 days. The relationships between shape of light curve and length of period have been well summarized by Payne-Gaposchkin (1954).

In a previous paper (Eggen 1951) the cepheids were divided into three groups, *A*, *B* and *C*, on the basis of the relationship between light and colour amplitudes and periods. From the material then available it was found that this classification, in general, divided the stars also into (i) those with δ Cephei-like or smooth, asymmetric light curves—type *A*; (ii) those with η Aquilae-like or asymmetric light curves showing a secondary hump—type *B*; and (iii) those with a nearly sinusoidal light curve, similar to ζ Geminorum—type *C*. In the light of the augmented material considered here, we have retained the classification system but altered the basic criterion to one of symmetry: if the maximum follows the minimum by an interval of more than $0^p.37$, we assign the star to type *C*; if less, to types *A* or *B* according to whether humps are absent or present, respectively. The somewhat arbitrary value of $0^p.37$ was suggested by the previous work. These criteria are not always free from ambiguity, and in particular there are a few stars, of which β Doradus and VY Carinae are examples, with humps superimposed on symmetrical light curves. In such cases the property of symmetry is taken as the fundamental one.

The colour and light amplitudes of the variables in Table IV have been plotted against the periods in Figs. 6*a* and 6*b*, respectively. The stars of type *A*, including three doubtful cases labelled type *AB* in Table IV, are shown by open circles, type *B* by filled circles, type *C* by crosses and population type II cepheids by plus signs; the four stars for which the classification is unknown or uncertain because of incomplete data, as indicated in column (9) by a question mark, are plotted as half-filled circles. A comparison of Fig. 6*a* with the corresponding Figs. 25 and 26 in the previous paper (Eggen 1951) shows why it was necessary to modify the original classification of the types *A*, *B* and *C* on the basis of colour amplitude alone. The increased scatter in Fig. 6*b* is due partly to revision of some of the previous data but mostly to newly observed cepheids such as RT Aurigae, ST Tauri and X Sagittarii. However, although the criteria have been changed, the classifications, except for seven stars, have not. These seven stars are: DT Cygni and SZ Tauri, which become type *C* instead of type *B*; SZ Aquilae, *B* instead of *A*; WZ Sagittarii, *A* instead of *B*; T Monocerotis and SV Vulpeculae, *A* instead of *C*; and Z Lacertae, *C* instead of *B*.

Preliminary to further discussion of Figs. 6*a* and 6*b* we should point out the existence of certain selection effects. The cepheids studied in this paper were

chosen primarily on the basis of apparent magnitude and, considered per unit volume of space, the intrinsically brighter cepheids, that is, those of longer period, are therefore disproportionally numerous, a bias that has been accentuated by the deliberate addition of long period cepheids to the programme. Also, as discussed below, the five faintest variables in Table IV may belong to population type II.

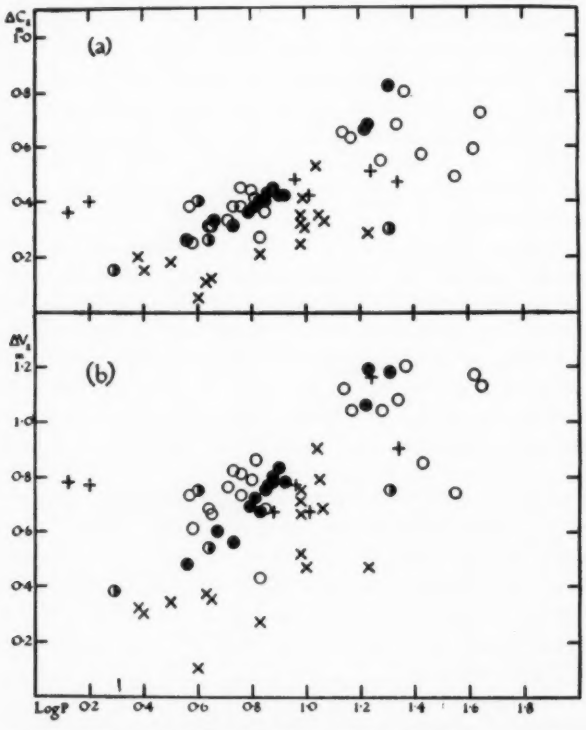

FIG. 6.—*Colour amplitudes (a) and light amplitudes (b) plotted against the logarithm of the periods. Open circles indicate cepheids of type A, including three doubtful cases indicated in Column 9 of Table IV as type AB, closed circles type B, crosses type C and plus signs population type II cepheids; the four stars indicated by question marks in Column 9 of Table IV are plotted as half-filled circles.*

It is apparent that the same broad features are common to both Figs. 6*a* and 6*b*. For example, omitting for the present the five faintest stars mentioned above, (i) the cepheids of type *C* have generally smaller amplitudes than those of types *A* and *B*; (ii) type *A* variables greatly predominate in the period range 3·5 to 6·5 days, and type *C* in the range from 9 to 12 days; (iii) all the type *A* stars in the period range from 3·5 to 6·5 days have greater light amplitudes than those of types *B* and *C*.

A selection of light curves illustrating the three types of cepheid is shown in Figs. 7, 8 and 9. Fig. 8 clearly shows the phenomenon noted by Hertzsprung (1926), that is, the relatively smooth progression of the hump from minimum light at periods near 3·5 days, up the descending branch of the curve to maximum light at 11 days, then down the ascending branch to minimum light again for

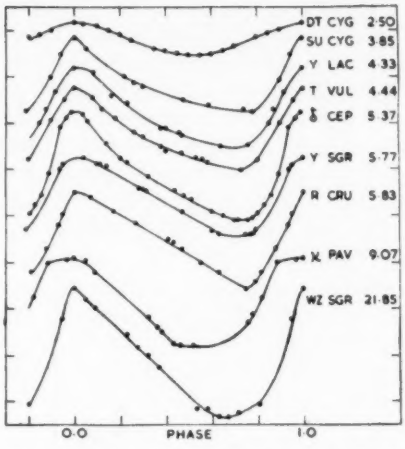

Fig. 7.—Light curves of typical type A cepheids.

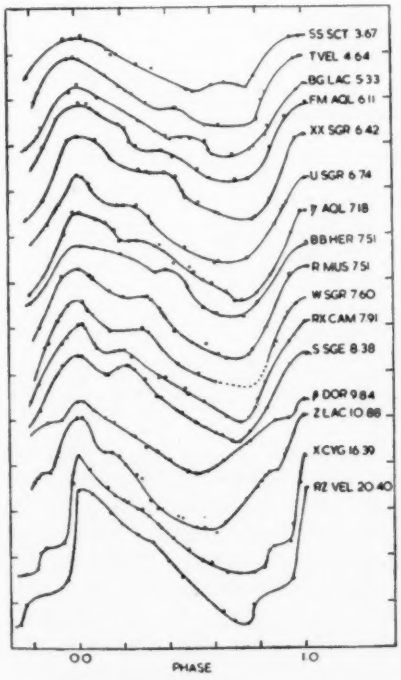

FIG. 8

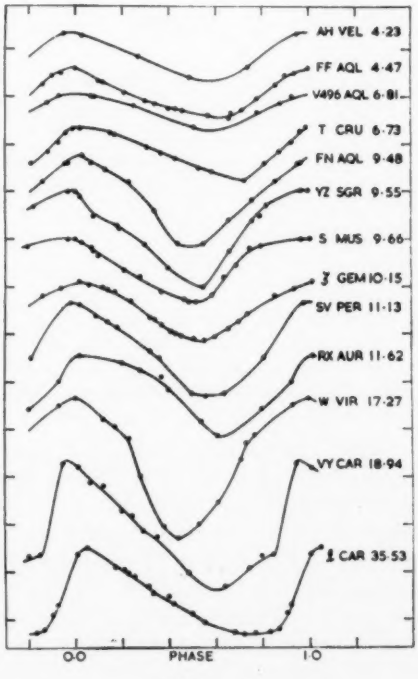

FIG. 9

FIG. 8.—*Light curves of typical type B cepheids. The light curves for β Doradus and Z Lacertae, which show type C light curves when the classification by symmetry is made but also have the hump characteristic of type B, are shown for comparison.*

FIG. 9.—*Light curves of typical type C cepheids. Two type A variables, T Crucis and l Carinae, and the population type II cepheid, W Virginis, are included in the figure for comparison. The peculiar variable VY Carinae is intermediate between types A and C.*

periods near 20 days. The only apparent break in this progression is the slightly misplaced hump in the light curve of BB Herculis which, since it has the high radial velocity of 100 km/sec relative to the stars near the Sun, may be a population type II object. The later star is included in Fig. 8 because such marked similarity between the light curves of population type I and type II variables is unusual; the light curves of such well-known population type II variables as W Virginis, RU Camelopardalis and, to a lesser extent, of κ Pavonis, are all quite distinctive. Two stars with periods near 10 days that are classified as type *C* on the basis of symmetry but which show the humps characteristic of type *B*, β Doradus and Z Lacertae, are included in Fig. 8.

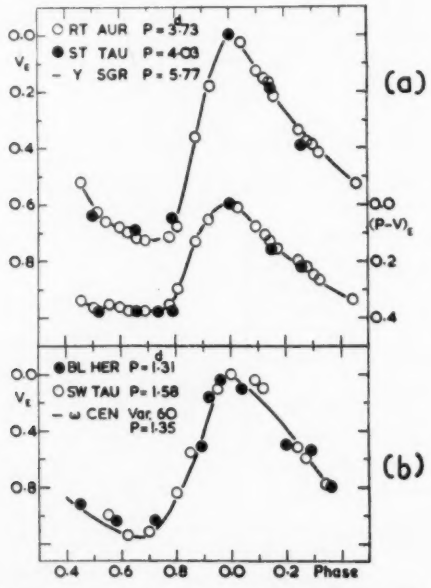

FIG. 10.—(*a*) *Light and colour curves of RT Aurigae, ST Tauri and Y Sagittarii.* (*b*) *Light curves of the population type II cepheids BL Herculis, SW Tauri and variable No.* 60 *in* ω *Centauri.*

Four additional variables that stand out from the general run in Figs. 6*a* and 6*b* need mention. The two of shortest period, near $1^d{\cdot}5$, are BL Herculis and SW Tauri, for which both the light and colour amplitudes seem much too large. In Fig. 10*b* we compare their light curves with that found for variable No. 60 in ω Centauri by Martin (1938); the similarity is striking. Spectroscopic evidence has led Joy (1949) to identify SW Tauri ($b = -28°$) with stars of similar periods in globular clusters and apparently BL Herculis ($b = +18°$) is also a galactic counterpart of the cluster variables. The systematic radial velocities of both variables are small but there is little doubt that the stars belong to population type II. The longer period variables RT Aurigae and ST Tauri also appear to have abnormally large light and colour amplitudes and Fig. 10*a* shows that their nearly identical light and colour curves match closely those for Y Sagittarii which has a fifty per cent longer period. Both RT Aurigae and ST Tauri lie within 10° of the galactic plane and except for their anomalously large amplitudes, are indistinguishable from the run of classical cepheids.

There appears to be little or no correlation between period length and light or colour amplitude for the six type *C* cepheids of shortest period although Fig. 9 shows their light curves to be quite similar; two type *A* variables, T Crucis and *l* Carinae, and the population type II cepheid, W Virginis, are included in Fig. 9 for comparison. The peculiar variable VY Carinae is intermediate between types *A* and *C*. The well-known break in the correlations between various observed characteristics of cepheids at periods near 10 days is reflected in Fig. 6*a* where only κ Pavonis and Z Lacertae have light amplitudes large enough to fit in with the general run of the *A* and *B* types. The radial velocity of κ Pavonis is not particularly high but the variable has a peculiar light curve (Fig. 2), variations in the shape of which are well established (Payne-Gaposchkin 1945), and an erratically varying period discussed above; it is probably a population type II cepheid. Although the symmetrical light curve of Z Lacertae classifies that variable as of type *C*, the presence of the hump at maximum light may mask the true maximum and therefore lead to a wrong classification.

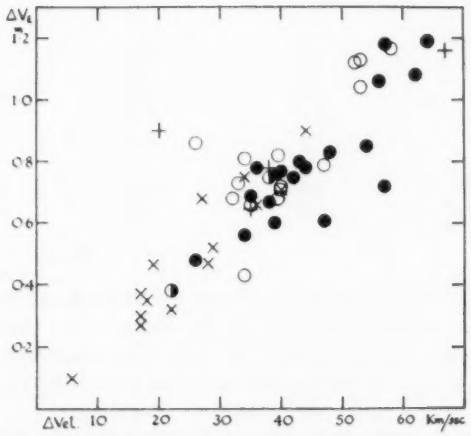

FIG. 11.—*The correlation between the velocity and light amplitudes. The symbols are those used in Fig.* 6.

The observed radial velocity amplitudes of the variables in Table IV are listed in column (10) and have been drawn from the sources listed in column (11) and plotted against the light amplitudes in Fig. 11, where the symbols are the same as those used in Fig. 6. The scatter in Fig. 11 is considerably greater than has been found in previous discussions of this correlation (Hellerich 1937; Eggen 1951) and is due mainly to the addition of new material including variables of population type II. A particularly clear-cut example of dispersion in this correlation is afforded by R and T Crucis, both of which have well-established velocity amplitudes of 34 km/sec but with visual magnitude ranges of $0^{m}\cdot81$ and $0^{m}\cdot43$, respectively. Also, T Monocerotis and SV Vulpeculae have very accurately determined velocity amplitudes of 54 and 53 km/sec, respectively, but the corresponding visual magnitude ranges are $0^{m}\cdot85$ and $1^{m}\cdot13$. Two stars that depart even more from the general run in Fig. 11 are XX Sagittarii and RR Lacertae, but for these the velocity data are less complete.

The present photometric data for 17 of the 18 cepheids used by Blaauw and Morgan (1954) to establish the zero-point of the period–luminosity relation are assembled in Table V. The magnitudes that are used by Blaauw and Morgan were obtained from a variety of sources but, presumably, are on the International

TABLE V

Magnitudes of zero-point cepheids (Blaauw and Morgan, 1954)

Name	m_{pg}	P_E	$m_{pg}-P_E$
α UMi	2·6	2·48	+0·12
SU Cas	6·5	6·50	0·00
SZ Tau	7·3	7·22	+0·08
β Dor	4·9	4·38	+0·52
RT Aur	6·0	5·90	+0·10
ζ Gem	4·7	4·66	+0·04
l Car	5·0	4·78	+0·22
X Sgr	5·4	5·13	+0·27
W Sgr	5·5	5·29	+0·21
Y Sgr	6·5	6·46	+0·04
U Sgr	7·8	7·54	+0·26
FF Aql	6·0	5·98	+0·02
η Aql	5·0	4·58	+0·42
S Sge	6·3	6·36	−0·06
T Vul	6·3	6·27	+0·03
DT Cyg	6·5	6·20	+0·30
δ Cep	4·7	4·40	+0·30
		Mean	+0·17

System; their adopted values are in the second column of the table while those determined in the present study are in the third. Our median photographic magnitudes, $\frac{1}{2}(P_{max}+P_{min})$, average $0^m\cdot17$ brighter than those used by Blaauw and Morgan and thus their determination of the zero-point requires a correction of $-0^m\cdot17$ to reduce it to the International P_E-system.

Acknowledgments.—The participation of the Mt Stromlo observers (S. C. B. G. and E. J. B.) in this programme was made possible by the generous loan of a multiplier and photometer from the Lick Observatory and the construction and maintenance of an amplifier by Mr D. G. Thomas.

Lick Observatory,
Mount Hamilton,
California, U.S.A.

Commonwealth Observatory,
Mount Stromlo,
Canberra.

1957 *January.*

References

Blaauw, A. and Morgan, H. R., 1954, *B.A.N.*, **12**, 95.
Cape, 1953, Royal Observatory, Cape of Good Hope, Mimeograms.
Eggen, O. J., 1951, *Ap. J.*, **113**, 367.
Eggen, O. J., 1955, *A. J.*, **60**, 65.
Gaposchkin, S. and Payne-Gaposchkin, C., 1946, *Harvard Annals*, **115**.
Harris, D. L., 1953, *Ap. J.*, **118**, 346.
Hertzsprung, E., 1926, *B.A.N.*, **3**, 115.
Jehoulet, D., 1953, *C.R.*, **236**, 663.

Joy, A. H., 1949, *Ap. J.*, **110**, 105.
Hellerich, J., 1937, *A.N.*, **261**, 280.
Kukarkin, B. V. and Parenago, P. P., 1948, *General Catalogue of Variable Stars*.
Lenouvel, F. and Jehoulet, D., 1953, *Ann. d'Aphysique*, **16**, 139.
Martin, W., 1938, *Leiden Ann.*, **17**, part 2.
Nielsen, A. V., 1954, *Medd. Ole Romer Obs.*, **24**, 343.
Oosterhoff, P. Th., 1936, *B.A.N.*, **8** 29.
Parenago, P. P., 1946, *Variable Stars*, **6**, 57.
Parenago, P. P. and Kukarkin, B. V., 1936, *Zeit. fr. Astroph.*, **11**, 337.
Payne-Gaposchkin, C., 1938, *Proc. Am. Phil. Soc.*, **81**, 189.
Payne-Gaposchkin, C., 1954, *Variable Stars and Galactic Structure*, London.
Stebbins, J., 1945, *Ap. J.*, **101**, 47.

CEPHEID VARIABLES AND GALACTIC ABSORPTION

S. C. B. Gascoigne and Olin J. Eggen

(Received 1957 February 9)

Summary

From a discussion of the colours and magnitudes of galactic and Magellanic Cloud cepheid variables, we have: (1) derived a reddening of $+0^{m}\cdot11$ for δ Cephei and $+0^{m}\cdot08$ for α Ursae Minoris from the colours and spectral types of their visual companions; (2) found similar values for the reddening of these bright cepheids by spectrophotometric comparisons with F- and G-type supergiants; (3) determined, from the proper motions of the brighter galactic cepheids, a correction of $-1^{m}\cdot7$ for the zero point of Shapley's period-luminosity relation; (4) derived the value $17\cdot5\pm1\cdot9$ km/sec/kpc for the rotation constant A and (5) discussed the large values of the mean absorption in the galactic plane that are derived from the assumption that the galactic and Magellanic Cloud cepheids have the same intrinsic colour.

---

1. *Introduction.*—Several years ago one of us (Eggen 1951) published photoelectric magnitudes and colours for 32 Population I galactic cepheid variables. Later, Gascoigne and Kron (1952) and Gascoigne (1955) made similar observations for a number of cepheids in the Magellanic Clouds and found these stars to be so much bluer than the variables observed by Eggen that it was difficult to attribute the same intrinsic colours to both groups without invoking an improbably high value for the interstellar absorption. These results raised two questions: what are the intrinsic colours of galactic cepheids, and to what extent can they be used as distance indicators or, more generally, what degree of similarity exists among galactic and extra-galactic cepheids? These problems have been briefly considered by Gascoigne and Eggen (1957) and the intrinsic colours of the galactic cepheids recently discussed by Stibbs (1956) and by Code (1957).

In this paper we have attempted to (*a*) determine the reddening of δ Cephei and α Ursae Minoris from the colours and spectral types of their visual companions (Section 2), (*b*) make spectrophotometric comparison between the cepheids and some F- and G-type supergiants (Section 3), (*c*) redetermine the zero-point of the period–luminosity relation from the proper motions (Blaauw and Morgan, 1954) of the brighter galactic cepheids (Section 4), (*d*) derive a value for the Oort rotation constant, A (Section 5), and (*e*) study the mean absorption in the galactic plane (Section 6).

The properties important for distance determination are absolute magnitude and colour. Our main conclusion can perhaps be best expressed by saying that as far as these two properties are concerned, there does not at present seem to be any convincing reason for supposing that the cepheids in our galaxy differ from those in other galaxies.

It has been necessary, in this discussion, to ignore possible dispersion in the period–luminosity and period-intrinsic colour relations; additional observations of cepheids in the Magellanic Clouds are needed before this dispersion can

be taken into account. Unless otherwise noted, the magnitudes and colours are on the $(P, V)_E$-system (Eggen 1955a).

2. *Cepheids with common proper motion companions.*—The bright variable δ Cephei forms ADS 15987 AC with the $6^m.5$ star BD $+57°2547$, 40″ distant. There has been no relative motion in this visual pair since its discovery by Struve in 1835. An unpublished velocity of the companion, -19 ± 4 km/sec, has been determined from five Mills plates by G. H. Herbig and, since the systematic velocity of the variable is -17 km/sec, the two stars apparently form a physical system. Stebbins and Kron (1956) have observed the companion in six-colours, and we use their results to determine its spectral type and reddening, following the Q method described by Johnson and Morgan (1953). Rather than make a somewhat uncertain transformation from the six-colours to the (U, B, V)-system, we will work with the six-colours directly; six-colour observations are here denoted by square brackets.

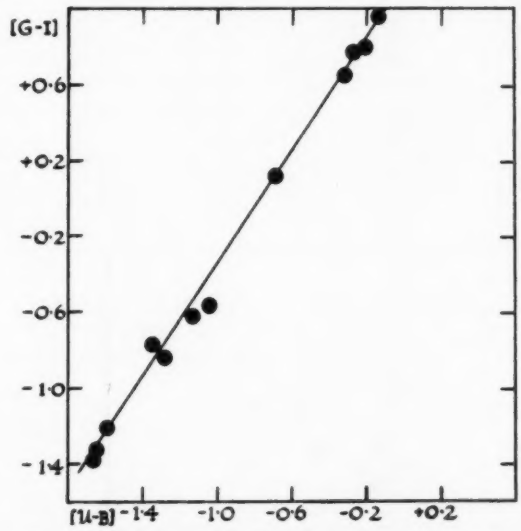

FIG. 1.—*The colours* [*G–I*] *and* [*U–B*] *for* O9·5 *to* B1·5, Ia *and* Ib *supergiants.*

The following stars of spectral type O9·5 to B1·5, Ia–Ib, have also been observed on the six-colour programme (Stebbins and Whitford 1945; Stebbins and Kron 1956):

Star	[*U–B*]	[*G–I*]	Spectrum	*Q*
	m	m		
HD 195592	−0·32	+0·66	O9·5 Ia	−0·76
ζ Ori	−1·66	−1·38	O9·5 Ib	−0·75
ε Ori	−1·64	−1·33	B0 Ia	−0·76
69 Cyg	−1·59	−1·21	B0 Ib	−0·79
HD 194839	−0·21	+0·81	B0·5 Ia	−0·75
26 Cep	−1·04	−0·55	B0·5 Ib	−0·68
κ Cas	−1·34	−0·77	B1 Ia	−0·83
HD 216411	−0·69	+0·12	B1 Ia	−0·77
HD 169454	−0·27	+0·78	B1 Ia+	−0·79
HD 190919	−1·13	−0·62	B1 Ib	−0·72
ζ Per	−1·28	−0·84	B1 Ib	−0·72
HD 194297	−0·14	+0·95	B1·5 Ia	−0·77

In Fig. 1 we plot $[G-I]$ for these stars against $[U-B]$. The line on which the points lie—the reddening line—is given by the equation:

$$[U-B]=0\cdot662[G-I]-0^{m}\cdot765.$$

This enables us to define a quantity

$$Q=[U-B]-0\cdot662[G-I],$$

which is independent of the degree of reddening and depends only on the spectral type of the star.

To find the intrinsic colour of a star with spectral type given by Q, we use the following list of stars considered by Johnson and Morgan (1953) and by Johnson (1955) to be almost or entirely unreddened:

Star	$[U-B]$	$[G-I]$	Sp.	Q	E_{GI}
η U Ma	−1·27	−1·34	B3 V	−0·38	−0·01
η Aur	−1·23	−1·28	B3 V	−0·38	+0·05
τ Her	−1·14	−1·29	B5 IV	−0·29	−0·02
μ Eri	−1·10	−1·23	B5 IV	−0·28	+0·03
19 Tau	−0·95	−1·16	B6 IV	−0·18	+0·04
17 Tau	−0·89	−1·13	B6 III	−0·14	+0·05
β Tau	−1·00	−1·17	B7 III	−0·22	+0·06
α Leo	−0·84	−1·15	B7 V	−0·08	−0·01
18 Tau	−0·82	−1·14	B8 V	−0·06	−0·01
β Cyg C	−0·74	−1·04	B8 V	−0·05	+0·08
δ Cep B	−0·80	−0·98	(B6)	−0·15	+0·20

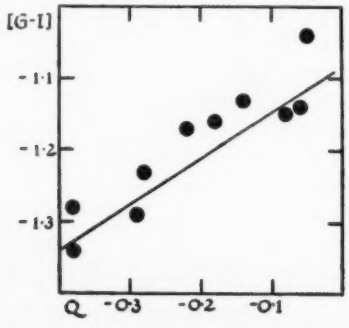

FIG. 2.—*The Q-values for* B3 *to* B8 *type stars.*

In Fig. 2 we plot $[G-I]$ for these stars against Q, and, giving greater weight to the bluer stars, find for the intrinsic colours,

$$[G-I]=0\cdot62Q-1^{m}\cdot09.$$

The colour excess E_{GI} on the $[G-I]$-system is then

$$E_{GI}=[G-I]-0\cdot62Q+1^{m}\cdot09.$$

The measured colours of δ Cep B give $Q=-0^{m}\cdot15$, corresponding to a spectral type of B6 and colour excess of $+0^{m}\cdot20$. Confirmatory evidence is provided by W. P. Bidelman who informs us that the spectrum of the star is similar to that of 16 Tauri, which is B7 IV on the MK system. It remains to put the colour excess on the $(P, V)_E$ system. From the data given by Johnson and Morgan (1953) we can find the relation between $[G-I]$ and $B-V$; that between $B-V$ and

$(P-V)_E$ has been given by Eggen (1955 a). Combining the two, we have, for reddened B-type stars only,

$$(P-V)_E = 0{\cdot}444 + 0{\cdot}55[G-I]$$

whence the colour excess for δ Cep B, and hence presumably for δ Cep itself, is $+0^m{\cdot}11$.

The important assumption in this procedure is that the companion is a normal star and not, for example, a binary with dissimilar components. Unfortunately the large absolute magnitude dispersion of the B-type stars, and the resulting uncertainty of the spectroscopic luminosity classification of δ Cep B preclude, at present, the use of this star for calibrating the zero-point of the period–luminosity relation.

Polaris also is a wide visual binary, and with an eighth magnitude star 18″ distant forms ADS 1477; the companion shares the proper motion, 0″·046, of the variable. The radial velocity of the companion from four Lick plates is −13 km/sec, and from seven Mt Wilson plates it is −5 km/sec; these figures are in only fair agreement with the systematic velocity of the variable, −16 km/sec (Roemer 1955). The magnitude and colour of the companion, determined by Kron and Eggen from one night of good seeing with the Crossley reflector, are $V_E = 8^m{\cdot}45$ and $(P-V)_E = +0^m{\cdot}31$. Since the median brightness of the variable is $V_E = 2^m{\cdot}00$, the photoelectric magnitude difference is $6^m{\cdot}45$, which agrees well with the visual magnitude difference found by the Harvard observers (Pickering, 1879) $6^m{\cdot}62$ and by Stebbins (1907), $6^m{\cdot}63$.

The most recent determinations of the spectral type of the companion are as follows:

Mt Wilson	dF1	(Adams *et al* 1935)
W. W. Morgan	F2 V	(1938)
W. P. Bidelman	F3 V	(unpublished).

For comparison we have the following F1 V to F3 V stars for which accurate colours and absolute magnitudes are known:

Star	$(P-V)_E$	M_V	Sp
37 U Ma	+0·21	+3·11	F1 V (Roman 1949)
78 U Ma	+0·235	+3·14	F2 V (Roman 1949)
HD 106946	+0·23	+3·01	F2 V (Weaver 1952)
ζ Ser	+0·255	+2·79	F3 V (Johnson and Morgan 1953)
Means	+0·23	+3·01	F2 V

The absolute magnitudes of the first three stars are found from cluster parallaxes and are taken from a previous paper (Eggen 1955 b) the luminosity of the last star was determined from the trigonometric parallax of 0·043 ± 0·005. If we adopt a spectral type of F2 V for the companion, the reddening is $+0^m{\cdot}08$. Also, if we adopt +3·0 as the visual absolute magnitude of the companion, we find $M_V = -3^m{\cdot}5$ for the variable at maximum; the corrected distance of Polaris is then about 100 parsecs. Since Polaris is a single-lined spectroscopic binary, the absolute magnitude of the cepheid component will, of course, be somewhat fainter than this.

3. *Spectral types and multi-colour photometry.*—One means of estimating the intrinsic colour of a cepheid is to compare the observed colour at some phase, say maximum light, with the colour of a non-variable, and supposedly unreddened,

star of the same spectral type. Code (1947), who has classified the spectra of 18 cepheids on the Yerkes system, finds that at maximum light they all have nearly the same spectral type, F6 Ib, and that the general features of cepheid spectra match those of standard supergiants well, although the hydrogen lines are abnormally strong at maximum and the *CN* band at $\lambda 4215$ is abnormally weak at minimum light.

The only reliable estimate of the intrinsic colour of an F-type non-variable supergiant is that for α Persei, F5 Ib, which is a member of the moving cluster in Perseus. It was previously shown (Eggen 1955 b) that the B-type stars in that cluster are reddened by $+0^{m}\cdot10$ on the $(P-V)_E$-system and this result has recently been confirmed by Harris (1956). Since the observed colour of α Persei is $(P-V)_E=+0^{m}\cdot36$, an intrinsic colour of $+0^{m}\cdot26$ will be assumed in the following discussion.

The following colour observations of non-variable supergiants have been taken from Stebbins and Whitford (1945) and Stebbins and Kron (1956); those of η Aquilae are from Stebbins, Kron and Smith (1952) and for δ Cephei from Stebbins (1945).

Star	Sp	$[B-G]$	$[R-I]$
		m	m
α Per	F5 Ib	−0·09	−0·09
35 Cyg	F5 Ib	+0·01	+0·06
44 Cyg	F5 Iab	+0·27	+0·42
HR 690	F7 Ib	+0·12	+0·21
45 Dra	F7 Ib	−0·03	−0·06
η Aql (Max)	F6 Ib	−0·02	+0·01
δ Cep ($0^{p}\cdot05$)	F6 Ib	−0·08	−0·09
β Aqr	G2 Ib	+0·15	+0·08
α' Cap	G3 Ib	+0·24	+0·20
ζ Cap	G4 Ib	+0·17	+0·04
9 Peg	G5 Ib	+0·23	+0·23
η Aql (Min)	G4 Ib	+0·22	+0·19
δ Cep (Min)	G2 Ib	+0·12	+0·09

The ultra-violet, which serves as such a useful discriminant between temperature and space reddening among the early type stars, loses its effectiveness for the later spectral types (Morgan, Harris and Johnson 1953) and has, therefore, not been included in this discussion. The values of $[B-G]$ and $[R-I]$ are plotted in Fig. 3 where the filled and open circles represent stars of types F5–F7 Ib and G2–G5 Ib, respectively. The continuous line is assumed to be the reddening path for the F5–F7 Ib stars; the broken line that of the G2–G5 Ib stars. The colour of δ Cephei near maximum light, indicated in the figure by a filled triangle, is almost identical with that of α Persei and the assumption that the $+0^{m}\cdot10$ reddening of the latter also applies to the variable is consistent with the reddening of $+0^{m}\cdot11$ found above for δ Cephei (B). Also, the colour of η Aquilae at maximum light, indicated in the figure by a filled square, is apparently reddened by $+0^{m}\cdot06$ in $[B-G]$ relative to δ Cephei and α Persei. From a comparison of the colours of the F5–F7 Ib stars we find $(P-V)_E=1\cdot5\,[B-G]+0^{m}\cdot5$ and, therefore, a reddening of $+0^{m}\cdot10+0^{m}\cdot09=+0^{m}\cdot19$ for η Aquilae.

The argument in the case of α Ursae Minoris, indicated in the figure by a cross, is not as straightforward as that given above for the other two variables because (*a*) the spectral type, F8 Ib, is intermediate between the two groups of non-variable supergiants plotted in the figure as open and filled circles and

(*b*) the known spectroscopic companion may influence the observed colours. In any case, the colour of α Ursae Minoris is slightly bluer than that of α Persei, which is consistent with the reddening value of $+0^{m}\cdot08$ for the former, obtained above from the visual companion.

4. *Intrinsic colours and absolute magnitudes.*—The available colours for galactic cepheids have been given in a previous paper (Eggen, Gascoigne and Burr, 1957). The colours of the observed variables in the Magellanic Clouds (Gascoigne and Kron 1952, and Gascoigne 1955), which have now been put on the $(P, V)_E$ system, are as follows:

Small Cloud			Large Cloud		
Var.	Log P	$(P-V)$ max	Var.	Log P	$(P-V)$ max
		m			m
HV 1342	1·254	+0·28	HV 886	1·379	+0·35
HV 817	1·276	+0·26	HV 1003	1·387	+0·35
HV 823	1·504	+0·40	HV 902	1·421	+0·25
HV 824	1·818	+0·39	HV 1002	1·483	+0·26
			HV 2294	1·563	+0·31
			HV 953	1·680	+0·44

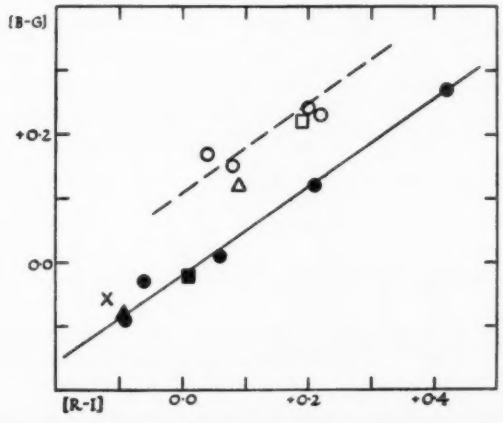

FIG. 3.—*The colours* [*B–G*] *and* [*R–I*] *for stars of types* F5–F7 Ib (*filled circles*), G2–G5 Ib (*open circles*), δ *Cephei at maximum* (*filled triangle*) *and minimum* (*open triangle*), η *Aquilae at maximum* (*filled square*) *and minimum* (*open square*), *and* α *Ursae Minoris* (*cross*). *The continuous line is the reddening path for the* F5–F7 Ib *stars and the broken line that of the* G2–G5 Ib *stars.*

The maximum colours of both the galactic and Cloud cepheids have been plotted in Fig. 4, where the crosses and open squares indicate respectively those of the galactic variables of population types I and II, and the open and filled circles those of the Small and Large Magellanic Clouds. The arrows attached to the colours of three galactic cepheids α Ursae Minoris, δ Cephei, and η Aquilae, indicate the amount of reddening derived for these variables in Section 2 and Section 3.

Fig. 4 brings us to the central question of the paper: do the galactic cepheids have the same intrinsic colours as those in the Clouds? The following points are relevant:

(i) With the exception of the population II variable W Virginis, *all* the Cloud cepheids are bluer than *all* the galactic cepheids of comparable period. In this connection, however, it should be remembered that (*a*) Cloud cepheids with periods less than 17 days have not been observed and (*b*) the longer period galactic variables, being more luminous, will in general be more distant and therefore more heavily reddened than those of shorter period (cf. Stibbs 1955 b). The marked difference between the colours of the observed galactic and Cloud cepheids is emphasized by the colour of the galactic variable β Doradus which, although only 6° from the centre of the Large Cloud and in the same galactic latitude, is decidedly redder than the Cloud cepheids. However, the absorbing material in the galaxy is known to be very patchy, and perhaps too much emphasis should not be placed on the colour of this one star.

(ii) The maximum intrinsic colours derived in Section 2 and Section 3 for three galactic cepheids are similar to these observed for the Cloud cepheids.

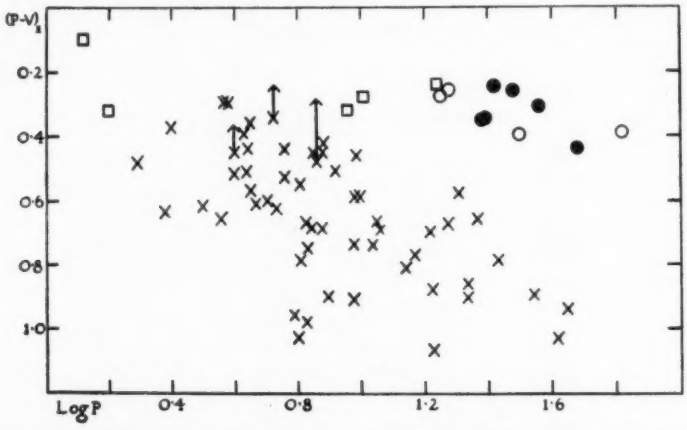

FIG. 4.—*Observed maximum colours of populations I and II galactic cepheids, crosses and open squares, respectively, and those of the Small and Large Magellanic Cloud, open and filled circles, respectively.*

(iii) The Cloud cepheids may themselves be reddened. Appreciable reddening seems unlikely in the direction of the Small Cloud, but unpublished colours, determined at Mt Stromlo by Gascoigne and Rodgers, indicate that some of the Large Cloud B-type stars are reddened $+0^{m}\cdot1$ or more by patchy obscuration either between us and the Cloud or within the Cloud itself. On the other hand, the existence of stars in both Clouds bluer than any so far observed in the galaxy (Code and Houck 1956) indicates that the Cloud cepheids are bluer than their galactic counterparts only because they are less reddened.

(iv) Although the observed sample is smaller, it may be significant that the dispersion in maximum colour of the Cloud cepheids is much smaller than that for the galactic variables of population I.

(v) The population I galactic cepheids do not themselves form a completely homogeneous group, but differ appreciably in almost all their observed characteristics, including the shape of light curve and the light, colour and velocity amplitudes. There is, moreover, the possibility that the intrinsic maximum colours may not be precisely the same for the three types A, B, and C.

(vi) There are a number of results, some well established, which tend to differentiate between the cepheids in the Small Cloud on one hand and those in the Large Cloud and in the galaxy on the other. Notable examples are the dissimilar correlations between period and light amplitude and the very marked differences in period distribution (cf. Gascoigne 1955).

(vii) The distinction between variables of populations I and II is neither clear-cut nor, in practice, easy to apply to individual cases. Of particular interest in this connection is the relation between such population II galactic variables as BL Herculis ($1^d \cdot 3$) and SW Tauri ($1^d \cdot 6$) and the variables with periods between one and two days that are so numerous in the Small Cloud (cf. Eggen, 1951).

(viii) The blueness of the galactic population II and of the Cloud variables, which lie, respectively, far above and below the galactic plane, and the redness of the population I galactic cepheids, which are closely clustered near the plane, may indicate that the stratum of absorbing material near the Sun is very patchy or very thin.

This evidence, though not conclusive as it stands, encourages us to investigate in detail the consequences of assuming an intrinsic colour at maximum of $0^m \cdot 25$ for both galactic and Cloud cepheids. There are some spectroscopic (Code 1947) and photometric indications of a dependence of maximum colour on period, but the effect seems small, and in what follows will be ignored. It has no effect on our main argument (cf. Section 6).

Support for these intrinsic colours comes from measures of polarization. Hiltner (1951) has published the following figures for seven cepheids observed by us (those for BG Lac were communicated privately):

Variable	l	b	δ (per cent)	E_1
	°	°		m
BG Lac	62·9	−9·7	1·8	0·19
Y Lac	66·5	−4·3	1·2	0·09
δ Cep	72·9	+0·4	0·6	0·04
RR Lac	73·4	−2·1	2·6	0·15
Z Lac	73·5	−1·7	2·3	0·24
RW Cas	96·8	−4·1	2·8	0·26
SU Cas	101·0	+9·1	1·9	0·12

The listed values of E_1 were derived from the values of A_{pg} in Table II with the assumption that $A_V = 0 \cdot 75\ A_{pg}$ and $A_V = 6 \cdot 1\ E_1$ (Morgan, Harris and Johnson, 1953). The percentage polarizations δ (per cent) and the colour excesses E_1 are plotted in Fig. 5, together with those for the B-type stars in the same galactic longitudes; the values of E_1 for the B-type stars were computed from the colours observed by Stebbins, Huffer and Whitford (1940) and the intrinsic colours derived by Morgan, Harris and Johnson (1953). This figure hardly suggests that the reddening of the cepheids has been overestimated. Although the material is too meagre for definite conclusions, the apparently better correlation between reddening and percentage polarization for the cepheids than for the B-type stars certainly deserves further investigation.

Blaauw and Morgan (1954) have recently redetermined the zero-point of the period–luminosity relation using accurate proper motions of 18 bright galactic cepheids. Accurate photometry is now also available for all these variables except W Gem and, after allowing for the absorption derived from the assumed intrinsic colour of $+0^m \cdot 25$, we have repeated the computations; the details are

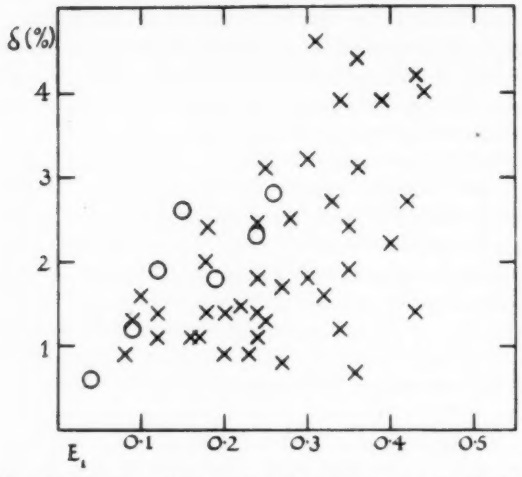

FIG. 5.—*Percentage polarizations,* δ (per cent), *and colour excesses,* E_1 *of cepheids* (*open circles*) *and B-type stars* (*crosses*).

listed in Table I. Assuming that the slope of the period–luminosity relation is as indicated by the cepheids in the Magellanic Clouds (Shapley 1940), the median absolute photographic magnitude, M, is given by the following expression:

$$M = C - 1{\cdot}74 \log P.$$

For convenience we will replace C by $(C' - 2^{m}{\cdot}0)$ and use the proper motions to determine C'. The second column of Table I contains the observed median

TABLE I

Proper motions of bright cepheids

v-components of proper motion for galactic cepheids ; unit is 0″·0001 p.a.

Star	$\dot{m}$	$\dot{m}_{corr}$	r_{kpc}	v	v'
α UMi	2·48	1·68	0·088	+557	+163
SU Cas	6·50	5·54	0·405	+ 99	+134
SZ Tau	7·22	5·74	0·526	+ 23	+ 40
β Dor	4·38	3·54	0·284	+ 17	+ 16
RT Aur	5·90	5·70	0·550	+104	+190
ζ Gem	4·66	3·30	0·257	+ 23	+ 20
l Car	4·78	2·22	0·242	+ 55	+ 44
X Sgr	5·13	4·33	0·363	+105	+127
W Sgr	5·28	4·48	0·400	+ 17	+ 23
Y Sgr	6·46	5·34	0·540	+155	+250
U Sgr	7·54	5·54	0·625	+116	+242
FF Aql	5·98	4·70	0·368	+ 26	+ 32
η Aql	4·58	3·66	0·269	+133	+120
S Sge	6·36	5·32	0·608	+ 53	+107
T Vul	6·28	5·84	0·622	+ 38	+ 79
DT Cyg	6·20	5·76	0·490	− 9	− 15
δ Cep	4·40	4·04	0·290	+167	+161

magnitudes, which are corrected in the third column for absorption as discussed above. The fourth column contains the computed distances in kiloparsecs with $C'=0$. The v-components of the cepheid motions (Blaauw and Morgan 1954) are listed in column 5 and, in column 6, are reduced to a mean distance of 300 parsecs. These reduced motions yield a mean parallax of $0''\cdot00328$ as compared with $0''\cdot00333$ derived from the distances in the sixth column of the table. The resulting value of C' is then $5\log(0''\cdot00328/0''\cdot00333)$ or $-0^{m}\cdot04$, and the period–luminosity relation then takes the following form:

$$\dot{M}=-2^{m}\cdot0-1\cdot74\log P,$$

which represents a correction of $-1^{m}\cdot7$ to the zero-point adopted by Shapley (1940). The distances of the galactic cepheids in Table I have been computed from this relation. Since Shapley also found that, for the observed median photographic magnitudes in the Magellanic Clouds,

$$\dot{M}=17^{m}\cdot04-1\cdot74\log P,$$

the distance modulus of the Clouds is then $19^{m}\cdot0$, if the magnitude systems are comparable (Gascoigne 1955).

5. *Distance and galactic rotation.*—We can now compute distances for the population I cepheids for which magnitudes and colours are known, and this is done in Table II. The photometric data are taken from Table IV of Eggen, Gascoigne and Burr (1957), and the colour excesses E converted to photographic absorptions A_{pg} by the result $A_{pg}=4E$ (Blanco 1956). These are listed in column 4. In the other columns are: the longitude measured from the galactic centre, $l+32^{\circ}$; the galactic latitude, b; the heliocentric, rectangular co-ordinates X, Y, and Z; the distance, R, of the variable from the galactic centre; and the radial velocity, v_r, corrected for a solar motion of 20·4 km/sec towards $l=17^{\circ}\cdot1$, $b=19^{\circ}\cdot6$ (Weaver 1955). The X-axis is directed towards the galactic centre, $l=328^{\circ}$ and $b=0^{\circ}$, the Y-axis towards $l=58^{\circ}$ and $b=0^{\circ}$ and the Z-axis towards the galactic pole. The Sun is assumed to be 8·4 kpc from the centre of the galaxy.

We have used the distances and radial velocities in Table II to discuss the differential galactic rotation in the manner first described by Camm (1938). If the circular velocity at a distance R from the galactic centre is V, then

$$v_r/\sin(l+32^{\circ})\cos b=R_{\odot}(V_{\odot}/R_{\odot}-V/R)$$

and the Oort constant is

$$A=-\frac{R}{2}\cdot\frac{d}{dR}\left(\frac{V}{R}\right).$$

No account is taken here of a possible K-term or of peculiar motions, that is, all the orbits are assumed to be circular. We also ignore the higher derivatives of V with respect to R. The 37 cepheids for which both radial velocity and accurate photometric data are available and for which $|\sin(l+32^{\circ})\cos b|>0\cdot3$ are plotted in Fig. 6. V Velorum, the radial velocity of which departs from the general run of values in the figure by nearly 50 km/sec, was omitted from the discussion and is plotted as a cross. Whilst most of the scatter in the figure comes from dispersion in the radial velocities, errors in distance determination cannot be disregarded, and give rise to a regression effect which we take

TABLE II

Distance, absorption, galactic coordinates and radial velocity for 55 population I galactic cepheids

Star	$l+32°$	b	A_{pg}	r_{kpc}	X	Y	Z	R	v_r
	°	°	m						
X Sgr	0·9	− 1·2	0·80	0·34	+0·34	+0·04	−0·01	8·06	− 0·9
W Sgr	1·2	− 5·4	0·80	0·40	+0·40	+0·01	−0·03	8·00	−13·0
WZ Sgr	11·8	− 2·8	2·44	1·51	+1·47	+0·31	−0·08	6·94	+ 2·3
Y Sgr	12·5	− 3·7	1·12	0·54	+0·53	+0·12	−0·03	7·87	+11·8
U Sgr	13·4	− 5·9	2·00	0·63	+0·61	+0·14	−0·07	7·79	+12·5
V350 Sgr	13·4	− 9·4	1·40	0·95	+0·92	+0·21	−0·16	7·48	+23·8
XX Sgr	14·7	− 3·4	2·16	1·51	+1·46	+0·38	−0·09	6·95	+18·0
YZ Sgr	17·4	− 8·6	1·96	0·94	+0·89	+0·28	−0·15	7·51	+33·6
Y Oph	20·3	+ 8·7	3·28	0·44	+0·41	+0·15	+0·06	7·99	+11·4
SS Scu	24·9	− 3·3	1·64	1·09	+0·99	+0·46	−0·06	7·42	+ 3·1
V496 Aql	28·5	− 8·7	2·92	0·74	+0·65	+0·36	−0·11	7·76	+21·0
U Aql	30·7	−13·1	1·72	0·65	+0·54	+0·32	−0·15	7·87	+ 9·2
SZ Aql	35·3	− 3·8	2·52	1·81	+1·48	+1·04	−0·12	7·00	+27·7
TT Aql	35·7	− 4·6	2·24	0·92	+0·74	+0·54	−0·07	7·68	+18·1
FN Aql	38·3	− 4·4	2·64	1·22	+0·95	+0·76	−0·09	7·49	+26·4
η Aql	40·8	−14·5	0·92	0·27	+0·19	+0·16	−0·06	8·21	+ 1·7
FM Aql	44·0	− 0·5	2·84	0·92	+0·66	+0·63	−0·01	7·76	+ 7·1
FF Aql	48·8	+ 5·1	1·28	0·37	+0·24	+0·28	+0·03	8·16	+ 5·3
S Sge	55·0	− 7·3	1·04	0·61	+0·35	+0·49	−0·07	8·06	+ 7·8
X Vul	63·6	− 2·4	3·12	1·13	+0·50	+1·01	−0·04	7·96	+ 5·4
SV Vul	63·7	− 0·8	2·76	1·33	+0·59	+1·19	−0·02	7·90	+16·1
SU Cyg	64·4	+ 1·5	0·20	1·00	+0·43	+0·90	+0·02	8·02	−17·1
T Vul	72·0	−11·1	0·44	0·62	+0·19	+0·59	−0·12	8·23	+14·7
DT Cyg	76·5	−11·6	0·44	0·49	+0·11	+0·47	−0·10	8·30	+15·0
X Cyg	76·7	− 5·1	1·80	0·84	+0·20	+0·81	−0·08	8·24	+25·6
BG Lac	92·9	− 9·7	1·52	1·79	−0·09	+1·77	−0·30	8·68	− 7·0
Y Lac	98·5	− 4·3	0·76	2·56	−0·38	+2·52	−0·19	9·13	− 5·9
δ Cep	104·9	+ 0·4	0·36	0·29	−0·08	+0·28	0·00	8·48	− 4·6
RR Lac	105·4	− 2·1	1·20	2·26	−0·61	+2·17	−0·09	9·27	−24·6
Z Lac	105·5	− 1·7	1·96	1·71	−0·46	+1·65	−0·05	9·01	−14·6
α U Mi	122·3	+26·8	0·80	0·09	−0·04	+0·07	+0·04	8·47	
RW Cas	128·8	− 4·1	2·08	2·86	−1·78	+2·22	−0·19	10·42	−59·8
SU Cas	133·0	+ 9·1	0·96	0·40	−0·27	+0·29	+0·06	8·67	− 3·7
RX Cam	145·5	+ 5·6	2·60	0·86	−0·70	+0·48	+0·08	9·11	−36·3
SV Per	162·3	− 0·3	1·68	2·21	−2·10	+0·67	−0·01	10·52	−16·9
RX Aur	165·5	+ 0·0	1·76	1·36	−1·32	+0·34	0·00	9·73	−29·4
SZ Tau	179·4	−17·3	1·48	0·53	−0·51	0·00	−0·15	8·91	−15·6
RT Aur	182·8	+10·3	0·20	0·55	−0·55	−0·02	+0·11	8·95	+ 9·6
ST Tau	192·8	− 6·6	1·08	1·45	−1·40	−0·32	−0·17	9·80	−15·2
ζ Gem	195·4	+13·4	1·36	0·26	−0·25	−0·02	+0·06	8·65	− 7·2
T Mon	203·3	− 1·1	2·16	0·77	−0·70	−0·31	−0·02	9·11	+14·6
RS Pup	252·1	+ 0·7	3·12	1·01	−0·33	−1·02	+0·01	8·79	+ 1·3
AH Vel	262·2	− 6·0	0·56	0·53	−0·08	−0·54	−0·06	8·52	+ 8·8
RZ Vel	262·6	− 1·2	1·32	1·57	−0·20	−1·56	−0·03	8·75	+ 8·9
T Vel	265·1	− 2·2	1·44	1·25	−0·11	−1·14	−0·04	8·58	− 8·4
SW Vel	265·8	− 2·4	1·64	2·46	−0·18	−2·45	−0·01	8·93	
β Dor	270·5	−32·3	0·84	0·28	0·00	−0·24	−0·14	8·40	−10·5
V Vel	276·2	− 3·8	1·04	1·12	−0·13	−1·11	+0·07	8·60	−43·0
l Car	282·7	− 6·8	2·56	0·24	+0·06	−0·24	−0·03	8·33	− 8·0
VY C r	286·2	+ 1·3	1·68	1·50	+0·41	−1·44	+0·04	8·12	−12·6
S Mus	299·1	− 7·8	1·36	0·70	+0·34	−0·61	−0·09	8·08	+ 3·0
T Cru	299·2	+ 0·2	1·68	0·67	+0·32	−0·58	0·00	8·11	−13·9
R Cru	299·4	+ 0·8	0·76	1·02	+0·52	−0·89	+0·01	7·93	−21·3
R Mus	301·6	− 6·9	0·68	0·92	+0·45	−0·73	−0·11	7·98	− 4·1
RY Sco	356·2	− 4·8	3·4:	0·95	+0·92	−0·06	−0·08	7·48	− 8·2

into account by Hertzprung's method (1922). The regression of R on $v_r/\sin(l+32^\circ)\cos b$ gives $A=22{\cdot}1$, and that of the v_r term on R gives 16·5. Assuming the errors in v_r to be about twice those in R (this is a minimum figure) we have the final result $A=17{\cdot}5\pm1{\cdot}9$(s.e.) km/sec/kpc.

In addition to the internal error of this result, there may be a further, systematic, error arising from the uncertainty of the zero-point of the period–luminosity relation; the dispersion in the proper motions alone (Section 4) introduces an uncertainty in A of 10 per cent. An independent determination of the zero-point would of course eliminate this uncertainty.

Stibbs (1956) has discussed in some detail the dependence of A, determined in this way, on the accuracy of the assumptions and of the observations involved. We may add that if the calculation is repeated with a value of 4·75 for the A_{pg}/E ratio instead of the 4·0 used here, the constant C in the period–luminosity relation becomes $-2^m{\cdot}2$ if the agreement with the mean parallaxes derived from the proper motions is to be preserved, and the resulting value of A is increased to 19·7 km/sec/kpc.

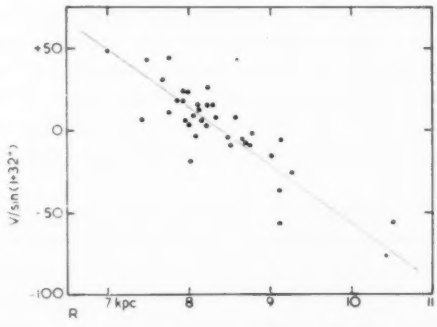

FIG. 6.—*Values of* $v_r/\sin(l+32^\circ)$, *and the distance,* R, *of* 37 *galactic cepheids.*

It is worth emphasizing that the value of A derived in this way is relatively insensitive to reasonable changes in the assumed intrinsic colours of the cepheids. For example, a change in the assumed intrinsic colour from $+0^m{\cdot}25$ to $+0^m{\cdot}35$ reduces the total absorption by $+0^m{\cdot}4$ for each variable and alters the constant, C, in the period–luminosity relation from $-2^m{\cdot}0$ to $-1^m{\cdot}6$ but leaves the distances, and hence the derived value of A, unchanged. In a previous computation (Gascoigne and Eggen, 1956) in which we assumed that the intrinsic colour was given by the expression $+0^m{\cdot}10+0^m{\cdot}13\log P$, the derived value of A was 18·4 km/sec/kpc, or only five per cent greater than the value derived above. This follows from the fact that the proper motions determine distances, not luminosities, and that any assumptions on luminosities and absorptions are, for the present purpose, only a means of extrapolating the distance scale from the nearer to the more distant cepheids.

Values of the rotation constant A have also been recently derived by Stibbs (1956), Weaver (1955) and Petrie, Cuttle and Andrews (1956). Stibbs found $A=19{\cdot}5$ or 19·9 km/sec/kpc, depending on particular assumptions for the K-term and for the longitude of the galactic centre. Our discussion differs from his in that it is confined to cepheids for which only photoelectric light-curves and

hence only measured colour excesses are available, and in the explicit derivation of the zero-point of the period–luminosity relation. It is the last point which enables us to establish the directness of the connection between the proper motions and Oort's A. Petrie, Cuttle and Andrews, using B-type stars with measured colour excesses and new spectroscopic absolute magnitudes, found 17·7 km/sec/kpc. Weaver, also using the cepheids, found $A = 10{\cdot}8$ km/sec/kpc, but a comparison between his distances and ours suggests that he may have underestimated the effect of absorption in the direction of the galactic centre and overestimated it in the direction of the anticentre.

6. *Galactic absorption.*—In a medium with large-scale variations of absorption, values of the "mean absorption" may have little significance, especially over large distances, but they do offer a convenient way of expressing relative amounts of photographic absorption derived from various assumptions and for that purpose will be used here. The mean absorption for the cepheids in Table I is +1·58 mag/kpc. The variables with periods respectively less than and greater than eight days yield absorptions of +1·44 and +1·73 mag/kpc; for the 18 stars in the quadrant $13^\circ \geq l > 289^\circ$ the absorption is +2·32 mag/kpc. These figures are appreciably smaller than the 3 mag/kpc previously derived (Gascoigne and Kron 1952), for three reasons: (*a*) the cepheids are here assumed to be $0^{m}{\cdot}4$ brighter than previously, (*b*) we have used the ratio $A_{pg}/E = 4{\cdot}0$ instead of 4·75 and (*c*) the mean has been computed in a different way. If the absorption and distance of the ith cepheid are A_i and r_i respectively, the mean used here is $\Sigma A_i/\Sigma r_i$ instead of, as previously, $\Sigma(A_i/r_i)$, which gives too much weight to the nearer stars.

The fact that the longer period cepheids show the larger mean absorption suggests that their colour excesses may have been slightly overestimated relative to the variables with shorter period. That the effect is small is shown by a previous computation (Gascoigne and Eggen 1956), in which the assumption that the intrinsic maximum colours are given by $+0^{m}{\cdot}10 + 0{\cdot}13 \log P$ led to mean absorptions of $+1^{m}{\cdot}89$ and $+1^{m}{\cdot}66$ for the cepheids with periods respectively less than and greater than eight days.

These mean absorptions are a good deal higher than those found by Joy and earlier workers, but larger values have come to be accepted in recent years, especially near the galactic plane, and our 1·6 mag/kpc now seems reasonable enough. For the nearer cepheids however the situation is different. The relevant data for the ten within 400 parsecs are listed in Table III. The mean absorption for the group is 1·5 mag for 400 parsecs, which is a rate of 3·5 mag/kpc. Such heavy absorption for the nearer cepheids implies that either they are redder than we have assumed, and especially that they are redder than the cepheids in the Magellanic Clouds, or that heavily obscuring clouds occur in the immediate vicinity of the Sun. Similar results were obtained from an analysis of the colours of the B-type stars (Oort 1938) which indicate an average photographic absorption of +2·4 mag/kpc for distances up to 800 parsecs and +2·8 mag/kpc for the region within 300 parsecs if $A_{pg}/E_1 = 8{\cdot}1$ (Morgan, Harris and Johnson 1953).

At first sight absorptions of this order seem quite at variance with those determined by the statistical astronomers. To examine the point more closely we compare some of our results with those obtained at the Warner and Swasey Observatory and recently summarized by McCuskey (1956); these investigations were chosen because of their extent and uniformity of treatment. The following

TABLE III

Distances and absorptions for the nearer cepheids

Star	l	b	A_{pg}	r_{kpc}
	°	°	m	
η Aql	8·8	−14·5	0·92	0·27
FF Aql	16·8	5·1	1·28	0·37
δ Cep	72·9	0·4	0·36	0·29
α UMi	90·3	26·8	0·80	0·09
SU Cas	101·0	9·1	0·80	0·40
ζ Gem	163·4	13·4	1·36	0·26
β Dor	238·5	−32·3	0·84	0·28
l Car	250·7	− 6·8	2·56	0·24
X Sgr	328·9	− 1·2	0·80	0·36
W Sgr	329·2	− 5·4	0·80	0·40

five cepheids in Table II lie within the "LF fields" discussed by McCuskey and his co-workers:

Star	l	b	A_{pg}	r_{kpc}	Reference	
	°	°	m			
SU Cyg	32·4	+1·5	0·20	1·00	LF2	*Ap. J.*, **106**, 1, 1947
RW Cas	96·8	−4·1	2·08	2·86	LF5	*Ap. J.*, **121**, 643, 1955
RX Cam	113·5	+5·6	2·60	0·86	LF6	*Ap. J.*, **115**, 479, 1954
SV Per	130·3	−0·3	1·68	2·21	LF7	*Ap. J.*, **109**, 414, 1949
RX Aur	133·5	0·0	1·76	1·36	LF7	*Ibid*

McCuskey's conclusions are that in LF2 "the absorption... appears to be negligible to a distance of 700 pc". For LF5 the absorption "sets in very near the Sun, within 100 parsecs at least, and increases rapidly to a value of 2 magnitudes at 2000 parsecs.... Thereafter the rate of increase is less rapid". For LF6 "the region is covered by an obscuring cloud which sets in at a distance of 200 parsecs and extends to 500 parsecs from the Sun.... The total absorption of this cloud is 2·0 mag at 500 parsecs (and) thereafter increases uniformly to 3 magnitudes at 2500 parsecs". Heeschen (1951) finds for this later region absorptions of about $+1^m{\cdot}0$ at 200 to 300 parsecs and $+2^m{\cdot}3$ at 800 parsecs. In LF7 the data "... are consistent with an absorption of 1·2 mag/kpc beginning 200 parsecs from the Sun", which would indicate absorptions of $+2^m{\cdot}4$ and $+1^m{\cdot}4$ for SV Persei and RX Aurigae respectively. Considering the nature of the problem and the necessity for averaging over large volumes of space, the general agreement is surprisingly good.

Commonwealth Observatory,
Mount Stromlo,
Canberra :
1957 *February.*

Royal Greenwich Observatory,
Herstmonceux Castle,
Hailsham, Sussex.

References

Adams, W. S., Joy, A. H., Humason, M. L. and Brayton, A. M., 1935, *Ap. J.*, **81**, 187 ; *Mt. Wilson Contr.* No. 511.
Blaauw, A. and Morgan, H. R., 1954, *B.A.N.*, **12**, 95 (No. 450).
Blanco, V., 1956, *Ap. J.*, **123**, 64.
Camm, G. L., 1938, *M.N.*, **99**, 71.
Code, A. D., 1957, *Ap. J.*, **106**, 309,
Code, A. D., 1957, *Report of the National Science Foundation Conference on the Cosmic Distance Scale* (in press).

Code, A. D. and Houck, T. E., 1956, *Ap. J.*, **61,** 173.
Eggen, O. J., 1951, *Ap. J.*, **113,** 367; *Lick Obs. Contr.*, Series II, No. 32.
Eggen, O. J., 1955 a, *A. J.*, **60,** 131; *Lick Obs. Bull.*, No. 532.
Eggen, O. J., 1955 b, *A. J.*, **60,** 407; *Lick Obs. Bull.*, No. 539.
Eggen, O. J., Gascoigne, S. C. B. and Burr, J., 1957, *M.N.*, **117,** 406.
Gascoigne, S. C. B., 1955, *Australian Journal of Science*, **17** : Supplement.
Gascoigne, S. C. B. and Kron, G. E., 1952, *P.A.S.P.*, **64,** 196.
Gascoigne, S. C. B. and Eggen, O. J., 1957, *Report of the National Science Foundation Conference on the Cosmic Distance Scale* (in press).
Harris, D. L., 1956, *Ap. J.*, **123,** 371.
Heeschen, D. S., 1951, *Ap. J.*, **114,** 132.
Hiltner, A. H., 1951, *Ap. J.*, **114,** 241; *Contr. McDonald Obs.*, No. 201.
Johnson, H. L., 1955, *Ann. d'Astroph.*, **18,** 292.
Johnson, H. L. and Morgan, W. W., 1953, *Ap. J.*, **117,** 313; *McDonald Obs. Contr.*, No. 216.
McCuskey, S. W., 1956, *Ap. J.*, **123,** 458.
Morgan, W. W., Harris, D. L. and Johnson, H. L., 1953, *Ap. J.*, **118,** 92.
Morgan, W. W., 1938, *Ap. J.*, **87,** 460.
Oort, J., 1938, *B.A.N.*, **8,** 233 (No. 308).
Petrie, R. M., Cuttle, P. M. and Andrews, D. H., 1956, *A. J.*, **61,** 289; *Dom. Astroph. Obs. Contr.*, No. 48.
Pickering, E. C., 1897, *H. A.*, **11.**
Roemer, E., 1955; Thesis, University of California.
Roman, N. G., 1949, *Ap. J.*, **110,** 205.
Shapley, H., 1940, *Proc. Nat. Acad. Sciences*, **9,** 541.
Stebbins, J., 1907, *Univ. Illinois Bulletin*, No. 25; 1945, *Ap. J.*, **101,** 45; *Mt. Wilson Contr.*, No. 704.
Stebbins, J., Huffer, C. M. and Whitford, A. E., 1940, *Ap. J.*, **91,** 20; *Mt. Wilson Contr.*, No. 621.
Stebbins, J. and Kron, G. E., 1956, *Ap. J.*, **123,** 440; *Lick Obs. Contr.*, Ser. II, No. 59.
Stebbins, J. and Whitford, A. E., 1945, *Ap. J.*, **102,** 318; *Mt. Wilson Obs. Contr.*, No. 712.
Stebbins, J., Kron, G. E. and Smith, J. L., 1952, *Ap. J.*, **115,** 292; *Lick Obs. Contr.*, Ser. II, No. 39.
Stibbs, D. W. N., 1955 a, *M.N.*, **115,** 323; 1955 b, *M.N.*, **115,** 363; 1956, *Obs.*, **76,** 85.
Weaver, H., 1952, *Ap. J.*, **116,** 612; *Lick Obs. Contr.*, Series II, No. 47; 1955, *A.J.*, **60,** 208.

THE PHOTOELECTRIC LIGHT CURVE OF V 499 SCO

G. G. Cillié and E. M. Lindsay

(Received 1957 March 8)

Summary

With the 60-inch Rockefeller reflector of the Boyden Observatory photoelectric light curves have been obtained in blue and yellow light for the star V 499 Sco. The star is a Beta Lyrae type with two fairly flat-topped equal maxima. The light elements are

$$\text{Min} = \text{JD } 2428340^{d}\cdot405 + 2^{d}\cdot3332977E.$$

The eclipsing variable V 499 Sco, which is the same as HD 158155 (spectrum B5) and CPD $-32^{\circ}4551$, was studied by Hertzsprung (**1**), who gave the following light elements for the system

$$\text{Min} = 2428339^{d}\cdot229 + 2^{d}\cdot33328E.$$

The star was stated to be either of the β-Lyrae or W Ursae Majoris type with equal minima, its magnitude varying between $8^{m}\cdot0$ and $8^{m}\cdot4$.

V 499 Sco was observed by us on a number of nights during 1952, 1953 and 1954 with the Linell–King photoelectric photometer with 1P21 tube attached to the Rockefeller reflector of the Boyden Observatory near Bloemfontein, South Africa. Altogether 1596 comparisons—862 in blue and 734 in yellow light—were made with a nearby star HD 157750 (spectrum G5) = CPD $-32^{\circ}4535$ (Ptm $8^{m}\cdot4$, Ptg $8^{m}\cdot8$). We used a third nearby star to check the constancy of our comparison star. On 3 nights we made 22 comparisons (11 in blue and 11 in yellow light) between the two comparison stars. The mean deviation from constancy for a single observation we found to be $\pm0^{m}\cdot021$ in blue light and $\pm0^{m}\cdot023$ in yellow light. We have taken this to indicate at least a very fair degree of constancy of our comparison star.

When plotting our observations according to Hertzsprung's light elements we found that his secondary minimum is $0^{m}\cdot088$ deeper in blue light and $0^{m}\cdot045$ deeper in yellow light than his primary minimum. We have therefore taken his secondary minimum as the true primary minimum. According to our observations the phase difference from true secondary to true primary minimum is 0·504. Hence we added $0\cdot504 \times 2^{d}\cdot3333$ to Hertzsprung's fundamental epoch, which gives the revised value JD $2428340^{d}\cdot405$. During 1953 we observed 3 primary minima of V 499 Sco whose Julian dates are given in Table I.

TABLE I

Date (1953)	JD of observed primary minimum	Wt.	JD of calculated primary minimum	O–C (in days)
July 4/5	2434563·3100	1	2434563·3100	$0^{d}\cdot0000$
July 18/19	2434577·3047	1	2434577·3098	$-0^{d}\cdot0051$
August 8/9	2434598·3105	5	2434598·3094	$+0^{d}\cdot0011$

Using the above revised fundamental epoch we find that the period which gives the best mean square fit is $2^{d}\cdot3332977$. We therefore propose the following light elements for the system V 499 Sco

$$\text{Min} = 2428340^{d}\cdot405 + 2^{d}\cdot3332977E.$$

These elements refer to what we consider as the true primary minimum. All the phases given in our subsequent tables and light curves were computed with

these elements. We should like to point out that the observation of an eclipsing variable whose period is so close to $2\frac{1}{3}$ days as that of V 499 Sco, presents a peculiar problem in view of the fact that the phases are practically exactly reproduced after 7 days. Even after 52 weeks there is very little shift. Hence, if one is not prepared to spread the observations of the star over a long period, say 5–10 years, it is very difficult to fill in all the gaps in the light curve. Even with our 1596 observations of the star, all told, we found that when all the observations were plotted, small stretches of the curve remained which were not very well observed, whereas other portions were well determined. This difficulty is somewhat enhanced by the fact that cloudy weather conditions at the Boyden Observatory sometimes show a tendency to be repeated with a period of a week.

TABLE II

Normal points of the blue light curve of V 499 Sco

Phase	Δm_b	M.e.	n	Phase	Δm_b	M.e.	n
0·002	+0m·273	±0m·002	26	0·569	−0m·102	±0m·004	22
·020	·228	·003	21	·589	·185	·003	27
·040	+0·101	·003	31	·616	·208	·006	12
·063	−0·072	·005	12	·640	·224	·006	14
·089	·194	·004	10	·667	·253	·003	14
·120	·225	·003	28	·685	·264	·003	21
·138	·241	·003	26	·700	·257	·004	23
·163	·254	·003	8	·716	·271	·003	20
·218	·273	·002	8	·762	·263	·003	7
·244	·269	·002	20	·778	·265	·003	7
·266	·285	·003	44	·818	·260	·002	28
·286	·278	·002	21	·841	·254	·002	36
·319	·263	·003	8	·852	·227	·003	29
·384	·231	·004	19	·882	·218	·004	14
·415	·190	·004	19	·901	·204	·005	20
·438	−0·086	·003	18	·924	·138	·003	32
·463	+0·076	·004	17	·942	−0·046	·002	29
·503	·185	·004	18	·960	+0·060	·002	26
·529	+0·113	·004	25	·976	·188	·003	44
0·550	−0·011	0·002	26	0·988	+0·244	0·003	32

TABLE III

Normal points of the yellow light curve of V 499 Sco

Phase	Δm_y	M.e.	n	Phase	Δm_y	M.e.	n
0·002	+0m·644	±0m·004	14	0·581	+0m·232	±0m·003	18
·020	·604	·003	12	·602	·196	·006	12
·039	·480	·004	16	·641	·175	·004	17
·067	·307	·004	11	·677	·149	·003	24
·101	·198	·004	19	·697	·153	·003	28
·121	·183	·004	16	·717	·129	·004	18
·136	·159	·005	18	·748	·138	·003	10
·155	·153	·003	15	·799	·144	·003	16
·227	·144	·003	15	·828	·147	·003	29
·253	·138	·003	27	·847	·164	·003	26
·270	·132	·003	28	·866	·172	·003	23
·286	·139	·002	23	·894	·184	·003	22
·367	·165	·002	29	·922	·246	·003	26
·425	·249	·004	32	·941	·348	·003	21
·457	·423	·004	19	·960	·459	·003	19
·503	·599	·004	20	·975	·564	·003	28
·536	·470	·004	40	0·988	+0·629	0·003	21
0·563	+0·319	0·003	22				

In Tables II and III the normal points of the blue and the yellow light curves of V 499 Sco are given, computed in the usual way. In the first and second columns are given the phases and magnitude differences of the normal points. The third column gives the mean error for each normal point and the fourth column the number of observations used in forming it. The mean errors are no larger than we expected from previous investigations of the same kind (**2**).

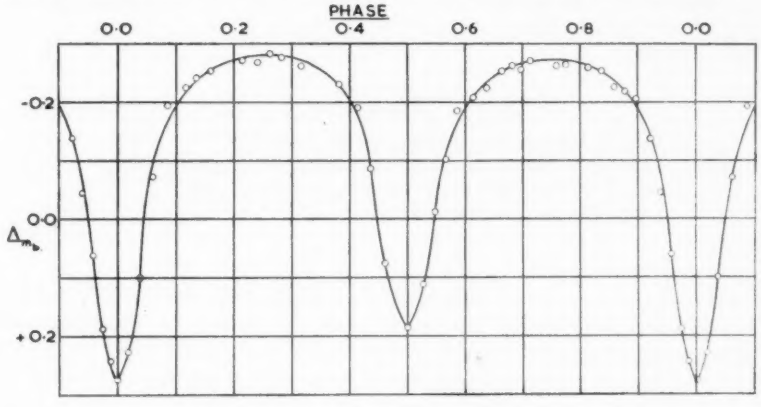

FIG. 1.—*Blue light curve of V 499 Scorpii.*

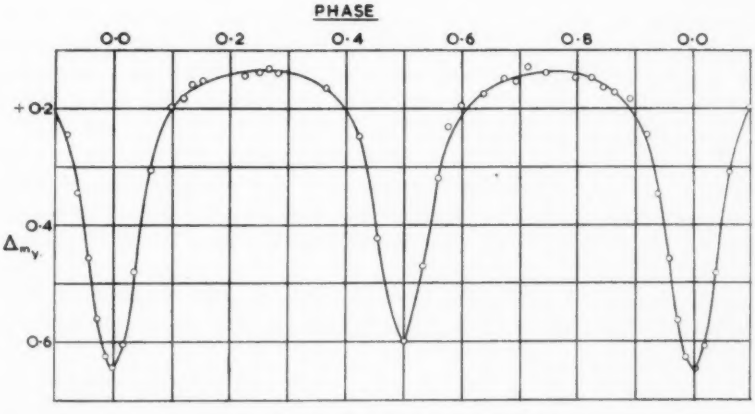

FIG. 2.—*Yellow light curve of V 499 Scorpii.*

Fig. 1 gives the blue light curve and Fig. 2 the yellow light curve of V 499 Sco. These curves clearly show that the primary minimum is somewhat deeper than the secondary minimum. There seems to be no significant difference between the two maxima, a result which is confirmed by our preliminary light curves drawn through the means of all plotted observations. These preliminary curves differ from our published ones in that the maxima are more flat-topped and that they show evidence of shoulders in both cases.

According to the Gaposchkins (**3**) V 499 Sco is a β-Lyrae star on account of its period being more than 12 hours. Our investigation reveals it as a β-Lyrae

star with two fairly flat topped equal maxima and evidence of shoulders in the light curve. Its components are presumably less elliptical than those of V 525 Sag (**4**) for instance.

In conclusion it is a pleasure to record our thanks to the staff of the Boyden Observatory for assisting with the observations of this star on a number of nights.

Department of Mathematics,
University of Stellenbosch,
Union of South Africa:
1957 *February* 21.

Armagh Observatory,
Northern Ireland.

References

(1) E. Hertzsprung, *B.A.N.*, **9**, 203, 1941.
(2) G. G. Cillié and E. M. Lindsay, *M.N.*, **113**, 516, 1953.
(3) *Variable Stars*, H. O. Monograph, No. 5, 1938.
(4) Cillié and Lindsay, *ibid.*

SPECTRAL TYPES AND LUMINOSITIES OF B, A AND F SOUTHERN STARS

Antoinette de Vaucouleurs

(Communicated by the Acting Commonwealth Astronomer)

(Received 1957 January 29)

Summary

Three hundred and sixty-six southern stars of B, A and F types brighter than 6·5 mag. were classified on the MK system. Microphotometer tracings were used to estimate the line ratios. A mean modulus for the members of the Scorpio-Centaurus cluster is determined. The calibration of absolute magnitudes of B stars is briefly discussed.

The spectrograms were obtained with a three-prism spectrograph at the Cassegrain focus of the Reynolds 30-inch reflector (dispersion 35 A/mm at Hγ; range Hζ to Hβ: $\lambda\lambda$ 3900–4900 A). As the spectra were taken primarily for radial velocity measurements in another programme, they were too narrow for classification by visual inspection. They were therefore recorded with a Hilger microphotometer and relative intensities of the pairs of lines used as criteria were estimated on tracings of small enlargement ($\times 7$). The extensions of the wings of the hydrogen lines were examined by a binocular microscope. The procedure was found most valuable for B and A stars and even for F stars which show a greater number of sensitive line ratios. The main difficulties encountered were due to the plate granulation which affected the depth of faint lines and the differences in density. Dense spectra were recorded with two sensitivity ratios in order to obtain more details in the darker region. Another difficulty, common to all procedures, was the shortage of standards.

The distribution of the 63 MK standards (**1**) recorded is given in Table I. The main gap occurs among A type stars and for luminosities II and IV among all types.

The 366 southern stars brighter than 6·5 mag., 263 of which are south of $-30°$, classified on the MK system (**1**), are listed in Table II. The columns give:

(1) the name of the star;

(2) the H.D. number;

(3) and (4) the galactic longitude and latitude to the nearest degree;

(5) the spectral type and luminosity class;

(6) the Harvard photovisual magnitude; an asterisk indicates that the magnitude has been corrected by +0·3 for a single-spectrum binary, or +0·6 for a two-spectra binary;

(7) the colour excess derived from various colour indices all converted to the B–V system: the value of the intrinsic colours were taken from (**1**). The main sources were the Cape Mimeograms (**2**) and the list published by J. Schilt and C. Jackson (**3**). The latter were corrected for lack of linearity by comparison with the converted B–V Cape colours. A few other colours were found in the

TABLE I

MK standards recorded

T \ L	I	II	III	IV	V	(*n*)
O 9			1			
O 9·5	1				1	
B 0	1				2	
B 0·5	1		1			
B 1	1	1	1		2	
B 2		1	1	2	2	
B 3	1	1			1	
B 5	2		1		1	
B 6			1		1	
B 7			2		1	
B 8	1	1			2	
B 9		1	1			(37)
A 0	1				1	
A 1					2	
A 2				1	1	
A 3			1	1	1	
A 5			1		1	
A 7			1			(12)
F 0	1		1	1	1	
F 2	1	1	1		1	
F 6		1		1	1	
F 7				1	1	
F 8					1	(14)
(*n*)	(11)	(7)	(14)	(7)	(24)	(63)

work of O. J. Eggen (**4**) and some $B-V$ indices were communicated by A. R. Hogg in advance of publication. When two or more different values were obtained for a star, the mean $B-V$ was used; the agreement was good except in two or three cases (see notes at the end of the table). Negative colour excesses were disregarded;

(8) the modulus $m_0-M=m-3E_y-M$, where M is the visual absolute magnitude as given by Morgan and Keenan (**5**) and corresponding to the spectral type and luminosity. When no colour-excess is available the value of the modulus is given in parentheses; and

(9) remarks and references to notes at the end of the Table. Recent classifications on the MK system taken from a variety of sources are given in parentheses.

B stars.—The catalogue includes 218 B stars, 75 of which are members of the Scorpio–Centaurus cluster. Fifteen stars which seemed intermediate between B_3 and B_5 were classified B_4, even though this subdivision does not exist in the MKK and MK systems. Type-differences in the B stars are shown mainly by the progressive increase of the hydrogen lines and the decrease of He I lines: λλ 4471, 4387, 4144 and 4026. The luminosity classification depends on the ratios 4009/4089, 4119/4144, 3995/4009, 4416/4387, 4481/4471 and the sharpness of the hydrogen lines. The classifications were made twice independently and the average difference between the two determinations is:

0·4 of a subclass both for types and luminosities. A comparison with M. L. Woods' catalogue (**6**), which gives the most extensive list of stars in common, indicates for about one hundred B stars the following average differences:

0·6 of a subclass for types, 0·5 for luminosities.

TABLE II

Name	HD	l	b	Sp	m(HP$_v$)	E_y	m_0–M	Remarks
49 G Cet	2696	49	−84	A3 V	5·21	...	(3·41)	
λ' Phe	2834	277	−68	A0 V	4·82	+0·02	4·46	
β^1 Tuc	2884	273	−54	B8 V	4·42	+0·04	4·8	
β^2 Tuc	2885	...	...	A2 IV			4·1	
70 G Phe	4293	270	−75	A7 III	5·95	...	(5·65)	
α Scl	5737	214	−86	B8 III	4·34	−0·05	7·34	
σ Scl	6178	227	−84	A2 V	5·48	...	(4·28)	
υ Phe	6767	252	−75	A3 V	5·10	+0·13	2·91	
ζ Phe	6882	263	−62	B6 V	4·62*	+0·07	5·51	
102 G Scl	7312	241	−78	A7 III	5·86	...	(5·56)	
12 G Hyi	9896	256	−58	F2 V	6·05	...	(2·85)	
α Eri	10144	255	−59	B5 V:	0·6	−0·01	1·9	
129 G Scl	10538	220	−75	A2 V	5·60	−0·02	4·40	
α Hyi	12311	255	−54	A9 III	2·95	+0·04	2·43	HD: Fo
μ For	13709	194	−70	A1 V	5·18	−0·02	4·38	
ϕ Eri	14228	240	−60	B8 V	3·67	+0·01	4·14	
δ Hyi	15008	257	−46	A2 V	4·20	−0·01	3·00	
λ Hor	15233	249	−54	F2 IIIp	5·40	−0·01	4·60	
κ Eri	15371	232	−61	B5 III	4·61*	+0·03	7·72	
ε Hyi	16978	254	−46	B9 III	4·16	+0·02	6·10	
π Cet	17081	159	−58	B6 III	4·54*	+0·03	7·55	(B7 V) (1)
93 Cet	18883	141	−44	B7 III	5·65	+0·05	8·50	
τ^3 Eri	18978	181	−59	A3 IV	4·03	+0·11	2·70	
71 G Eri	20121	220	−56	F6 III	5·89*	−0·07	4·89	
55 G Hyi	20313	262	−36	Fo II	5·63	...	(7·63)	
ζ Eri	20320	159	−50	Am	4·80	...	...	H lines A3
ξ Tau	21364	142	−36	B8 V	4·22*	+0·03	4·63	
59 G Hyi	21722	251	−42	F5 IV	5·88	...	(3·18)	
44 G Hor	21981	223	−52	A2 V	5·93	+0·12	4·37	
7 G Ret	22252	249	−43	B7 V	5·68	+0·07	6·27	
τ For	22789	191	−51	A0 V	6·04	+0·01	5·71	
17 G Ret	25346	234	−45	F2 III	6·07	...	(5·27)	
210 G Eri	27563	169	−35	B5 III	5·77	...	(8·97)	
4 G Dor	27604	228	−43	F5 IV	5·98	+0·02	3·22	
1 G Cae	28246	215	−43	F6 V	6·12	...	(2·32)	
α Dor	29305	230	−41	A0 V:	3·39	−0·05	3·09:	
253 G Eri	29435	198	−40	B9 IV–V	6·24	0·0	6·74	
268 G Eri	30422	195	−37	A3 III–IV	6·00	...	(5·70)	
19 G Cae	31093	204	−37	A1: V	5·75	+0·09	4·68	K line A2
ι' Pic	31203	227	−38	Fo IV	5·46	...	(3·46)	
ζ Dor	33262	232	−36	F7 V	4·68	+0·05	0·53	
12 G Col	34868	197	−30	A0 IV	5·73	−0·02	6·13	or B9?
18 G Col	36060	213	−32	Am	5·79	...	...	K line A3
82 G Lep	40972	198	−20	A1 V	5·90	−0·02	5·10	
74 G Col	41843	203	−21	A1: V	5·71	0·0	4·91	
94 G Lep	42301	196	−17	A0 IV	5·41	−0·02	5·81	
90 G Col	44506	209	−20	B2 Vn	5·86*	+0·02	8·40	(B1·5 V:)
36 G Mon	45320	179	−04	A7 IIIp	5·69	...	(5·39)	
α Car	45348	228	−24	Fo Iab	−0·79	−0·13	3·71	
74 G CMa	49131	208	−13	B3 V	5·83	−0·02	7·83	

TABLE II—(*cont.*)

Name	HD	l	b	Sp	$m(HP_v)$	E_{y}	m_0-M	Remarks
80 G Mon	49643	182	00	B8 V	5·61	...	(6·11)	HD: Ao
ζ Men	50506	258	−27	A5 III	5·58	...	(5·58)	
101 G Mon	52312	189	−01	B9 III	5·80	...	(7·80)	HD: Ao
120 G CMa	54031	209	−09	B3 IV	6·92*	+0·01	9·39	
122 G CMa	54309	203	−06	B1: Ve	5·75	+0·07	8·74	
δ Mon	55185	183	−06	Ao IV	4·08	0·0	4·48	
158 G CMa	57593	208	−05	B3 V	5·84	−0·02	7·84	
δ Vol	57623	246	−22	F8 I–II	3·94	+0·27	7·63	
96 G Pup	59550	212	−05	B3 IV	5·80	−0·03	8·60	
108 G Pup	60532	205	00	F7 IV	4·37	+0·01	1·34	
f Pup	61330	217	−06	B8 V	4·59	−0·01	5·09	
3 l Pup	62623	212	−02	A2 Iab	4·03	+0·09	11·19	
161 G Pup	62747	208	−01	B1 V	5·61	+0·04	8·69	
o Pup	63462	209	−01	B1 Ve	4·54	+0·17	7·23	(Bo V: pe) (2)
P Pup	63922	227	−09	Bo·5 III	4·17	+0·08	8·33	
b Pup	64503	221	−04	B2: V	4·84*	+0·04	7·32	
D Car	66591	243	−16	B3 IV	4·84	+0·02	7·58	
16 Pup	67797	207	−08	B3 V	4·64*	+0·02	6·58	
ϵ Vol	68520	248	−18	B5 III	4·64*	+0·02	7·78	
280 G Pup	69253	225	−02	B3 V	6·63	...	(8·63)	
q Pup	70060	222	−01	A7 III	4·42	+0·03	4·00	
α Cha	71243	256	−21	F2 IV	4·01	+0·02	1·45	
48G e Vel	73634	229	00	A9 I–II	4·08	−0·15	8·58	
o Vel	74195	237	−06	B3 III	3·86*	+0·01	7·53	
d Car	74375	232	−01	B1 III	4·60*	+0·11	8·57	
δ Vel	74956	239	−06	Ao: V	2·23*	+0·04	1·81	
f Car	75311	241	−08	B3 Vne	4·51	+0·03	6·42	
c Car	76728	245	−09	B8 II	3·88	−0·02	8·12	
b Car	77002	244	−09	B3 IV	4·93	...	(7·73)	
91G w Vel	77258	231	+04	F8 IV	4·32	+0·11	0·89	
α Vol	78045	250	−13	A5 III	4·42*	+0·03	4·33	
G Car	78791	255	−16	F6 II–III	4·42	+0·12	6·06	
105 G Vel	79275	236	+02	B2 IV	5·80	+0·01	9·07	
a Car	79351	245	−07	B2 IV	4·03*	+0·05	7·18	
i Car	79447	247	−09	B3 IV	4·06	+0·01	6·83	
z Vel	79735	234	+04	B5 Vn	5·09	0·0	6·39	
k Vel	79940	230	+09	F5 III	4·62	+0·01	3·59	
β Car	80007	253	−14	A1 IV	1·72	−0·05	1·82	
ι Car	80404	246	−07	Fo Iab	2·18	−0·13	5·68	
κ Vel	81188	243	−03	B2 IV	2·81*	+0·06	5·93	
ψ Vel	82434	234	+09	F2 IV	3·84*	−0·02	1·34	
32 τ^2 Hya	82446	204	+36	A3 III	4·65*	+0·03	4·86	(A3 III)
145 G Vel	82984	240	+03	B4 Vn	5·53*	0·0	7·23	
m Car	83944	249	−06	B9 V	4·87*	−0·01	4·87	
O Vel	84461	245	00	Ao V	5·93*	−0·03	5·63	
157 G Vel	84816	239	+07	B2:Vn	5·62	+0·04	8·10	
υ CarA	85123	253	−09	A9 II	3·08	+0·01	5·05	HD: Fo
165 G Vel	85953	244	+03	B2 III	5·88	+0·06	9·80	
166 G Vel	85980	241	+07	B3 V	5·69	+0·04	7·57	
ϕ Vel	86440	247	00	B5 I–II	3·58	+0·04	7·96	(3)

TABLE II—(*cont.*)

Name	HD	l	b	Sp	$m(HP_v)$	E_u	m_0-M	Remarks
υ^2 Hya	87504	221	+34	B8 III	4·67	+0·02	7·61	
α Sex	87887	210	+43	Ao III	4·44	−0·03	5·54	
183 G Car	88907	253	−04	B3 Vn	6·36	+0·05	8·21	
q Vel	88955	242	+12	A2 V	4·04	−0·02	2·78	
ω Car	89080	258	−11	B7 IV	3·44	+0·04	5·12	
J Vel	89890	251	+01	B3 IV	4·53	+0·06	7·15	
I Car	90589	261	−14	F2 III	4·30*	−0·02	3·50	
s Car	90853	253	−01	Fo I–II	4·00	+0·01	5·97:	
p Car	91465	255	−03	B3 Ve	3·44	+0·06	5·26	
212 G Car	92287	253	+01	B3 III	6·50*	+0·04	10·08	
θ Car	93030	257	−05	09·5 V	3·21*	+0·07	6·90	
228 G Car	93163	257	−05	B3: V	6·02	+0·13	7·63	
229 G Car	93194	257	−04	B5 Vn	4·97	0·0	6·27	
236 G Car	93540	258	−05	B7: V	5·42	+0·02	6·16	
238 G Car	93607	257	−04	B4 IV	4·98	0·0	7·48	
δ^2 Cha	93845	265	−19	B3 V	4·50	+0·02	6·44	
i Vel	95370	250	+16	A2 IV	4·52	+0·03	3·43	
β Crt	97277	243	+35	A2 III–IV	4·52	−0·06	4·82	
y Car	97534	259	00	F2 Ip	4·65	+0·14	8·73	(Fo Ia) (4)
74 ϕ Leo	98058	232	+52	A7 IV	4·59	+0·03	2·80	(A7 III–IV)
π Cen	98718	258	+06	B6 Vn	4·74*	−0·04	5·84	
15 γ Crt	99211	244	+41	A7 IV	4·08	+0·02	2·32	
33 G Cen	99556	261	00	B5 Iv	5·41	+0·05	7·46	
λ Cen	100841	262	−01	B9 II:	3·24	−0·01	7·04	
50 G Cen	100929	262	00	B3 IV	5·69	+0·08	8·25	
λ Mus	102249	264	−05	A7 II–III	3·74	−0·04	5·74	
j Cen	102776	264	−02	B3: Vne	4·40	+0·03	6·31	
18 G Mus	103079	264	−03	B4 IV	5·28*	+0·05	7·63	
1 G Cru	103884	264	00	B3 V	5·57	+0·03	7·48	
θ' Cru	104671	265	−01	Ap	5·02*	...	...	Am ?
θ^2 Cru	104841	265	−01	B2 IV	5·09*	+0·13	8·00	
η Cru	105211	266	−02	Fo III	4·23	+0·03	3·54	
92 G Cen	105382	264	+12	B6 III–IV	4·68	−0·02	7·28	
δ Cen	105435	264	+12	B3 Vne	2·73v	+0·03	4·6	
ρ Cen	105937	265	+10	B4 V	4·06	+0·02	5·60	
δ Cru	106490	266	+04	B2 IV	2·93	0·0	6·23	
γ Crv	106625	260	+44	B8 IV	2·88*	−0·01	4·95	(B8 III)
β Cha	106911	268	−17	B6 V	4·25	+0·03	5·26	
ζ Cru	106983	267	−01	B3 IV	4·11	+0·01	6·88	
113 G Cen	107832	265	+27	B9 III	5·35	−0·01	7·35	
25 G Cru	108250	268	−01	B4 IV	5·31*	+0·05	7·66	
119 G Cen	108257	267	+11	B5 Vn	4·90	0·0	6·20	
σ Cen	108483	267	+12	B3 Vn	4·01	−0·01	6·01	
γ Mus	109026	269	−10	B5 V	3·91	0·0	5·21	
η Crv	109085	266	+46	Fo IV	4·95*	+0·07	2·74	
α Mus	109668	269	−07	B3 IV	2·79	−0·01	5·59	
45 G Cru	110956	270	+06	B3 IV	4·71	+0·04	7·39	
β Cru	111123	270	+03	Bo·5 IV	1·65*	+0·04	5·53	
p Cen	111597	271	+29	Ao IV	4·98	−0·03	5·38	
n Cen	111968	272	+12	A7 III	4·32	+0·02	3·96	

TABLE II—(*cont.*)

Name	HD	l	b	Sp	$m(HP_v)$	E_y	m_0-M	Remarks
λ Cru	112078	271	+03	B5: Vn	4·70	−0·01	6·00	
μ^2 Cru	112091	271	+05	B5 Ve	5·32	+0·02	6·56	
μ' Cru	112092	271	+05	B3 IV	4·11	+0·01	6·88	
f Cen	113703	273	+14	B4 IV	4·81	+0·02	7·25	
ξ^2 Cen	113791	273	+13	B2 IV	4·56*	+0·02	7·80	
51 θ Vir	114330	291	+56	A1 III–IV	4·66*	−0·06	5·16	
202 G Cen	115823	275	+10	B5 III	5·55	0·0	8·75	
ι Cen	115892	278	+25	A2 V	2·90	−0·02	1·70	
J Cen	116087	274	+01	B5 V	4·50	+0·02	5·74	
ϵ Cen	118716	278	+08	B1 V	2·41	+0·03	5·52	
1 i Cen	119756	284	+28	F2 III	4·54*	−0·01	3·74	
ν Cen	120307	282	+19	B2 V	3·76*	0·0	6·36	
μ Cen	120324	282	+18	B3 Ve	3·24	0·0	5·24	
278 G Cen	120640	282	+14	B4 III	6·02*	0·0	9·52	
3 k Cen	120709	285	+27	B5 IV	4·59	+0·01	6·76	
3 CenB	120710	285	+27	B8 V	6·04	+0·01	6·51	
283 G Cen	120908	280	+08	B5 V	5·94	+0·11	6·91	
4 h Cen	120955	286	+29	B5 IV	5·00*	+0·01	7·17	
ϕ Cen	121743	284	+18	B2 V	3·96	0·0	6·56	
υ^1 Cen	121790	283	+16	B3 IV	4·09	−0·02	6·89	
υ^2 Cen	122223	284	+15	F7 I–II	4·61*	+0·10	6·31	
β Cen	122451	280	+01	B1 III	1·02*	+0·03	5·23	
χ Cen	122980	286	+19	B2 V	4·47	+0·02	7·01	
318 G Cen	123335	280	+01	B5 IV	6·43	+0·14	8·21	
328 G An	124367	282	+03	B3 Ve	5·20	+0·07	6·99	
ϵ Aps	124771	274	−18	B4 IV	5·07	+0·07	7·36	
ι Lup	125238	286	+13	B3 V	4·02	0·0	6·02	
v Cen	125288	283	+04	B5 II	4·28	+0·21	8·15	(5)
a Cen	125823	290	+19	B6 III	4·51	−0·06	7·61	
σ Lup	127381	287	+08	B2 V	4·45	+0·03	6·96	
η Cen	127972	291	+15	B3 III	3·13*	−0·02	6·83	+ A comp.
ρ Lup	128345	288	+09	B5 V	4·01	−0·01	5·31	
α CirA	128898	282	−05	Fo Vp	3·34	−0·05	0·34	
α Lup	129056	289	+11	B1 III	3·06*	+0·05	7·21	
b Cen	129116	294	+20	B3 V	4·06	+0·01	6·03	
21 G Cir	129557	286	+03	B2 IV	6·09	+0·09	9·12	
57 Hya	130274	301	+28	B9 V	5·62	+0·04	5·50	
o Lup	130807	293	+13	B6 III	4·43	−0·02	7·53	
ζ Cir	131058	282	−06	B5 Vn	6·01	0·0	7·31	
θ' Cir	131492	284	−03	B3 Vne	5·27	+0·09	7·00	
β Lup	132058	294	+13	B2 V	3·03*	0·0	5·63	
κ Cen	132200	295	+13	B2 III	3·58*	+0·02	7·62	
45 G Lup	132955	301	+22	B4 IV	5·37	+0·03	7·78	
π Lup	133242–3	293	+09	B5 IV	(4·7)	0·0	6·9	
58 G Lup	133937	296	+13	B6 V	5·92	+0·02	6·96	
λ Lup	133955	295	+10	B3 IV	4·89*	+0·01	7·66	
e Lup	134687	296	+10	B3 III	5·16*	0·0	8·86	
β Cir	135379	289	−01	A3 IV	4·12	+0·01	3·09	
γ TrA	135382	283	−10	A1 V	2·98	−0·05	2·18	
79 G Lup	135876	299	+13	B9 V	5·97*	−0·06	5·97	

TABLE II—(*cont.*)

Name	HD	l	b	Sp	$m(HP_v)$	E_y	m_0-M	Remarks
δ Lup	136298	299	+13	B3 IV	3·33	−0·03	6·13	
ϵ Lup	136504	297	+10	B3 IV	3·95*	0·0	7·05	
ϕ^2 Lup	136664	301	+16	B3 IV	4·66	+0·03	7·37	
k Lup	137058	301	+14	A0 IV	4·64	+0·02	4·18	
100 G Lup	137432	303	+16	B4 V	5·48	+0·02	7·02	
35 ζ^2 Lib	138485	317	+30	B3 III	5·90*	0·0	9·60	
γ Lup	138690	301	+11	B3 V	3·48*	−0·02	5·48	
90 G Lib	138764	324	+35	B6 IV	5·16	0·0	7·26	
d Lup	138769	299	+08	B3 IV	4·74	0·0	7·55	
τ Lib	139365	309	+20	B4 V	4·00*	−0·02	5·60	
g Lup	139664	300	+08	F2 IV	4·60	+0·03	2·01	
ψ^2 Lup	140008	307	+15	B6 V	5·38*	−0·02	6·48	
128 G Lup	140784	307	+15	B6 Vn	5·57	+0·04	6·55	
β SerA	141003	354	+47	A2: IV	3·57	0·0	3·37	(A2 IV)
14 G Nor	141318	294	−02	B2 III	5·72	+0·17	9·31	
χ Lup	141556	309	+15	A0 III–IV	4·69*	−0·04	5·49	HD: B9
1(b) Sco	141637	314	+21	B3 V	4·74	+0·09	6·47	
β TrA	141891	309	−08	F0 V	2·97	−0·02	0·0	
2(A) Sco	142114	315	+20	B3 Vn	4·59	+0·08	6·35	(B3 V)
4 G Sco	142165	316	+21	B6 Vn	5·36	+0·10	6·16	
5G Sco	142184	316	+21	B3 Vne?	5·35	+0·11	7·02	
ρ Sco	142669	312	+17	B3 IV	3·97	−0·02	6·77	(B2 V)
6 π Sco	143018	315	+19	B2 IV	3·52*	+0·02	6·76	(B1 V)
η Lup	143118	307	+10	B3 V	3·56	−0·03	5·56	
151 G Lup	143699	307	+10	B5 V	4·96	0·0	6·26	
β ScoA	144217	321	+22	B1 V	2·83	+0·20	5·43	(B0·5 V)
θ Lup	144294	309	+10	B3 IV	4·27	+0·01	7·04	
229 G Sco	144892	331	+28	F7 V	6·48	...	(2·5)	
13 Sco	145482	316	+15	B3 Vn	4·65	+0·01	6·62	
ν Sco	145502	323	+21	B3 V	4·50*	+0·20	5·90	(B2 IV ?)
o Sco	147084	320	+17	A5 III :	4·73	+0·63	2·84	(A5 II) (6)
52 G Nor	147152	302	−01	B6 V	5·36	...	6·46	
ϵ' Nor	147971	304	00	B3: V	5·18*	+0·11	6·85	
7 χ Oph	148184	326	+20	B3 V: e	5·04*	+0·40	5·84	(B2 IVp)
26 G Oct	148542	274	−26	A3 IV	6·05	...	(5·05)	
71 G Sco	148688	308	+03	B1 Ia	5·39	+0·47	10·98	(B1 Ia)
N Sco	148703	314	+08	B2 V	4·61*	+0·05	7·06	
62 G Nor	149711	308	+01	B3 III–IV	5·99	+0·12	8·93	
μ' Sco	151890	314	+03	B3 Vp	3·74*	−0·02	5·74	(B1·5 V)
μ^2 Sco	151985	315	+03	B2 IV	3·67	+0·01	6·94	
101 G Sco	152234	311	00	B0·5 II	5·19	+0·33	9·40	(B0·5 Ia)
117 G Sco	153613	320	+05	B8 V	5·03	−0·02	5·53	
32 G Ara	153716	300	−11	B4 V	5·74	+0·06	7·16	
k Sco	154090	318	+03	B1 II–IIIe	4·86	+0·43	8·37	
116 G Sco	154368	318	+02	O9·5 I–II	6·17	+0·71	10·04	(O9·5 Iab) (7)
80 G Oph	154481	325	+07	A0 III–IV	6·16	−0·06	6·86	
η Sco	155203	312	−03	F2 III	3·36	+0·03	2·47	
130 G Sco	155450	321	+03	B1 III	5·92	+0·20	9·62	(B2 IV)
46 G Ara	156838	296	−16	B2 V	5·73	+0·04	8·21	
40 ξ Oph	156897	331	+07	F2 V	4·35	0·0	1·15	

TABLE II—(*cont.*)

Name	HD	l	b	Sp	$m(HP_v)$	E_y	m_0-M	Remarks
θ Oph	157056	328	+05	B2 IV	3·61*	+0·01	6·88	(B2 IV)
146 G Sco	157243	313	−06	B6 V	5·03	+0·07	5·92	
γ Ara	157246	302	−12	B1 III	3·36	+0·12	7·30	(8)
δ Ara	158094	299	−15	B8 V	3·68	−0·03	4·18	
α Ara	158427	308	−10	B3 Vn	2·82	0·0	4·82	(B2·5 V)
λ Sco	158926	319	−04	B2 IV	1·96*	0·0	5·26	(MKK Std)
6 G Sco	159358	342	+10	B8 V	5·50	...	(6·00)	
κ Sco	160578	319	−06	B2 IV	2·62*	+0·02	5·86	
167 G Oph	161056	346	+10	B3 Vn	6·50*	+0·42	7·24	
77 G Ara	161783	306	−14	B3 V	6·05*	+0·05	7·90	
13 G Sgr	163685	329	−04	B3 IV	5·94	+0·10	8·94	
ζ Ser	164259	351	+08	F3 V	4·60	−0·03	1·30	(F3 V)
66 Oph	164284	358	+12	B2 Vn	4·75	+0·11	7·02	(B2 Ve)
π Pav	165040	299	−21	Ap	4·69*	+0·15	...	Am ?
102 Her	166182	15	+17	B2 V	4·24	...	(6·84)	(B2 V)
6 G Tel	167128	306	−19	B3 V	5·71*	+0·11	6·38	
45 G Sgr	167356	340	−02	A2 I	6·10	+0·02	10·74	(Ao Ia)
Ser	167833	348	+01	A5 III	6·24	...	(6·24)	
8 G CrA	168905	318	−15	B3 Vn	5·34	+0·01	7·31	
α Tel	169467	316	−17	B3 III	3·68	+0·02	7·32	
γ Sct	170296	345	−04	A2 V	4·60	−0·01	3·40	(A3 V)
δ' Tel	170465	316	−17	B6 IV	5·28*	+0·02	6·22	
δ^2 Tel	170523	316	−17	B5 IV	5·50*	0·0	7·70	
9 G Sct	170740	349	−02	B2 V	5·66	+0·40	7·06	(B2 V)
77 G Sgr	171034	329	−13	B3 IV	5·34	+0·04	8·02	
83 G Sgr	171856	340	−08	A7 IIIp	5·75	...	...	Am ?
λ CrA	172777	325	−16	A1 V	5·15	+0·11	5·62	
91 G Sgr	172910	327	−15	B3 V	4·82	0·0	6·82	
94 G Sgr	173117	338	−11	B5: V	5·76	+0·18	6·52	
λ Pav	173948	301	−25	B1 Ve	4·28	+0·11	7·15	
32 G Sct	175156	347	−09	B3 III	4·93	+0·31	7·70	
31 G CrA	175362	327	−18	B8 IV	5·42	−0·03	7·12	
λ Tel	175510	311	−23	B9 III	5·23*	+0·03	7·14	
ϵ CrA	175813	327	−19	Fo V	4·84	+0·07	1·63	
ζ Sgr	176687	334	−17	A2 V:	2·98*	+0·01	1·75	
134 G Sgr	177074	334	−17	Ao IV	5·53	+0·06	5·75	
λ Aql	177756	358	−07	B7 V	3·34	+0·05	3·89	
45 G CrA	178322	323	−23	B5 V	5·80	+0·08	6·86	
47 G CrA	178628	326	−22	B6 V	6·48*	+0·10	7·28	
162 G Sgr	180885	330	−22	B4 IV	5·62	+0·05	7·97	
α Sgr	181869	325	−24	B9 III	4·34*	−0·04	6·34	
186 G Sgr	182681	336	−21	B9 V	5·58	+0·08	5·34	
63 G Tel	183806	321	−27	Ap	5·79	...	...	Am ?
55 Sgr	186005	352	−20	Fo III	5·07	...	(4·47)	
70 G Pav	186219	289	−31	Am	5·47	...	...	
228 G Sgr	186500	336	−26	B8 Vn	5·53	+0·12	5·67	
ν Tel	186543	308	−31	A5p	5·48	...	...	
73 G Pav	186837	303	−31	B5 V	6·27	0·0	7·57	
51 Aql	187532	358	−20	Fo IV	5·49	...	(3·49)	
75 G Pav	187653	303	−32	A3 V	6·27	...	(4·47)	

TABLE II—(*cont.*)

Name	HD	l	b	Sp	$m(HP_v)$	E_y	m_0-M	Remarks
76 G Pav	188097	294	−32	Am	5·77	...	...	
79 G Pav	188164	294	−32	A3p	6·42	...	...	
61 Sgr	188899	354	−23	A2 IV	5·01	+0·05	4·66	
259 G Sgr	189198	322	−32	A7 IIIp	5·90	+0·13	5·21	
κ' Sgr	193571	326	−36	A1 V	5·57	−0·02	4·77	
ψ' Pav	195267	303	−37	Fo V	4·78	−0·01	1·78	
υ Pav	196519	295	−36	B8 V	5·26	+0·02	5·70	
...	196775	28	−17	B4 Vn	5·98	...	(7·58)	
α Del	196867	28	−17	B8 V	3·61	+0·03	4·02	(B9 V)
52 G Cap	198174	348	−38	B6 V	5·74	+0·10	6·54	
64 G Cap	199443	360	−36	A5 IIIp	5·88	...	(5·88)	
α Oct	199532	283	−34	F5 IIIp	5·17	...	(4·17)	
8 G Ind	199623	314	−42	F6 V	5·80	...	(2·00)	
χ Cap	201184	354	−41	Ao V	5·25	+0·05	4·80	
23 G Ind	202103	310	−44	A5 III	5·80	...	(5·80)	
ϵ Mic	202627	341	−45	A2p	4·73	+0·03	4·44 :	
γ Pav	203608	294	−41	F5 V	4·22	+0·02	0·66	
18 Aqr	203705	007	−41	A9 III	5·54	...	(5·14)	
γ Ind	203760	309	−45	Fo III	6·17	+0·04	5·45	
6 PsA	204854	339	−48	A2 IV	5·95	...	(5·75)	
ξ Aqr	205767	15	−41	A7 IV	4·71	−0·01	3·01	(A7 V)
5 Peg	205852	41	−25	Fo IV	5·88*	...	(3·88)	
54G B Oct	206553	271	−29	A7 IV	6·50	...	(4·80)	
λ Cap	207052	11	−45	A2 V	5·46	...	(4·26)	
20 G Gru	208321	333	−53	A3 V	5·50	...	(3·70)	
δ Ind	208450	306	−49	Fo IV	5·29*	−0·02	3·29	
66 G Oct	208741	281	−37	F3 III	5·84	...	(4·94)	
η PsA	209014	292	−38	B8 V	5·37	+0·01	5·84	
o Aqr	209409	26	−44	B6: Vn	4·51	+0·09	5·34	(B8 V)
25 G PsA	209522	352	−55	B5 Vn	5·84	−0·03	7·14	
ι Aqr	209819	12	−50	B8 IV	4·84*	+0·05	7·39	
ι Peg	210027	51	−25	F5 V	4·35*	0·0	0·85	
λ PsA	210934	351	−57	B8 III	5·31	−0·02	8·31	
ρ Aqr	211838	24	−51	B8 V	5·31	+0·04	5·69	
48 γ Aqr	212061	31	−47	Ao IV	4·07*	−0·05	4·47	
π^2 Gru	212132	318	−57	Fo IVp	5·76	+0·09	3·49	
δ Tuc	212581	291	−47	B8 V	4·70	+0·07	4·99	
40 G PsA	213135	352	−60	Fo V	5·89	...	(2·89)	
72 G Ind	212728	288	−45	A3 V	5·65	...	(3·85)	
57 σ Aqr	213320	21	−54	A1 IV	5·09*	−0·09	5·19	
η Aqr	213998	35	−49	B8 V	3·95	+0·01	4·42	
49 G PsA	214484	340	−62	A2 Vp	6·15*	0·0	4·95	
ϵ PsA	214748	353	−63	B8 V	4·26	−0·02	4·76	
ϵ Gru	215789	304	−57	A2 V	3·63	+0·01	2·40	
52 Peg	217232	53	−43	Fo V	5·68	...	(2·68)	
π PsA	217792	336	−67	Fo IV	5·07	...	(3·07)	
80 G Ind	217831	283	−46	F2 IIIp	5·57	...	(4·77)	
α Peg	218045	57	−41	B9 V	2·86*	+0·03	2·77	(B9 V)
83 Aqr	218060	36	−59	F2 V	5·83*	−0·07	2·63	
υ Gru	218242	325	−67	A1 V	5·54	−0·02	4·74	

TABLE II—(*cont.*)

Name	HD	l	b	Sp	m(HP$_v$)	E_y	m_0–M	Remarks
88 G Gru	218630	316	−66	F6 V	5·68	...	(1·88)	
59 Peg	218918	54	−47	A2 V	5·10	...	(3·90)	
ψ^3 Aqr	219832	37	−63	A0 V	5·13	...	(4·83)	
107 G Gru	220729	295	−61	F3 IV	5·48	...	(2·88)	
β Scl	221507	322	−72	B9 III	4·49	−0·05	6·49	
11 G Phe	222095	302	−68	A2 V	4·82	+0·01	5·99	
ω^2 Aqr	222661	39	−71	B9 V	4·45	+0·05	4·30	(B9·5 V)
106 Aqr	222847	30	−74	B8 V	5·19	+0·04	5·67	
δ Scl	223352	352	−78	A0 V	4·61	+0·03	4·22	
27 G Phe	224022	305	−73	F8 V	5·91	...	1·81	
35 G Scl	224113	337	−78	B5 IV	6·00	+0·06	8·02	
42 G Tuc	224361	279	−54	A2p	5·98	...	...	
ϵ Tuc	224686	277	−51	B7 V	4·61	+0·05	5·26	
ζ Scl	224990	345	−80	B4 III	5·21*	+0·04	8·59	
2 Cet	225132	44	−76	A0: IV	4·64	−0·02	5·04	(B9 IV)
45 G Tuc	225253	274	−46	B8 III	5·54	−0·03	8·54	

NOTES

(1) π Cet—the classification B7 V given by A. Slettebak and R. F. Howard (*Ap. J.*, **121**, 102, 1955) seems difficult to justify ; the star has sharp lines and is indicated as B5 I or II by S. L. Lippincott and D. Hoffleit (*A. J.*, **58**, 167, 1953).

(2) o Pup—four values of converted B–V colours were found as follows : $-0{\cdot}09$ $-0{\cdot}20$ -13_5 $-0{\cdot}02_5$.

(3) ϕ Vel—B5 I or II by S. L. Lippincott and D. Hoffleit.

(4) y Car—classification Fo Ia by W. P. Bidelman (*P.A.S.P.*, **66**, 249, 1954) ; λ 4226 weak for F2, strong Fe lines 4233 and 4172–78.

(5) HD 125288=HR 5358, B5 I or II by S. L. Lippincott and D. Hoffleit.

(6) o Sco—class III doubtful, faint spectrum. On the basis of its proper motion and position the star was recently found to be a member of the Scorpio–Centaurus cluster (*Ap. J.*, **121**, 557, 1955) with $M_v=-3{\cdot}6$ and a provisional classification of A5 II.

(7) HD 154368—a B–V colour of $+0{\cdot}605$ which would give a total absorption of nearly 3 mag. was rejected. Schilt and Jackson's converted B–V is $+0{\cdot}37$ giving a total absorption of 2·1 mag. in agreement with the value 7 $E_1=2{\cdot}1$ mag. obtained by P. Th. Oosterhoff (*B.A.N.*, **11**, 299, 1951).

(8) γ Ara—three values of converted B–V colours were found as follows : $-0{\cdot}17$ $-0{\cdot}21$ $-0{\cdot}10_5$.

A referee has called my attention to a recent Cape Mimeogram* (not available at Mt Stromlo) which contains a few MK types for some stars in Table II :

HD		
4293	A7 V	
33262	F8 V	
128898	Fo III	(A strontium star which shows a false absolute magnitude effect)
176687	A2 III	(The Stromlo spectrum was very dark and the luminosity class is uncertain)
202103	A5 V	
203608	F8 V	
213135	Fo V	

*Fundamental data for southern stars—First List.

A stars.—In A stars the helium lines have disappeared and the metallic lines and the K line have become progressively stronger. Useful line ratios are 4481/4385, 4128–32/4030–4 and 4300/4385. Luminosity differences are shown

by the intensity of the blend 4171–4179, the Fe II line 4233, the appearance of the hydrogen lines and the ratio 4417/4481. Among 94 A stars, 7 have been classified as metallic-line stars or peculiar. Because of the false absolute magnitude effect observed in these stars, a few, possibly two or three, may have been missed and classified A5 III or A7 III. In such cases the K line, lost in the granulation, may have been too weak to remove the ambiguity. The average difference between the two determinations is about one subclass for types and luminosities.

F stars.—For F stars type-differences are shown mainly by the rapid decrease of the hydrogen lines and the increasing strength of the lines 4325, 4226, 4045 and the G band. The line ratios used for luminosity classifications are 4417/4481, 4444/4481, 4171/4226, 4063/4077, 4045/4077. The very luminous F stars are distinguished by the appearance of the G band, the strength of the pair of lines 4172–4179 and the numerous sharp metallic lines. Table II contains 54 F stars for which the average difference is 0·5 of a subclass both for types and luminosities.

Cepheid β Dor.—In addition, eight spectra of the cepheid β Dor (**7, 8**), taken by S. Gaposchkin, were recorded and classified and the variation with the phase was found to be as follows:

Plate	JD 2,430,000+	Phase (in days)	Sp
1477	5746·205	7·79	F6 Ia
1496	5769·101	1·15	F8 Ia
1498	5769·128	1·18	F8 Ia
1511	5771·222	3·27	Go + I
1523	5773·140	5·19	G2 I
1525	5773·177	5·23	G2 I
1550	5777·169	9·17	F6–8 I
1552	5777·144	9·19	F6 Ia

Scorpio–Centaurus cluster.—The certain and probable members of the Scorpio–Centaurus cluster according to A. Blaauw (**9**) are listed in Table III. Column 1 gives the name of the star, column 2 the HD number, column 3 the spectral classification and column 4 the modulus $m_0 - M$ as in Table II.

The mean moduli are:

(*a*) certain members	6·87 ± 0·09 p.e.	($n = 34$),
(*b*) probable members	6·59 ± 0·13 p.e.	($n = 38$),
all members	6·72 ± 0·11 p.e.	($n = 72$).

Three emission line stars giving small distance moduli, δ Cen, μ Cen and α Ara were rejected from the means. Emission line stars are not supposed to be intrinsically brighter than normal stars but because of broad diffuse lines the luminosity classes may be uncertain.

The 72 members were grouped according to spectral type as follows:

	B0, 1, 2	B3, 4	B5–8
$m_0 - M$	6·68	6·72	6·79
p.e.	±0·15	±0·13	±0·18
(n)	(20)	(33)	(19)

No systematic effect in relation to the spectral type is evident.

Although the cluster contains few giants the members were divided into three luminosity classes as follows:

	III	IV	V
m_0-M	7·58	7·02	6·35
p.e.	±0·27	±0·11	±0·11
(n)	(6)	(29)	(37)

TABLE III

Scorpio-Centaurus cluster

Name	HD	Sp	m_0-M	Name	HD	Sp	m_0-M
Certain members				*Probable members*			
a Car	79351	B2 IV	7·18	b Car	77002	B3 IV	7·73
166 G Vel	85980	B3 V	7·57	i Car	79447	B3 IV	6·83
1 G Cru	103884	B3 V	7·48	145 G Vel	82984	B4 Vn	7·23
92 G Cen	105382	B6 III–IV	7·28	δ^2 Cha	93845	B3 V	6·44
δ Cen	105435	B3 Vne	(4·6)	π Cen	98718	B6 Vn	5·84
ζ Cru	106983	B3 IV	6·88	33 G Cen	99556	B5 IV	7·46
α Mus	109668	B3 IV	5·59	18 G Mus	103079	B4 IV	7·63
λ Cru	112078	B5: Vn	6·00	ρ Cen	105937	B4 V	5·60
f Cen	113703	B4 IV	7·25	δ Cru	106490	B2 IV	6·23
ν Cen	120307	B2 V	6·36	119 G Cen	108257	B5 Vn	6·20
μ Cen	120324	B3 Ve	(5·2)	γ Mus	109026	B5 V	5·21
3 k Cen	120709	B5 IV	6·76	45 G Cru	110956	B3 IV	7·39
283 G Cen	120908	B5 V	6·91	β Cru	111123	B0·5 IV	5·53
4 h Cen	120955	B5 IV	7·17	μ^2 Cru	112091	B5 Ve	6·56
ϕ Cen	121743	B2 V	6·56	μ' Cru	112092	B3 IV	6·88
χ Cen	122980	B2 V	7·01	ξ^2 Cen	113791	B2 IV	7·80
a Cen	125823	B6 III	7·61	202 G Cen	115823	B5 III	8·75
α Lup	129056	B1 III	7·21	J Cen	116087	B5 V	5·74
b Cen	129116	B3 V	6·03	ϵ Cen	118716	B1 V	5·52
o Lup	130807	B6 III	7·53	υ' Cen	121790	B3 IV	6·89
κ Cen	132200	B2 III	7·62	β Lup	132058	B2 V	5·63
45 G Lup	132955	B4 IV	7·78	λ Lup	133955	B3 IV	7·66
δ Lup	136298	B3 IV	6·13	100 G Lup	137432	B4 V	7·02
ϕ^2 Lup	136664	B3 IV	7·37	γ Lup	138690	B3 V	5·48
90 G Lib	138764	B6 IV	7·26	d Lup	138769	B3 IV	7·55
ψ^2 Lup	140008	B6 V	6·48	τ Lib	139365	B4 V	5·60
ρ Sco	142669	B3 IV	6·77	1 Sco	141637	B3 V	6·47
η Lup	143118	B3 V	5·56	2 Sco	142114	B3 Vn	6·35
σ Sco	147165	(B1 III)	6·8*	π Sco	143018	B2 IV	6·76
N Sco	148703	B2 V	7·06	151 G Lup	143699	B5 V	6·26
τ Sco	149438	(Bo V)	6·65†	β' Sco	144217	B1 V	5·43
μ' Sco	151890	B3 Vp	5·74	θ Lup	144294	B3 IV	7·04
μ^2 Sco	151985	B2 IV	6·94	ν Sco	145502	B3 V	5·90
32 G Ara	153716	B4 V	7·16	χ Oph	148184	B3 V : e	5·84
91 G Sgr	172910	B3 V	6·82	22 Sco	148605	(B2 V)	7·22‡
31 G CrA	175362	B8 IV	7·12	θ Oph	157056	B2 IV	6·88
				α Ara	158427	B3 Vne	(4·82)
				9 G Sct	170740	B2 V	7·06
				45 G CrA	178322	B5 V	6·86
	Mean		6·87		Mean		6·59
	±0·09 pe.				±0·13 pe.		

* MK Std $E_y=+0·26$
† MK Std $E_y=+0·05$

‡MK Std $E_y=+0·08$

A systematic effect depending on luminosity is well marked. It is partly due to errors in the classification and partly to errors in the calibration of standard absolute magnitudes. The number of objects of class III is small but even class IV with a comparable number of stars with that of class V gives a mean modulus 0·67 magnitude larger.

A. Blaauw (**10**) has recently determined from the proper motions of the cluster members (and two other associations), mean visual absolute magnitudes per volume of space, for types B1, 2, 3 of class V and B2 class IV. With these new values for 27 members of the corresponding spectral types, the following mean moduli are obtained:

	B2 IV	B1, 2, 3 V
m_0-M	6·37	6·07
p.e.	±0·21	±0·15
(n)	(6)	(21)

The difference between the mean moduli of class IV and class V is reduced to 0·3 magnitude. This results mainly from the fact that the Δm between Blaauw's absolute magnitudes for classes B2 IV and B2 V is only of 0·3 magnitude while it is of 0·7 mag. for Morgan and Keenan standard absolute magnitudes (**5**).

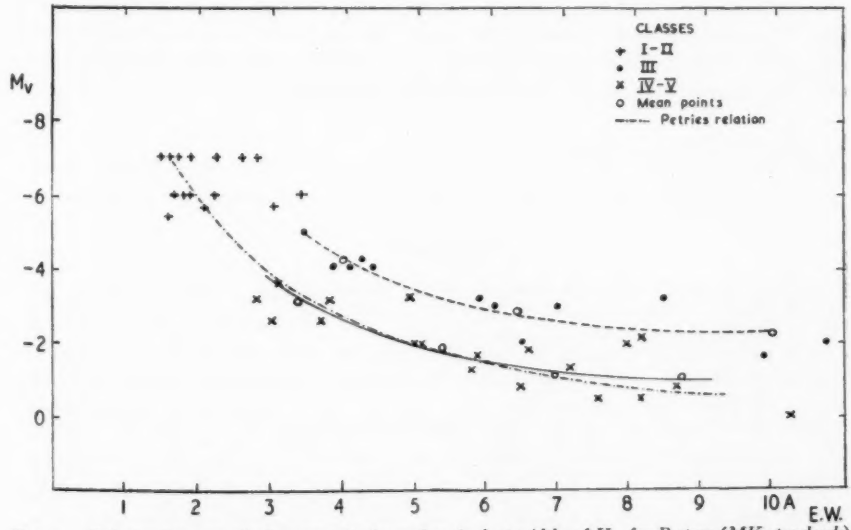

FIG. 1.—*Relation between absolute magnitudes and equivalent widths of $H\gamma$ for B stars (MK standards).*

Absolute magnitudes of B stars from $H\gamma$ line intensities.—Absolute magnitudes of B stars may be determined from equivalent widths of $H\gamma$ and R. M. Petrie (**11**) has obtained a mean relation between luminosity and $H\gamma$ intensity which shows a systematic difference from the absolute magnitudes of Morgan and Keenan (Victoria–Yerkes = +0·7 mag.).

Among the B stars measured for equivalent widths by Petrie there are only 19 MK standards, but the extensive list published by S. Günther (**12**) contains 46 MK standards for B stars. In Fig. 1 the equivalent widths of $H\gamma$ in angstroms (EW) for these stars are plotted against the mean visual absolute magnitudes of

Morgan and Keenan. The supergiants and bright giants, classes I and II, are clustered around $M = -6$ and EW between 1·5 and 3 A; the class III giants form a distinct sequence from $M \approx -5$ and EW $\approx 3{\cdot}5$ A to $M - \approx 2$ and EW ≈ 10 A; the mean points for classes IV and V fit closely the mean relation obtained by Petrie, except of course where this relation reaches the group of the very luminous stars. The sequence of the class III giants is from 1·2 to 1·4 magnitudes above Petrie's relation.

The equivalent widths published by J. Stock (**13**) for some MK standards for B stars show the same effect.

This may explain, at least in part, the disagreement between the Victoria and Yerkes luminosities. Either Petrie's relation is valid only for the Main Sequence and class IV, or the mean absolute magnitudes of the B stars of class III in the MK system are too bright. The systematic effect depending on luminosity classes in the Scorpio–Centaurus cluster tends to indicate that the latter alternative is more probable. But it is equally possible that the mean relation between absolute magnitudes and equivalent widths of Hγ, being based on only one parameter, is approximately a Main Sequence relation for B stars. It does not show up the finer distinction of luminosities which can be made by visual inspection of the spectra or their tracings.

Acknowledgments.—The author wishes to express her thanks to Dr Gollnow and Dr Buscombe for the use of the observational material in their programme and particularly Dr Buscombe who has organized the necessary observations of the MK standards, and for some helpful suggestions.

Commonwealth Observatory,
Mount Stromlo,
Canberra:
1956 *December.*

References

(1) H. L. Johnson and W. W. Morgan, *Ap. J.*, **117**, 313, 1953.
(2) A. W. J. Cousins, Cape Mimeogram No. 1, 1953.
(3) J. Schilt and C. Jackson, *A.J.*, **56**, 209, 1952.
(4) O. J. Eggen, *A.J.*, **60**, 131, 1955 ; *L.O.B.* No. 532.
(5) W. W. Morgan and P. C. Keenan, in " Astrophysics " (edit. by J. A. Hynek), McGraw-Hill, New York, 1951, Chap. 1.
(6) M. L. Woods, *Mem. Comm. Observ.*, **111**, No. 12, 1955.
(7) L. Gratton, *Ap. J.*, **118**, 570, 1953.
(8) A. W. Rodgers, *M.N.*, **117**, 85, 1957.
(9) A. Blaauw, *Publ. Kapteyn Ast. Lab. Groningen*, No. 52, 1946.
(10) A. Blaauw, *Ap. J.*, **123**, 408, 1955.
(11) R. M. Petrie, *Publ. Dominion Astro. Observ.*, IX, No. 8, 1953.
(12) S. Günther, *Zs. f. Ast.*, **7**, 106, 1933.
(13) J. Stock, *Ap. J.*, **123**, 253, 1955.

THE EFFECT OF DEPARTURES FROM THERMODYNAMIC EQUILIBRIUM ON THE INTENSITY RATIO OF ^2D–^4S DOUBLETS IN GASEOUS NEBULAE

Ali M. Naqvi and S. P. Talwar*

(Received 1957 January 18)†

Summary

A revised calculation of transition probabilities in ground configuration of [O II], [S II], and [A IV] is made. Using these transition probabilities and allowing for collisional effects, the relative level populations in ^2D and ^2P terms and the intensity ratio, $r=\frac{I(D_{5/2}-S_{3/2})}{I(D_{3/2}-S_{3/2})}$, are calculated as a function of the electron density N_e and the electron temperature T_e. The theory is made use of to estimate $N_e/T_e^{1/2}$ for regions of maximum emission of [O II], [S II], and [A IV] in nebulae for which the intensity ratio r of ^2D–^4S doublets are observed. It is suggested that the accurate measurements of this intensity ratio in a nebula, together with the use of theoretical calculations, give the electron density in the nebulae. This may prove to be a very simple and powerful method for determining the electron density.

---

1. *Introduction.*—The doublets ($^2D_{5/2,3/2}\rightarrow{}^4S$) in [O II], [S II], and [A IV] are observed in numerous emission nebulae. The intensity ratio

$$r=\frac{I(^2D_{5/2}\rightarrow{}^4S)}{I(^2D_{3/2}\rightarrow{}^4S)}$$

for [O II] has been calculated by Aller, Ufford and Van Vleck (**7**) and by Garstang (**11**), assuming the ^2D levels to be populated in the statistical weight ratio 6:4. The values obtained for [O II] were 0·58 and 0·47 respectively.

The amount of accurate data on the intensity ratio r for the ions under consideration is somewhat limited, yet it can be said that the variation in the values of r for an ion from nebula to nebula is real (see Table I). There are marked variations for [O II]; the value for NGC 40 is 0·85, whereas for IC 4997 it is 0·38. For IC 4997, which is a "stellar" nebula, and for which the measurements are probably difficult, two independent measurements were made by Aller, Ufford and Van Vleck (hereafter abbreviated as AUV) which gave r equal to 0·36 and 0·40.

The value of r for the corresponding [S II] doublet has been calculated by Garstang. The theoretical value $r=0{\cdot}55$ is significantly smaller than the observed values in gaseous nebulae.

The assumption of the Boltzmann distribution for level population is not justified for most of the nebulae. This assumption cannot account for the observed variation of the intensity ratio. As we shall see later, *the Boltzmann*

* Now at University of Sind, Pakistan.

† Received in original form 1955 April 30.

value must always be smaller or at most equal to any of the observed values. This however, is not the case with the theoretical values of AUV *and Garstang.* The Boltzmann value depends only on the transition probabilities. Earlier, one of us (Naqvi (**13**)) had calculated the transition probabilities of [O II] lines, including the effects of the mutual magnetic interactions. Using Naqvi's transition probabilities, we recalculated the Boltzmann value of r for [O II] doublet. The value thus obtained, $r=0{\cdot}34$, is lower than the observed value for any nebula. When the Boltzmann distribution does not apply, the value of r depends on the electron density, N_e, and the electron temperature, T_e, of the nebula. In the present paper, the departures from the Boltzmann distribution are considered in detail.

TABLE I

Observed intensity ratios of the ^2D–^4S *lines*

Nebulae	r (O II)	r (S II)	r (A IV)
NGC 7662	0·62 (**24**)	0·74 (**5**)	1·25 (**24**)
NGC 2440	0·60 (**24**)	...	1·25 (**24**)
NGC 7027	0·49 (**4**)	0·72 (**4**)	0·43 (**24**)
NGC 6572	0·50 (**24**) 0·45 (**7**)	0·67 (**24**) 0·75 (**23**)	1·33 (**24**)
Orion	0·6 (**24**)	0·75 (**24**)	3·3 (**24**)
IC 418	0·4 (**24**)	0·83 (**24**)	...
NGC 40	0·84 (**7**)	...	...
NGC 2392	0·46 (**7**)	...	...
NGC 6210	0·47 (**7**)	...	...
BD+30 3639	0·46 (**7**)	0·70 (**23**)	...
IC 4593	0·67 (**7**)	...	...
NGC 6543	0·50 (**7**)	1·00 (**23**)	...
NGC 6826	0·48 (**7**)	...	...
IC 4997	0·38 (**7**)	...	...
NGC 7009	0·50 (**7**)	...	1·00 (**24**)
NGC 6803	...	...	0·87 (**1**)
IC 2165	...	...	1·00 (**24**) 1·10 (**1**)
IC 5217	...	...	1·14 (**24**)
Humason Planetary	0·42*	...	...
Cannor Planetary	0·54*	...	...

* Private communication (Osterbrock, 1956)†.

2. *Transition probabilities.*—The transitions under consideration are not allowed according to the selection rules for the electric dipole radiation but are allowed for the electric quadrupole and the magnetic dipole radiations. The theory of the transition probabilities is well known (Condon and Shortley (**10**); Shortley (**21**)). Earlier calculations of the transition probabilities were performed by Pasternack (**15**) and by Shortley, Aller, Baker and Menzel (**22**), hereafter abbreviated as SABM. The effects of the mutual magnetic interactions are very important for atoms having p^3 as their ground configuration. In general, the effect of the inclusion of the M–M interactions on the transformation coefficients is twofold. First, ζ, M_0 and F_2 (the spin–orbit, the mutual magnetic and the electrostatic integrals respectively) are calculated empirically by equating the

† One of us (S.P.T.) is thankful to Professor Osterbrock for letting him know his experimental results.

theoretical expressions for the energy levels with their observed values, and therefore the values of ζ, M_0 and F_2 depend upon whether the mutual magnetic interaction terms are included in the energy level expressions or not. The integral η used by AUV is five times our integral M_0. Second, the expressions for the transformation coefficients (**13**) contain the M_0 terms explicitly. The empirical determination of ζ, M_0 for the p^3 configuration is further complicated, due to the fact that the diagonal elements of the spin–orbit interaction for this configuration are zero. Therefore ζ and M_0 must be determined by interpolation between the neighbouring configurations p^2 and p^4.

For the calculation of the transition probabilities of O II listed in Table II, we have employed the following values of the various integrals, calculated according to the above-mentioned procedure:

$\zeta = 181$ cm^{-1}.

$M_0 = 0{\cdot}35$ cm^{-1}.

$F_2 = 2979$ cm^{-1}.

$s_q = 0{\cdot}59ea_H^2$ (Garstang's value based upon wave functions with exchange).

For comparison, we have included in Table II the transition probabilities calculated by AUV and Garstang. The differences between their values and ours arise due to the different choices of ζ, M_0 and s_q. AUV have used values of ζ obtained from the observed energy levels but ignoring the mutual magnetic interactions.

There is a further difference between our procedure and that used by AUV. In the formulae for the transformation coefficients, the denominators consist of the unperturbed term differences as given by the Slater formulae in terms of the electrostatic interaction integral F_2. AUV have instead used the observed term differences which are affected by the configuration interaction. We feel that AUV's procedure is not justified, and it may not correctly take into account the contribution of the configuration interaction to the transformation coefficients. In our procedure, the effect of the configuration interaction is taken into account at one step only, namely in the determination of F_2, but not in the subsequent determination of the transition probabilities.

TABLE II

Transition probabilities (in sec^{-1})

Transition	O II	S II	A IV
$D_{5/2}$–$S_{3/2}$	$3{\cdot}78\times10^{-5}$ $5{\cdot}41\times10^{-5}$ (7) $3{\cdot}94\times10^{-5}$ (11)	$6{\cdot}31\times10^{-4}$ (11)	$2{\cdot}59\times10^{-3}$
$D_{3/2}$–$S_{3/2}$	$16{\cdot}51\times10^{-5}$ $14{\cdot}01\times10^{-5}$ (7) $13{\cdot}06\times10^{-5}$ (11)	$17{\cdot}36\times10^{-4}$ (11)	$27{\cdot}02\times10^{-3}$
$P_{3/2}$–$S_{3/2}$	0·0466	0·2711	...
$P_{1/2}$–$S_{3/2}$	0·0179	0·0663	...
$P_{3/2}$–$D_{5/2}$	0·1643	0·4262	...
$P_{1/2}$–$D_{5/2}$	0·0780	0·1087	...
$P_{3/2}$–$D_{3/2}$	0·0478	0·1440	...
$P_{1/2}$–$D_{3/2}$	0·1255	0·4830	...

Transition probabilities for A IV.—The ground configuration of A IV is $3p^3$. For atoms having this configuration the effects of the mutual magnetic interactions

are not as important as for O II (ground configuration $2p^3$). Earlier, we mentioned that in general the effect of the inclusion of the mutual magnetic interactions is twofold. For atoms having $3p^3$ configuration, the first effect alone is significant, namely the effect on the calculation of ζ and F_2. The M_0 terms in the expressions for the transformation coefficients have negligible magnitude. Hence for atoms having $3p^3$ configuration all we need to know is the accurate values of ζ and F_2 but values of M_0 are not required. The values of ζ and F_2 given by Naqvi (**13**) are: $\zeta = 1256$ cm^{-1}; $F_2 = 2353$ cm^{-1}.

The wave functions for A IV are not known. Therefore, the integral s_q has been determined by the screening constant method, similar to that used by Pasternack (**15**). This method is approximate, and for A IV we find

$$s_q = 0{\cdot}974 e a_H^2.$$

The transition probabilities are given in Table II.

Transition probabilities for S II.—The transition probabilities for the ^{2}D–^{4}S transition in S II have been calculated by Garstang (**11**). For calculating the probabilities of other transitions we have used the following values of ζ and F_2 (**13**) and s_q (**11**):

$$\zeta = 497 \text{ cm}^{-1}$$
$$F_2 = 1653 \text{ cm}^{-1}$$
$$s_q = 2{\cdot}10 e a_H^2.$$

The transition probabilities for S II are also included in Table II.

3. *Collision strengths.*—Recently Seaton (**16, 17**) calculated the collision strengths (the dimensionless parameter related to cross-section) for excitation by electron collisions between different terms of the ground configuration of O II and S II. In our calculations in Section 5 we have needed to know these collision strengths (henceforth called as the collision cross-section parameters) from a level of one term to another term, and we have assumed them to be proportional to the statistical weights of the levels concerned. That is to say, if A and B are two terms and A consists of two levels, A_j and $A_{j'}$, then the various collision cross-section parameters are given by,

$$\frac{\Omega(A_j, B)}{\omega_j} = \frac{\Omega(A_{j'}, B)}{\omega_{j'}} = \frac{\Omega(A, B)}{\omega_j + \omega_{j'}}. \tag{1}$$

Further, the collision cross-section parameters for excitation and de-excitation between any two states are equal, i.e.

$$\Omega_{AB} = \Omega_{BA}.$$

The collision cross-section parameters between the levels of the same doublet term are not known for the atoms considered here. The frequency of collisional processes between them is hence ignored. Since we completed this work, we have seen an estimation made by Seaton (**18**) of the cross-section parameters between the two levels of the ^{2}D term of O II and S II, but his procedure and the values do not appear to us to be justified. Until proper calculations for the cross-section parameters between the ^{2}D levels of p^3 ions are made, it is considered safer to neglect the collisional processes between the doublet levels although considerable differences in the electron densities for regions of maximum emission of O II, S II and A IV (as given in Table III) may result if different assumptions were made regarding the cross-section parameters for the ^{2}D levels in p^3 ions.

We have used in Section 5 the cross-section parameters calculated according to equation (1); for A IV the cross-sections are estimated following a suggestion made by Seaton (**16**).

4. *Departure from thermodynamic equilibrium.*—The p^3 configuration consists of the following levels: $^4S_{3/2}$, $^2D_{3/2}$, $^2D_{5/2}$, $^2P_{1/2}$, $^2P_{3/2}$. In O II the doublet terms are normal, but in S II and A IV they are inverted. For convenience we shall adopt the following abbreviations.

Term	Abbreviations	Level	Abbreviations
^4S	S	$^4S_{3/2}$	s
^2D	D	$^2D_{5/2}$	d'
		$^2D_{3/2}$	d
^2P	P	$^2P_{1/2}$	p'
		$^2P_{3/2}$	p

The intensity ratio of the D–S lines can be written as

$$r = \frac{I(d'-s)}{I(d-s)} = \frac{N_{d'}}{N_d} \cdot \frac{A(d'-s)}{A(d-s)} \cdot \frac{h\nu(d'-s)}{h\nu(d-s)} \qquad (2)$$

where ν is the frequency of the line A, the transition probability, and N_d, $N_{d'}$ are the equilibrium populations of the levels concerned. In thermodynamic equilibrium,

$$r_{Th} = 1{\cdot}5 \, \frac{A(d'-s)}{A(d-s)} \frac{h\nu(d'-s)}{h\nu(d-s)}.$$

Substituting the transition probabilities given in Table II, and the frequencies of the lines involved, the following values of r_{Th} are obtained

$$r_{Th}(\text{O II}) = 0{\cdot}34,$$
$$r_{Th}(\text{S II}) = 0{\cdot}546,$$
$$r_{Th}(\text{A IV}) = 0{\cdot}14.$$

A comparison with Table I will show that there is no thermodynamic equilibrium in gaseous nebulae.

Bowen (**9**) showed that the atoms giving rise to the forbidden lines in gaseous nebulae are excited due to electron collisions. Radiative excitations are negligible on account of the extreme dilution of the radiation from the central star. The fact that stellar radiation is extremely diluted forms an essential reason for departure from thermodynamic equilibrium in gaseous nebulae. Proton impact could also produce transitions between the metastable ground configuration terms of ions with outer p^q shells ($q = 2, 3, 4$) but recently Seaton (**20**) has shown that under the conditions prevailing in gaseous nebulae the number of such transitions is small compared to that produced by electron impact.

The radiative and collisional de-excitations compete with each other. When the frequency of radiative de-excitations is small compared to that of collisional de-excitations, the collisional processes alone are responsible for excitation as well as de-excitation and virtually detailed balancing and thermodynamic equilibrium is obtained. On the other hand, when the number of radiative de-excitations is significant, we cannot expect to find thermodynamic equilibrium. Therefore the state of thermodynamic equilibrium can be expected only when

(1) N_e is large;
(2) T_e is small; and
(3) transition probabilities are small.

The large departures of the observed ratio r for A IV from the Boltzmann value, as compared to that for O II, are due to the larger transition probabilities for A IV.

5. *Relative populations of the levels.*—The equations of equilibrium have been discussed earlier by Hebb and Menzel (**12**) and more recently by Seaton (**17, 18**) and Aller (**2**). Ignoring the frequency of transitions between the levels of the doublet terms (i.e. $^2P_{3/2} \rightleftarrows {}^2P_{1/2}$ and $^2D_{3/2} \rightleftarrows {}^2D_{5/2}$) and neglecting the de-excitations from ^2P term in the equations of the steady state for d' and d levels, we can write for the ratio of the level populations

$$\frac{N_{d'}}{N_d} = 1{\cdot}5\,\frac{CN_e(\Omega_{SD}+\Omega_{DP}e^{-\chi_{DP}/kT_e})+\omega_D A(d-s)}{CN_e(\Omega_{SD}+\Omega_{DP}e^{-\chi_{DP}/kT_e})+\omega_D A(d'-s)} \tag{3}$$

$$\frac{N_{p'}}{N_p} = 0{\cdot}5\,\frac{CN_e(\Omega_{PD}+\Omega_{PS})+\omega_P A(p-s)+A(p-d)+A(p-d')}{CN_e(\Omega_{PD}+\Omega_{PS})+\omega_P A(p'-s)+A(p'-d)+A(p'-d')} \tag{4}$$

where $C = 8{\cdot}54\times 10^{-6}/T_e^{1/2}$. These ratios depend upon N_e and T_e. The curves showing the variation of $N_{d'}/N_d$ with $N_e/T_e^{1/2}$ for the ions under consideration are given in Fig. 1. For large values of $N_e/T_e^{1/2}$, all the curves in Fig. 1 asymptotically approach the Boltzmann values.

The variation of $N_{p'}/N_p$ is very small and hence is not included in Fig. 1.

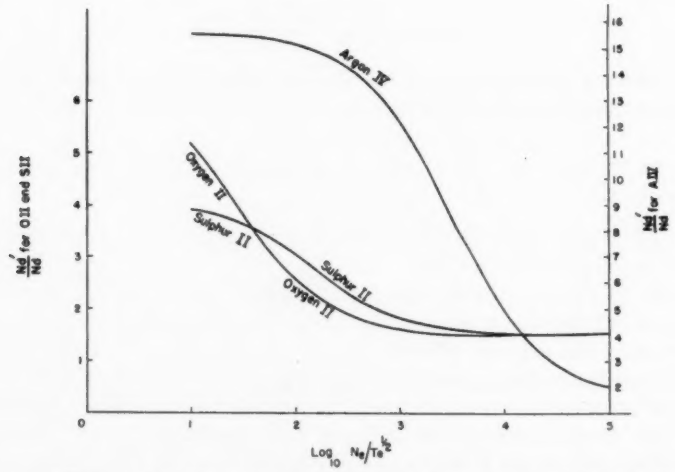

FIG. 1.—*Theoretical population ratio of* $^2D_{5/2}$ *and* $^2D_{3/2}$ *as a function of* $N_e/T_e^{1/2}$.

6. *Intensity ratio* $I(d'-s)/I(d-s)$ *and the estimation of* $N_e/T_e^{1/2}$.—From equations (2) and (3), we obtain,

$$r = I(d'-s)/I(d-s) = 1{\cdot}5\,\frac{\left[1+\dfrac{CN_e}{\omega_D}(\Omega_{SD}+\Omega_{DP}e^{-\chi_{DP}/kT_e})\dfrac{1}{A(d-s)}\right]}{\left[1+\dfrac{CN_e}{\omega_D}(\Omega_{SD}+\Omega_{DP}e^{-\chi_{DP}/kT_e})\dfrac{1}{A(d'-s)}\right]}\cdot\frac{\nu(d'-s)}{\nu(d-s)} \tag{5}*$$

* The exponential term in parenthesis is much smaller than the other term. Therefore, while calculating $N_e/T_e^{1/2}$ (Table III, cols. 2, 3 and 4) T_e in the exponential term only is taken equal to 10^4.

The values of r, computed for various values of $N_e/T_e^{1/2}$ for O II, S II and A IV are plotted in Fig. 2. All three curves asymptotically approach their thermodynamic equilibrium values r_{Th} (0·34 for O II, 0·546 for S II, and 0·14 for A IV). The curve for O II reaches near the asymptotic value at $N_e/T_e^{1/2} \sim 10^3$, that for S II at about 10^4 and that for A IV at about 10^6.

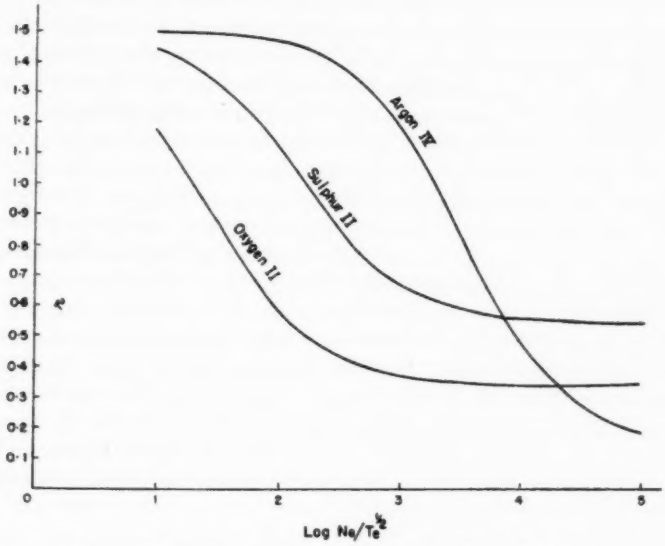

FIG. 2.—*Theoretical intensity ratio r as a function of* $N_e/T_e^{1/2}$.

It would be worthwhile to utilize the theoretical curves to estimate the ratio $N_e/T_e^{1/2}$ in the nebulae for which the intensity ratios are known observationally. The electron temperature T_e is usually computed from the relative intensities of the $\lambda 4363$ and the green nebular lines of [O III]. The electron densities N_e are then estimated using the surface brightness method of Aller and Liller (**3**). However, on account of stratification which exists in most of the nebulae, real differences in electron density do occur within the body of the nebula. The surface brightness method should give essentially an overall average value of the electron density throughout the volume of the nebula, which may be much smaller than that in a cloud of maximum emission from an ion.

More recently Seaton (**17**) obtained estimates of the electron temperature T_e, and electron density N_e, from the relative intensities of the forbidden lines. For ions like N II, O II, O III, and S II, the intensity ratio of the nebular to the auroral or transauroral transitions gives a relation between T_e and N_e. Thus simultaneous transcendental equations involving N_e and T_e are formed for each ion. They are then solved simultaneously to give N_e and T_e. However, with this method, one can expect a unique solution for N_e and T_e only when the ions considered arise in the same strata. Recently Aller and Minkowski (**6**) found that in NGC 7027 the simultaneous solution of N_e, T_e equations for [O III] and [N II] lines gave (after applying corrections for space absorption) $N_e \sim 6{\cdot}3 \times 10^4$ electrons per cm^3 and $T_e \sim 14\,000$ deg. K. On the other hand employing only the [O III] data together with the photoelectrically measured surface brightness corrected for space absorption and the distance derived

by Berman (**8**), Aller (**2**) found $N_e \sim 1{\cdot}7 \times 10^4$ electrons per cm^3 and $T_e \sim 15\,600$ deg. K. These results may imply that [N II] and [O III] radiations originate predominantly in different regions within the nebula, and that the forbidden line method (**17**) gives essentially an average density for the regions of maximum emission of the ions considered.

The electron densities in the clouds of maximum emission of an ion in a nebula are not known. We can, however, make use of the theoretical curves in Fig. 2, to estimate the values of $N_e/T_e^{1/2}$ in a nebula for the regions of maximum concentration of the ions considered here and thus get an idea of how this varies within a nebula for clouds of maximum emission of different ions.

The various atomic constants used and the experimental intensity ratio r for O II are quite accurate and hence the curve for O II is quite reliable. The reliability of the theoretical curve for S II is somewhat less, and that for A IV still less. It is difficult to give an exact measure of the reliability of these curves, but for A IV it may give no better than an order of magnitude estimate. This determination is most accurate for the steep portion of the curves.

In Table III, we give the estimates of $N_e/T_e^{1/2}$ for O II, S II and A IV for various nebulae. The values for O II are perhaps quite accurate, whereas for A IV they are rough estimates only. But still it appears that [S II] and [A IV] radiations are produced in filaments of much higher density than those from which [O II] radiation is more predominant, assuming that the variations in T_e are small. Hence a nebula, perhaps, consists of numerous filaments, knots, and tenuous regions such that the density may very well range from less than 10^4 electrons/cm^3 to something like 10^6 electrons/cm^3.

TABLE III

Values of $N_e/T_e^{1/2}$ *for* O II, S II *and* A IV

Nebulae	$N_e/T_e^{1/2}$ O II	$N_e/T_e^{1/2}$ S II	$N_e/T_e^{1/2}$ A IV	$\frac{N_e(\text{SB})}{T_e^{1/2}}$	$\frac{N_e(\text{FL})}{T_e^{1/2}}$
NGC 7662	80	550	760	51	440
NGC 2440	92	...	760	...	310
NGC 7027	174	562	$1{\cdot}2 \times 10^4$	38	290
NGC 6572	160 254	1000 540	480	88	440
Orion	92	540	...	...	180
IC 418	500	340	...	117	60
NGC 40	38	...	...	...	...
NGC 2392	230	...	...	8	...
NGC 6210	230	...	...	84	...
BD+30 3639	230	740	...	...	...
IC 4593	66	...	...	33	...
NGC 6543	176	160	...	65	300*
NGC 6826	190	...	...	21	286*
IC 4997	750	...	...	...	...
NGC 7009	160	...	$1{\cdot}9 \times 10^3$	53	253*
NGC 6803	...	...	$2{\cdot}82 \times 10^3$	...	...
IC 2165	...	...	$1{\cdot}9 \times 10^3$ $1{\cdot}35 \times 10^3$	...	...
IC 5217	...	...	$1{\cdot}15 \times 10^3$	...	...
Humason Planetary	400	...	...	...	...
Cannor Planetary	125	...	...	...	...

*Estimated from surface brightness (Seaton, (**19**)).

For the sake of comparison, we have included in Table III, the values of $N_e/T_e^{1/2}$ computed from the surface brightness method of Aller and Liller (3) (abbreviated as SB) and the values obtained by Seaton (17) using the forbidden line method (abbreviated as FL).

Our values of $N_e/T_e^{1/2}$ for regions of maximum [O II] emission are, in all but two cases, about 2 to 5 times greater than Aller's values. The values of $N_e/T_e^{1/2}$ given by the FL method (17) are all larger (with the exception of IC 418, for which Wyse's intensities may not be reliable) than our values for O II, which can be explained if [O II] radiation predominantly originates from less dense portions of the nebulae, since the values given by the FL method are essentially average values for the regions of maximum emission of the ions considered.

Very recently Osterbrock (14) observed the $\lambda 3727$ intensity ratio at many points in the Orion Nebula. The intensity ratio is observed to vary much at different points, thus supporting the theory. All the observed values lie between the lower limit 0·34 and the upper limit 1·5.

It is admitted without reservation that this method of estimating the electron density in clouds of maximum emission of p^3 ions can be effectively applied only if the intensity ratio r of the ^2D–^4S lines is known accurately. Further, this determination should be particularly accurate for the steep portion of the curves. It is here assumed that there are no large scale variations in the value of electron temperature T_e within a nebula. But, strictly speaking, one should determine T_e for the ion concerned from the ratio of the nebular and the auroral or transauroral lines. Thus accurate intensity measurements of [D–S], [P–D], and [P–S] lines for O II, S II and A IV in gaseous nebulae are much to be desired.

We are grateful to Professor D. S. Kothari for helpful discussions.

Department of Physics,
University of Delhi:
1955 *April.*

References

(1) Aller, L. H., *Ap. J.*, **113**, 125, 1951.
(2) Aller, L. H., *Ap. J.*, **120**, 401, 1954.
(3) Aller, L. H. and Liller, W., *Ap. J.*, **120**, 48, 1954.
(4) Aller, L. H., Bowen, I. S. and Minkowski, R., *Ap. J.*, **122**, 62, 1955.
(5) Aller, L. H. and Minkowski, R., *P.A.S.P.*, **58**, 258, 1946.
(6) Aller, L. H. and Minkowski, R., *Ap. J.*, **124**, 110, 1956.
(7) Aller, L. H., Ufford, C. W. and Van Vleck, J. H., *Ap. J.*, **109**, 42, 1949.
(8) Berman, L., *Lick Obs. Bull.*, **18**, 73, 1937.
(9) Bowen, I. S., *Ap. J.*, **81**, 1, 1928.
(10) Condon, E. U. and Shortley, G. H., Cambridge University Press, 1935.
(11) Garstang, R. H., *Ap. J.*, **115**, 506, 1952.
(12) Hebb, M. H. and Menzel, D. H., *Ap. J.*, **92**, 408, 1940.
(13) Naqvi, A. M., *Thesis*, Harvard University, 1951.
(14) Osterbrock, D. E., *Ap. J.*, **122**, 235, 1955.
(15) Pasternack, S., *Ap. J.*, **92**, 129, 1940.
(16) Seaton, M. J., *Proc. Roy. Soc.* A, **218**, 400, 1953.
(17) Seaton, M. J., *M.N.*, **114**, 154, 1954.
(18) Seaton, M. J., *Ann. d'Ap.*, **17**, 74, 1954.
(19) Seaton, M. J., *Ann. d'Ap.*, **17**, 296, 1954.
(20) Seaton, M. J., *Ann. d'Ap.*, **17**, 550, 1954.
(21) Shortley, G. H., *Phys. Rev.*, **57**, 225, 1940.
(22) Shortley , G. H., Aller, L. H., Baker, J. G. and Menzel, D. H., *Ap. J.*, **92**, 178, 1940.
(23) Swings, P. and Jose, P. D., *P.A.S.P.*, **61**, 181, 1949.
(24) Wyse, A. B., *Ap. J.*, **95**, 356, 1942.

NOTICE TO AUTHORS

1. *Communications.*—Papers must be communicated to the Society by a Fellow. They should be accompanied by a summary at the *beginning* of the paper conveying briefly the content of the paper, and drawing attention to important new information and to the main conclusions. The summary should be intelligible in itself, without reference to the paper, to a reader with some knowledge of the subject; it should not normally exceed 200 words in length. **Authors are requested to submit MSS. in duplicate. These should be typed using double spacing and leaving a margin of not less than one inch on the left-hand side. Corrections to the MSS. should be made in the text and not in the margin.** Unless a paper reaches the Secretaries more than seven days before a Council meeting it will not normally be considered at that meeting. By Council decision, MSS. of accepted papers are retained by the Society for one year after publication; unless their return is then requested by the author, they are destroyed.

2. *Presentation.*—Authors are allowed considerable latitude, but they are requested to follow the general style and arrangement of *Monthly Notices*. References to literature should be given in the standard form, including a date, for printing either as footnotes or in a numbered list at the end of the paper. Each reference should give the **name and initials** of the author cited, irrespective of the occurrence of the name in the text (some latitude being permissible, however, in the case of an author referring to his own work). The following examples indicate the style of reference appropriate for a paper and a book, respectively :—

A. Corlin, *Zs. f. Astrophys.*, **15**, 239, 1938.
H. Jeffreys, *Theory of Probability*, 2nd edn., section 5.45, p. 258, Oxford, 1948.

3. *Notation.*—For technical astronomical terms, authors should conform closely to the recommendations of Commission 3 of the International Astronomical Union (*Trans. I.A.U.*, Vol. VI, p. 345, 1938). Council has decided to adopt the I.A.U. 3-letter abbreviations for constellations where contraction is desirable (Vol. IV, p. 221, 1932). In general matters, authors should follow the recommendations in *Symbols, Signs and Abbreviations* (London : Royal Society, 1951) except where these conflict with I.A.U. practice.

4. *Diagrams.*—**These should be designed to appear upright on the page, drawn about twice the size required in print and prepared for direct photographic reproduction except for the lettering, which should be inserted in pencil. Legends should be given in the manuscript indicating where in the text the figure should appear.** Blocks are retained by the Society for 10 years; unless the author requires them before the end of this period they are then destroyed.

5. *Tables.*—**These should be arranged so that they can be printed upright on the page.**

6. *Proofs.*—Costs of alteration exceeding 5 per cent of composition must be borne by the author. Fellows are warned that such costs have risen sharply in recent years, and it is in their own and the Society's interests to seek the maximum conciseness and simplification of symbols and equations consistent with clarity.

7. *Revised Manuscripts.*—When papers are submitted in revised form it is especially requested that they be accompanied by the original MSS.

Reading of Papers at Meetings

8. When submitting papers authors are requested to indicate whether they will be willing and able to read the paper at the next or some subsequent meeting, and approximately how long they would like to be allotted for speaking.

9. Postcards giving the programme of each meeting are issued some days before the meeting concerned. Fellows wishing to receive such cards whether for Ordinary Meetings or for the Geophysical Discussions or both should notify the Assistant Secretary

CONTENTS

Printed in London by Taylor & Francis, Ltd., 1957 October